Studies on Structures and Redox Properties of Mixed Addenda Heteropolyoxometalates

1997

Isao Kawafune

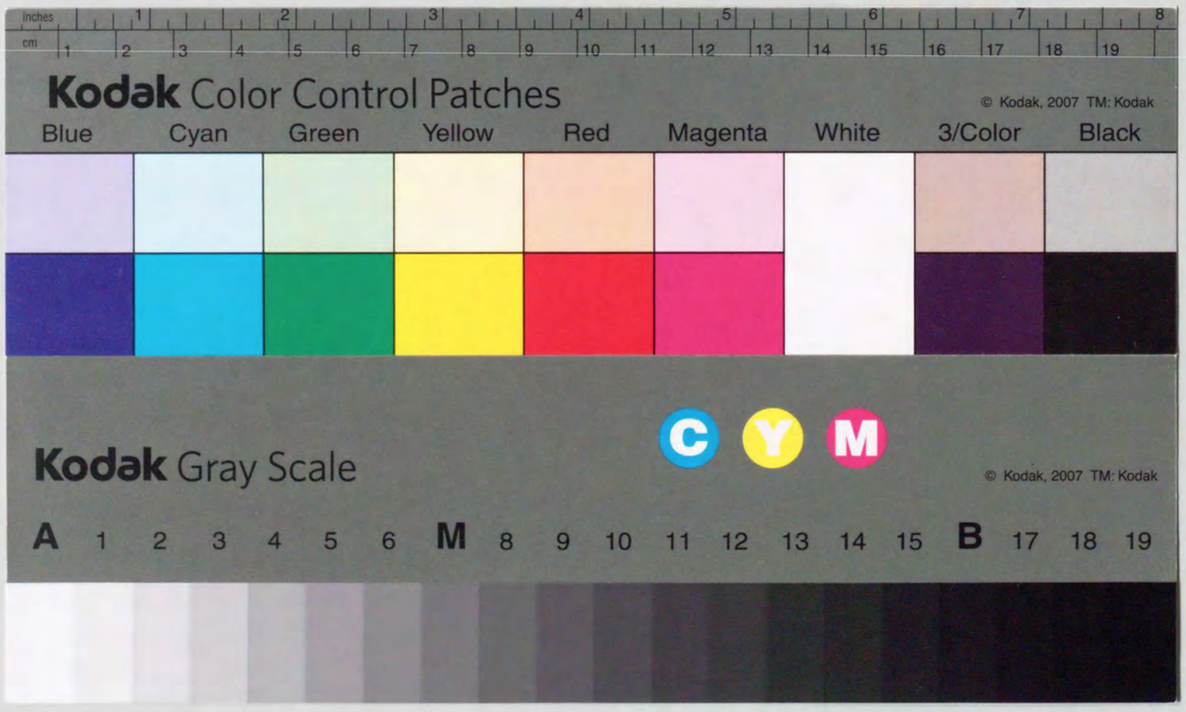

Studies on Structures and Redox Properties of Mixed Addenda Heteropolyoxometalates

（混合配位型ヘテロポリ酸塩の構造と酸化還元特性に関する研究）

1997

Isao Kawafune

Preface

The work of this thesis was performed under the guidance of Professor Gen-etsu Matsubayashi at Department of Applied Chemistry, Faculty of Engineering, Osaka University.

The studies of this thesis are directed toward development of preparation methods of mixed addenda heteropolyoxometalates with the specific positional isomerism concerning the substituted metal atoms and establishment of the relationships between the structures and the redox properties of heteropolyoxometalates. The author hopes that the findings obtained in this work will benefit in progress in elucidation of electronic states of heteropolyoxometalates as well as introduction of the concept of molecular design to a wide range of functional materials of metal oxides.

Isao Kawafune

Isao Kawafune

Osaka Municipal Technical Research Institute

1-6-50 Morinomiya, Joto-ku, Osaka 536,

Japan

December 1997

Contents

General Introduction

Heteropolyoxometalates have extensively been used as practical catalysts for oxidation and acidic processes in various industrial fields [1a, 2, 3]. In recent years, a wide range of their potential applications are spread in many fields [1a, 2] such as magnetic and conducting [4, 5], electrodes [6], non-linear optical [7], and biomedical materials [8] because of their versatile properties.

Heteropolyanions are formed by the condensation of an oxo acid of metal (M) and that of heteroatom (X) and classified into various types of structures according to the composition of X:M, as summarized in Table 1 [1b, 1c, 9, 10]. Among them, the Keggin anions

Table 1. Typical Classes of Heteropolyanions

X:M	Formula	Name of Structure
1:12	$[PW_{12}O_{40}]^{3-}$	Keggin
1:12	$[CeMo_{12}O_{42}]^{8-}$	Silverton
2:18	$[P_2W_{18}O_{62}]^{6-}$	Dawson
1:9	$[MnMo_9O_{32}]^{6-}$	Waugh
1:6	$[TeMo_6O_{24}]^{6-}$	Anderson
1:11	$[PW_{11}O_{39}]^{7-}$	defect Keggin
1:10	$[PW_{10}O_{36}]^{7-}$	defect Keggin
1:9	$[PW_9O_{34}]^{9-}$	defect Keggin

(X:M = 1:12) are representative, because they are easily prepared, thermally and chemically stable, and widely used as catalysts [3]. The Keggin structure [11], having overall T_d symmetry, is constructed with a central XO_4 tetrahedron (X= P, Si, As, etc.) surrounded by twelve metal-centered MO_6 octahedra (M= W, Mo, V, Nb, etc.) arranged in four groups of three edge-shared octahedra, M_3O_{13}; these triplet groups are linked by shared corners to one another and to the central XO_4 tetrahedron [1d] (Fig. 1). The oxygen atoms of the Keggin anion are classified into four species [10]: four internal ones (O_i) binding the X and three M

atoms, twelve terminal ones (O_t) bound to the M atoms, twelve edge-sharing ones (O_{be}) bridging between two MO_6 octahedra within the same M_3O_{13} triplet, and twelve corner-sharing ones (O_{bc}) bridging between two M_3O_{13} triplets; O_{be} and O_{bc} atoms are expressed in terms of O_b atoms put together.

Figure 1. Polyhedral representation of the Keggin anion, α-$[XM_{12}O_{40}]^{n-}$. Hatched and plain parts indicate the central XO_4 tetrahedron and MO_6 octahedra, respectively.

Heteropolyoxometalates resemble discrete fragments of solid metal oxides and, in addition, are superior to conventional metal oxides in the respects that they are soluble in water and organic solvents and that their structures can be well-defined at the molecular level of polyanions [3]. Thus, from the viewpoint of molecular design of catalysts, their properties as a model complex of metal oxide catalysts as well as their inherent catalytic activities have been attracting particular attention. Furthermore, since their properties can be controlled by modifying the constituent elements (heteroatoms and addenda atoms) of polyanions and counter cations, the relationships between the structures and the properties of heteropoly compounds have systematically been investigated [10].

Mixed addenda heteropolyoxometalates, which contain two or more kinds of elements as addenda atoms, have recently attracted much interest, because the metal atoms substituted for the parent ones furnish the polyanions with novel properties such as enhancement of the catalytic activities and selectivities [3, 12–18], supporting for transition metal catalysts [19], introducing of sites of direct ligand binding [20], magnetic interactions [21–23], and formation of new types of geometrical isomers [24–27]. One of the major problems for this class of heteropoly compounds is that it is difficult to synthesize one with precise structure including the location of the different addenda atoms. Mixtures containing a variety of species with different composition of the addenda atoms tend to be afforded [28], and even

for the species with a unique composition there are numerous possibilities [29, 30] of positional isomers [1e, 31] of the different addenda atoms as well as geometrical isomers [32].

Stereospecific positional isomers of metal(M)-trisubstituted dodecatungsto-heteropolyanions of the Keggin type, $[XM_3W_9O_{40}]^{n-}$ (X = heteroatom), are demonstrated in Fig. 2 [33]. The A-type positional isomers (a and c) have three adjacent corner-shared MO_6 octahedra of the substituted metal and the B-type one (b) has three adjacent edge-shared MO_6 octahedra constructing the M_3O_{13} triplet. The geometrical isomers are also demonstrated in Fig. 2. The Keggin anions (a and b) are denoted by the α-isomer [11]. The structure of the β-isomer (c) has an edge-shared W_3O_{13} triplet rotated by 60° about the three-fold axis of the α-isomer, thereby reducing the overall symmetry of the anion from T_d to C_{3v} [32].

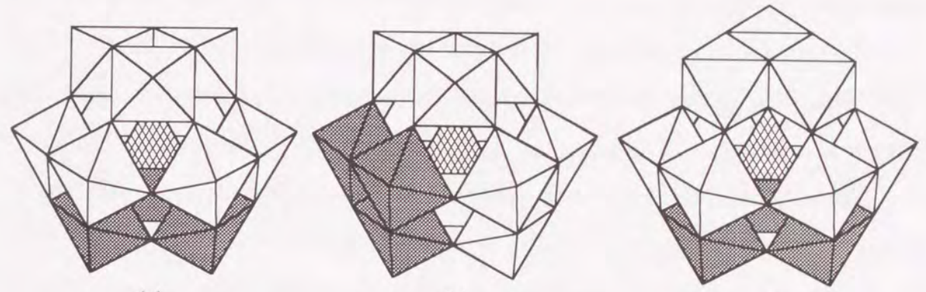

Figure 2. Polyhedral representation of the positional and geometrical isomers of metal-trisubstituted dodecatungsto heteropolyanions of the Keggin type. A-α-$[XM_3W_9O_{40}]^{n-}$ (a), B-α-$[XM_3W_9O_{40}]^{n-}$ (b), and A-β-$[XM_3W_9O_{40}]^{n-}$ (c). Hatched, plain, and shaded parts indicate the central XO_4 tetrahedron, WO_6 octahedra, and MO_6 octahedra, respectively.

The first object of this study is to confirm the methods for the syntheses of specific positional isomers of the mixed addenda heteropolyoxometalates derived from the trivacant lacunary nonatungstophosphate precursor, A-$Na_9[PW_9O_{34}]$ [34, 35]. The precise structures of the β-isomers of the A-type metal-trisubstituted dodecatungstophosphate anion salts, A-β-$[PM_3W_9O_{40}]^{n-}$ (M = V(V) and Nb(V), n = 6, M = Mo(VI), n = 3), have been

determined by the single-crystal X-ray analyses, the sites of the substituted addenda atoms having been clarified.

The redox mechanisms of heteropolyoxometalates of the Keggin type have systematically been studied in relation to their catalytic functions [10, 36–41]. Although a heterogeneous (vapor/solid phase) reduction of the α-dodecamolybdophosphate (α-$[PMo_{12}O_{40}]^{3-}$) compounds in catalytic processes is known to be accompanied by an elimination of the bridging oxygen atoms in the Mo–O–Mo bonds [10, 36, 38, 40], no investigations have been done to clarify the difference in the reactivity between the corner-sharing and the edge-sharing oxygen atoms. In this study, the individual reactivity of both the bridging oxygen atoms has been evaluated through the stoichiometric reductions of the α-$[PMo_{12}O_{40}]^{3-}$ anion salt and of the A-β-$[PMo_3W_9O_{40}]^{3-}$ anion salt with triphenylphosphine in a homogeneous system.

Chapter 1 describes syntheses and spectroscopic properties of A-β-$[PV_3W_9O_{40}]^{6-}$, A-β-$[PNb_3W_9O_{40}]^{6-}$, and A-β-$[PMo_3W_9O_{40}]^{3-}$ anion salts in comparison with their geometrical α-isomers.

Chapter 2 describes the determination of the crystal structures of three β-isomers of these salts.

Chapter 3 refers the isomerization of these β-isomers to the corresponding α-isomers together with their kinetics.

In chapter 4, reduction of α-$(NBu^n_4)_3[PMo_{12}O_{40}]$ and of A-β-$(NBu^n_4)_3[PMo_3W_9O_{40}]$ with triphenylphosphine are examined in acetonitrile. Some oxygen-deficient reduced species of these heteropoly compounds are isolated and their spectroscopic properties are discussed.

In chapter 5, the kinetics of the above-mentioned oxygen-transfer reactions are discussed.

List of Publications

1. Reduction of the Dodecamolybdophosphate Anion with Triphenylphosphine in a Homogeneous System,
   Isao Kawafune,
   Chem. Lett., 1503–1506 (1986).
2. Isolation and Characterization of Some Oxygen-Deficient Reduced Forms of Dodecamolybdophosphate Anion Salts,
   Isao Kawafune,
   Chem. Lett., 185–188 (1989).
3. Isolation and Characterization of Oxygen-Deficient Reduced Forms of the Dodecamolybdophosphate Anion Salt,
   Isao Kawafune and Gen-etsu Matsubayashi,
   Inorg. Chim. Acta, **188**, 33–39 (1991).
4. Synthesis and Crystal Structure of Molybdenum-Trisubstituted Tungstophosphate Anion Salt, A-β-$[N(CH_3)_4]_3[PMo_3W_9O_{40}]$,
   Isao Kawafune and Gen-etsu Matsubayashi,
   Chem. Lett., 1869–1872 (1992).
5. Oxygen-Transfer Reaction of the A-Type Molybdenum-Trisubstituted Tungstophosphate Anion Salt and Spectroscopic Properties of the Isolated Oxygen-Deficient Reduced Species,
   Isao Kawafune and Gen-etsu Matsubayashi,
   Bull. Chem. Soc. Jpn., **67**, 694–698 (1994).
6. Kinetics of Oxygen-Atom Transfer Reactions of α-$[PMo_{12}O_{40}]^{3-}$ and of A-β-$[PMo_3W_9O_{40}]^{3-}$ Anion Salts with PPh_3 in Non-Aqueous Solution,
   Isao Kawafune and Gen-etsu Matsubayashi,
   Bull. Chem. Soc. Jpn., **68**, 838–842 (1995).

7. Isolation and Spectroscopic Properties of A-β-$[PV_3W_9O_{40}]^{6-}$ Anion Salts and Their Isomerization to the α-Isomers,
Isao Kawafune and Gen-etsu Matsubayashi,
Bull. Chem. Soc. Jpn., **69**, 359–365 (1996).

8. Crystal Structure of Cesium Salt of β-Isomer of A-Type Vanadium-Trisubstituted Dodecatungstophosphate Anion, A-β-$Cs_{5.4}H_{0.6}[PV_3W_9O_{40}]\cdot 12H_2O$,
Isao Kawafune, Hatsue Tamura, and Gen-etsu Matsubayashi,
Bull. Chem. Soc. Jpn., **70**, 2455–2460 (1997).

9. Syntheses of α- and β-Isomers of the A-Type Niobium-Trisubstituted Dodecatungstophosphate Anion Salts and Crystal Structure of Cesium Salt of the β-Isomer, A-β-$Cs_6[PNb_3W_9O_{40}]\cdot 14H_2O$,
I. Kawafune, H. Tamura, and G. Matsubayashi,
in preparation.

References

1 (a) M. T. Pope, "Heteropoly and Isopoly Oxometalates", Springer-Verlag, Berlin, p.31 (1983), and references therein. (b) *ibid.*, p.18. (c) *ibid.*, p.58. (d) *ibid.*, p.23. (e) *ibid.*, p.27.

2 M. T. Pope and A. Müller, *Angew. Chem. Int. Ed. Engl.*, **30**, 34 (1991), and references therein.

3 N. Mizuno and M. Misono, *J. Mol. Catal.*, **86**, 319 (1994), and references therein.

4 P. L. Maguerès, L. Ouahab, S. Golhen, D. Grandjean, O. Peña, J. -C. Jegaden, C. J. Gómez-García, and P. Delhaès, *Inorg. Chem.*, **33**, 5180 (1994), and references therein; C. J. Gómez-García, C. Giménez-Saiz, S. Triki, E. Coronado, P. L. Maguerès, L. Ouahab, L. Ducasse, C. Sourisseau, and P. Delhaès, *Inorg. Chem.*, **34**, 4139 (1995), and references therein.

5 C. Bellitto, M. Bonamico, V. Fares, F. Federici, G. Righini, M. urmoo, and P. Day, *Chem. Mater.*, **7**, 1475 (1995), and references therein.

6 P. J. Kulesza, L. R. Faulkner, J. Chen, and W. G. Klemperer, *J. Am. Chem. Soc.*, **113**, 379 (1991), and references therein.

7 J. Niu, X. You, C. Duan, H. Fun, and Z. Zhou, *Inorg. Chem.*, **35**, 4211 (1996).

8 M. Inoue and T. Yamase, *Bull. Chem. Soc. Jpn.*, **68**, 3055 (1995), and references therein; M. Inoue and T. Yamase, *Bull. Chem. Soc. Jpn.*, **69**, 2863 (1996).

9 T. J. R. Weakley, *Structure and Bonding*, **18**, 131 (1974).

10 M. Misono, *Proc. Int. Conf. Chem. Uses Molybdenum, 4th*, **1982**, 289, and references therein.

11 J. F. Keggin, *Nature*, **131**, 908 (1933), **132**, 351 (1933); J. F. Keggin, *Proc. Roy. Soc.*, **A144**, 75 (1934).

12 E. G. Zhizhina, L. I. Kuznetsova, R. I. Maksimovskaya, S. N. Pavlova, and K. I. Matveev, *J. Mol. Catal.*, **38**, 345 (1986).

13 T. Yamase and M. Sugeta, *Inorg. Chim. Acta*, **172**, 131 (1990), and references therein.

14 J. K. Burdett and C. K. Nguyen, *J. Am. Chem. Soc.*, **112**, 5366 (1990).

15 M. W. Droege and R. G. Finke, *J. Mol. Catal.*, **69**, 323 (1991), and references therein.

16 A. M. Khenkin and C. L. Hill., *J. Am. Chem. Soc.*, **115**, 8178 (1993), and references therein.

17 E. Cadot, M. Fournier, A. Tézé, and G. Hervé, *Inorg. Chem.*, **35**, 282 (1996), and references therein.

18 K. Nomiya, H. Yanagibayashi, C. Nozaki, K. Kondoh, E. Hiramatsu, and Y. Shimizu, *J. Mol. Catal.*, **114**, 181 (1996).

19 B. Rapko, M. Pohl, and R. G. Finke, *Inorg. Chem.*, **33**, 3625 (1994), and references therein.

20 J. Liu, F. Ortéga, P. Sethuraman, D. E. Katsoulis, C. E. Costello, and M. T. Pope, *J. Chem. Soc., Dalton Trans.*, **1992**, 1901, and references therein; H. Y. Woo, H. So, and M. T. Pope, *J. Am. Chem. Soc.*, **118**, 621 (1996).

21 M. Kozik, N. Casan-Pastor, C. F. Hammer, and L. C. W. Baker, *J. Am. Chem. Soc.*, **110**, 7697 (1988).

22 C. J. Gómez-García, E. Coronado, and L. Ouahab, *Angew. Chem. Int. Ed. Engl.*, **31**, 649 (1992); C. J. Gómez-García, E. Coronado, P. Gómez-Romero, and N. Casañ-Pastor, *Inorg. Chem.*, **32**, 89 (1993); C. J. Gómez-García, E. Coronado, P. Gómez-Romero, and N. Casañ-Pastor, *Inorg. Chem.*, **32**, 3378 (1993).

23 X. Zhang, G. B. Jameson, C. J. O'Connor, and M. T. Pope, *Polyhedron*, **15**, 917 (1996).

24 P. J. Domaille and R. L. Harlow, *J. Am. Chem. Soc.*, **108**, 2108 (1986); P. J. Domaille, *Inorg. Synth.*, **27**, 96 (1990).

25 J. Canny, R. Thouvenot, A. Tézé, G. Hervé, M. Leparulo-Loftus, and M. T. Pope, *Inorg. Chem.*, **30**, 976 (1991).

26 X. Zhang, C. J. O'Connor, G. B. Jameson, and M. T. Pope, *Inorg. Chem.*, **35**, 30 (1996).

27 E. Cadot, V. Béreau, B. Marg, S. Halut, and F. Sécheresse, *Inorg. Chem.*, **35**, 3099 (1996).

28 E. Cadot, R. Thouvenot, A. Tézé, and G. Hervé, *Inorg. Chem.*, **31**, 4128 (1992).

29 W. H. Knoth, *J. Am. Chem. Soc.*, **101**, 759 (1979).

30 J. Canny, A. Tézé, R. Thouvenot, and G. Hervé, *Inorg. Chem.*, **25**, 2114 (1986).

31 M. T. Pope and T. F. Scully, *Inorg. Chem.*, **14**, 953 (1975).

32 L. C. W. Baker and J. S. Figgis, *J. Am. Chem. Soc.*, **92**, 3794 (1970).

33 R. G. Finke, B. Rapko, R. J. Saxton, and P. J. Domaille, *J. Am. Chem. Soc.*, **108**, 2947 (1986)

34 P. J. Domaille and G. Watunya, *Inorg. Chem.*, **25**, 1239 (1986).

35 The trivacant lacunary heteropolyanions which correspond to removal of three adjacent corner-shared MO_6 octahedra and three adjacent edge-shared MO_6 octahedra from the Keggin anion are also denoted by an A-type and a B-type, respectively.

36 H. Tsuneki, H. Niiyama, and E. Echigoya, *Chem. Lett.*, **1978**, 645 and 1183.

37 M. Akimoto, Y. Tsuchida, and E. Echigoya, *Chem. Lett.*, **1980**, 1205; M. Akimoto and E. Echigoya, *Chem. Lett.*, **1981**, 1759; M. Akimoto, Y. Tsuchida, K. Sato, and E. Echigoya, *J. Catal.*, **72**, 83 (1981); S. Yoshida, H. Niiyama, and E. Echigoya, *J. Phys. Chem.*, **86**, 3150 (1982); M. Akimoto, K. Shima, and E. Echigoya, *J. Chem. Soc., Faraday Trans. 1*, **79**, 2467 (1983); M. Akimoto, K. Shima, H. Ikeda and E. Echigoya, *J. Catal.*, **86**, 173 (1984).

38 K. Katamura, T. Nakamura, K. Sakata, M. Misono, and Y. Yoneda, *Chem. Lett.*, **1981**, 89; N. Mizuno, K. Katamura, Y. Yoneda, and M. Misono, *J. Catal.*, **83**, 384 (1983).

39 M. Misono, T. Komaya, H. Sekiguchi, and Y. Yoneda, *Chem. Lett.*, **1982**, 53; Y. Konishi, K. Sakata, M. Misono, and Y. Yoneda, *J. Catal.*, **77**, 169 (1982); N. Mizuno, T. Watanabe, and M. Misono, *J. Phys. Chem.*, **89**, 80 (1985).

40 K. Eguchi, Y. Toyozawa, K. Furuta, N. Yamazoe, and T. Seiyama, *Chem. Lett.*, **1981**, 1253; K. Eguchi, Y. Toyozawa, N. Yamazoe, and T. Seiyama, *J. Catal.*, **83**, 32 (1983).

41 K. Eguchi, N. Yamazoe, and T. Seiyama, *Chem. Lett.*, **1982**, 1341; H. Taketa, S. Katsuki, K. Eguchi, T. Seiyama, and N. Yamazoe, *J. Phys. Chem.*, **90**, 2959 (1986).

Chapter 1

Syntheses and Spectroscopic Properties of the α- and β-Isomers of the A-Type Vanadium-, Niobium-, and Molybdenum-Trisubstituted Dodecatungstophosphate Anion Salts

1.1 Introduction

The redox properties of mixed addenda heteropolyoxometalates, which contain two or more kinds of elements as addenda atoms, can be precisely controlled by modifying the constituent addenda atoms [1]. Therefore, the relationships between the structures and the redox properties of such compounds have attracted much attention in relation to discrete model complexes of mixed metal oxides catalysts [1–4]. One of the major problems for these compounds is that it is difficult to synthesize one with precise structure including the number and the location of the substituted metal atoms. Mixtures containing various species with different compositions of the addenda atoms tend to be afforded [5], and even for the species with a unique composition there are numerous possibilities [6, 7] of positional isomers [8, 9] of the different addenda atoms as well as geometrical isomers [10].

Stereospecific syntheses of metal-trisubstituted dodecatungstosilicate compounds ($[SiM_3W_9O_{40}]^{7-}$, M = V and Nb) [11–13] were done by using structurally well-characterized A-type trivacant lacunary nonatungstosilicate precursors, the A-α-$[SiW_9O_{34}]^{10-}$ [14] and A-β-$[SiW_9O_{34}]^{10-}$ anion salts [15]. On the other hand, it is uncertain whether the trivacant lacunary nonatungstophosphate anion, $[PW_9O_{34}]^{9-}$, is an α- or β-isomer [16]. By using the A- and B-$[PW_9O_{34}]^{9-}$ anion salts as precursors, two α-isomers of nonatungstotrivanadophosphate compounds, the A-α-$[PV_3W_9O_{40}]^{6-}$ [11] and B-α-$[PV_3W_9O_{40}]^{6-}$ anion salts [16], were synthesized, respectively.

In this chapter, by using the sodium salt of the A-type trivacant lacunary nonatungstophosphate anion, A-$Na_9[PW_9O_{34}]$ [16], as a precursor, A-type vanadium-, niobium-, and molybdenum-trisubstituted dodecatungstophosphate anion salts, A-β-$[PV_3W_9O_{40}]^{6-}$, A-α-$[PV_3W_9O_{40}]^{6-}$, A-β-$[PNb_3W_9O_{40}]^{6-}$, A-α-$[PNb_3W_9O_{40}]^{6-}$, and A-β-$[PMo_3W_9O_{40}]^{3-}$, were synthesized and their structures were characterized by their spectroscopic properties.

1.2 Experimental

Materials. Nonasodium nonatungstophosphate heptahydrate [16], A-$Na_9[PW_9O_{34}]\cdot 7H_2O$, and heptapotassium monohydrogen hexaniobate tridecahydrate [17], $K_7H[Nb_6O_{19}]\cdot 13H_2O$, were prepared according to the procedures in the literatures.

Preparation of Nonatungstotrivanadophosphate Anion Salts.

A-β-$Cs_{5.4}H_{0.6}[PV_3W_9O_{40}]$. To an aqueous (90 cm^3) solution of $NaVO_3$ (4.23 g, 34.4 mmol) was added 12 mol dm^{-3} HCl (50 cm^3) and then 1,4-dioxane (50 cm^3). To the vigorously stirred pale-yellow solution, freshly prepared A-$Na_9[PW_9O_{34}]\cdot 7H_2O$ (14.2 g, 5.54 mmol) was added slowly in small portions (about 50 mg) to turn red immediately. After stirring for 1 h at room temperature, CsCl solids (13.2 g, 78.4 mmol) were added to the solution. The resulting red precipitates were collected by filtration, washed with methanol, and dried in vacuo to afford a red powder (12.5 g). It was dissolved in water (350 cm^3), yellow insoluble materials being removed by centrifugation. The supernatant solution was cooled to give dark-red columns of A-β-$Cs_{5.4}H_{0.6}[PV_3W_9O_{40}]\cdot 12H_2O$ (10.5 g, 56% yield). The composition of the cation was determined by the single-crystal X-ray analysis described in chapter 2. Twelve molar amounts of water were determined by thermogravimetry based on the weight loss of the salt heated up to 300°C (Found 6.0%, Calcd 6.33%). The compound contained no sodium ion based on atomic absorption spectroscopy. Anal. Found: H, 0.67; Cs, 22; P, 0.91; V, 4.4; W, 48%. Calcd for $H_{24.6}Cs_{5.4}O_{52}PV_3W_9$: H, 0.73; Cs, 21.03; P, 0.91; V, 4.48; W, 48.48%.

A-β-$(NBu^n_4)_4H_2[PV_3W_9O_{40}]$. To the above-mentioned supernatant solution was added an aqueous (25 cm^3) solution of NBu^n_4Br (6.45 g, 20.0 mmol). The resulting red precipitates were collected by filtration, washed with water and ethanol, and dried in

vacuo to afford a red powder of A-β-$(NBu^n_4)_4H_2[PV_3W_9O_{40}]$ (8.20 g, 43% yield). Anal. Found: C, 22.29; H, 4.20; N, 1.57; P, 0.88; V, 4.1; W, 47%. Calcd for $C_{64}H_{146}N_4O_{40}PV_3W_9$: C, 22.28; H, 4.27; N, 1.62; P, 0.90; V, 4.43; W, 47.96%.

A-β-$(NBu^n_4)_6[PV_3W_9O_{40}]$. To an acetonitrile (10 cm^3) solution of A-β-$(NBu^n_4)_4H_2[PV_3W_9O_{40}]$ (1.00 g, 0.290 mmol) was added a methanol solution containing 10 wt% of NBu^n_4OH (1.51 g, 0.582 mmol) and the solution was stirred for 5 min at room temperature. After the solvent was evaporated to dryness under reduced pressure, the residue was washed with diethyl ether, collected by filtration, and dried in vacuo to afford a red powder of A-β-$(NBu^n_4)_6[PV_3W_9O_{40}]$ (0.930 g, 81% yield). Anal. Found: C, 30.17; H, 5.70; N, 2.17%. Calcd for $C_{96}H_{216}N_6O_{40}PV_3W_9$: C, 29.32; H, 5.54; N, 2.14%.

A-α-$Cs_6[PV_3W_9O_{40}]$. The α-isomer of the A-$[PV_3W_9O_{40}]^{6-}$ anion was prepared by the condensation of A-$Na_9[PW_9O_{34}]\cdot 7H_2O$ and $NaVO_3$ in an acetate buffer solution at pH 4.8 according to the procedure in the literature [11, 18] as follows. To an acetate buffer solution (pH 4.8, 100 cm^3) was added $NaVO_3$ (3.50 g, 28.7 mmol) and then A-$Na_9[PW_9O_{34}]\cdot 7H_2O$ (14.0 g, 5.46 mmol). After stirring for 48 h at room temperature, CsCl solids (10.0 g, 59.4 mmol) were added to the solution. The resulting orange precipitates were collected by filtration, washed with water and methanol, and dried in vacuo to afford an orange powder of A-α-$Cs_6[PV_3W_9O_{40}]$ (14.2 g, 79%).

A-α-$(NBu^n_4)_4H_2[PV_3W_9O_{40}]$. A-α-$Cs_6[PV_3W_9O_{40}]$ (7.10 g, 2.17 mmol) was dissolved in water (1000 cm^3) and followed by addition of an aqueous (25 cm^3) solution of NBu^n_4Br (6.45 g, 20.0 mmol). The resulting red precipitates were collected by filtration, washed with water and ethanol, and dried in vacuo to afford a red powder of A-α-$(NBu^n_4)_4H_2[PV_3W_9O_{40}]$ (3.40 g, 45% yield). Anal. Found: C, 22.30; H, 4.11; N, 1.70%. Calcd for $C_{64}H_{146}N_4O_{40}PV_3W_9$: C, 22.28; H, 4.27; N, 1.62%.

Preparation of Triniobononatungstophosphate Anion Salts.

A-β-$Cs_6[PNb_3W_9O_{40}]$. $K_7H[Nb_6O_{19}]\cdot 13H_2O$ (2.02 g, 1.47 mmol) was dissolved in a 30% H_2O_2 aqueous solution (17 cm^3) at room temperature [12, 17] and to the

solution was added water (220 cm^3). After stirring for 10 min at the temperature, 12 mol dm^{-3} HCl (1.0 cm^3) was added and then 1,4-dioxane (1.0 cm^3). To the vigorously stirred pale-yellow solution, freshly prepared A-$Na_9[PW_9O_{34}]\cdot 7H_2O$ (7.12 g, 2.78 mmol) was added slowly in small portions (about 50 mg) to turn yellow gradually. After stirring for 1 h at room temperature, the yellow suspensions were filtered and to the filtrate were added CsCl solids (6.00 g, 35.6 mmol). The resulting yellow precipitates were collected by filtration, washed with methanol, and dried in vacuo to afford a yellow powder (4.94 g). It was dissolved in water (320 cm^3), white insoluble materials being removed by centrifugation. The supernatant solution was cooled to give yellow crystals of A-β-$Cs_6[PNb_3W_9O_{40}]\cdot 14H_2O$ (1.51 g, 15% yield). Fourteen molar amounts of water were determined by thermogravimetry based on the weight loss of the salt heated up to 300°C (Found 6.4%, Calcd 6.90%). The compound contained neither sodium nor potassium ion based on atomic absorption spectroscopy. Anal. Found: Cs, 20; Nb, 7.5; P, 0.86; W, 46%. Calcd for $H_{28}Cs_6Nb_3O_{54}PW_9$: Cs, 21.82; Nb, 7.63; P, 0.85; W, 45.28%.

A-β-$(NBu^n_4)_5H[PNb_3W_9O_{40}]$. To the above-mentioned supernatant solution was added an aqueous (15 cm^3) solution of NBu^n_4Br (3.40 g, 10.5 mmol). The resulting pale-yellow precipitates were collected by filtration, washed with water and ethanol, and dried in vacuo to afford a pale-yellow powder of A-β-$(NBu^n_4)_5H[PNb_3W_9O_{40}]$ (2.39 g, 23% yield). Anal. Found: C, 24.92; H, 4.65; N, 1.86; Nb, 7.9; P, 0.74; W, 43%. Calcd for $C_{80}H_{181}N_5Nb_3O_{40}PW_9$: C, 25.17; H, 4.78; N, 1.83; Nb, 7.30; P, 0.81; W, 43.34%.

A-α-$Cs_6[PNb_3W_9O_{40}]$. An acetate buffer solution (pH 4.8, 50 cm^3) containing A-$Na_9[PW_9O_{34}]\cdot 7H_2O$ (1.88 g, 0.735 mmol) was heated at 60°C for 1 h and then cooled to room temperature. Separately, $K_7H[Nb_6O_{19}]\cdot 13H_2O$ (0.500 g, 0.368 mmol) was dissolved in a 30% H_2O_2 aqueous solution (4.0 cm^3) at room temperature and to the solution was added water (40 cm^3). To the solution was added the above-mentioned buffer solution containing A-$Na_9[PW_9O_{34}]\cdot 7H_2O$ to turn yellow immediately. After stirring for 2 h at room temperature, CsCl solids (1.50 g, 8.91 mmol) were added to the solution and stirred for

2 h. The resulting yellow precipitates were collected by filtration, washed with methanol, and dried in vacuo to afford a yellow powder of A-α-$Cs_6[PNb_3W_9O_{40}]\cdot 11H_2O$ (0.894 g, 34% yield). Eleven molar amounts of water were determined by thermogravimetry based on the weight loss of the salt heated up to 300°C (Found 5.1%, Calcd 5.51%). The compound contained neither sodium nor potassium ion based on atomic absorption spectroscopy. Anal. Found: Cs, 21; Nb, 7.7; P, 0.83; W, 45%. Calcd for $H_{22}Cs_6Nb_3O_{51}PW_9$: Cs, 22.15; Nb, 7.74; P, 0.86; W, 45.96%.

A-α-$(NBu^n_4)_5H[PNb_3W_9O_{40}]$. To the above-mentioned buffer solution containing A-$Na_9[PW_9O_{34}]\cdot 7H_2O$ (1.88 g, 0.735 mmol) and $K_7H[Nb_6O_{19}]\cdot 13H_2O$ (0.500 g, 0.368 mmol) was added an aqueous (50 cm^3) solution of NBu^n_4Br (1.10 g, 3.41 mmol). The resulting pale-yellow precipitates were collected by filtration, washed with water, and dried in vacuo to afford a pale-yellow powder of A-α-$(NBu^n_4)_5H[PNb_3W_9O_{40}]$ (1.34 g, 48% yield). Anal. Found: C, 24.76; H, 4.58; N, 1.86; Nb, 7.3; P, 0.61; W, 45%. Calcd for $C_{80}H_{181}N_5Nb_3O_{40}PW_9$: C, 25.17; H, 4.78; N, 1.83; Nb, 7.30; P, 0.81; W, 43.34%.

Preparation of Trimolybdononatungstophosphate Anion Salts.

A-β-$K_3[PMo_3W_9O_{40}]$. To an aqueous (35 cm^3) solution of $Na_2MoO_4\cdot 2H_2O$ (7.30 g, 30.2 mmol) was added 12 mol dm^{-3} HCl (50 cm^3) and then 1,4-dioxane (50 cm^3). To the vigorously stirred solution, freshly prepared A-$Na_9[PW_9O_{34}]\cdot 7H_2O$ (14.2 g, 5.54 mmol) was added slowly in small portions (about 100 mg) to turn yellowish-green suspensions. After stirring for 1 h at room temperature, KCl solids (3.00 g, 40.2 mmol) were added to the solution. The resulting yellow precipitates were collected by filtration, washed with a saturated KCl aqueous solution, and dried in vacuo to afford a yellow powder of A-β-$K_3[PMo_3W_9O_{40}]$ (12.0 g, 79% yield).

A-β-$(NMe_4)_3[PMo_3W_9O_{40}]$. A-β-$K_3[PMo_3W_9O_{40}]$ (12.0 g, 4.39 mmol) was dissolved in methanol (300 cm^3) and to the solution was added NMe_4Br (2.80 g, 18.2 mmol) dissolved in methanol (100 cm^3). The resulting yellow precipitates were collected by filtration, washed with methanol, and dried in vacuo to afford a yellow powder of A-β-

$(NMe_4)_3[PMo_3W_9O_{40}]$ (7.97 g, 64% yield). It was recrystallized from acetonitrile to give yellow columns. Anal. Found: C, 5.23; H, 1.42; N, 1.40; Mo, 9.6; P, 1.2; W, 56%. Calcd for $C_{12}H_{36}Mo_3N_3O_{40}PW_9$: C, 5.08; H, 1.28; N, 1.48; Mo, 10.15; P, 1.09; W, 58.35%.

A-β-$(NBu^n_4)_3[PMo_3W_9O_{40}]$. A-β-$K_3[PMo_3W_9O_{40}]$ (12.0 g, 4.39 mmol) was dissolved in methanol (300 cm^3) and to the solution was added NBu^n_4Br (5.00 g, 15.5 mmol) dissolved in methanol (50 cm^3). The resulting yellow precipitate was collected by filtration, washed with methanol, and dried in vacuo to afford a yellow powder of A-β-$(NBu^n_4)_3[PMo_3W_9O_{40}]$ (11.0 g, 75% yield). It was recrystallized from acetonitrile to give yellow columns. Found: C, 17.24; H, 3.20; N, 1.24; Mo, 8.3; P, 0.90; W, 49%. Calcd for $C_{48}H_{108}N_3Mo_3O_{40}PW_9$: C, 17.26; H, 3.26; N, 1.26; Mo, 8.26; P, 0.93; W, 49.53%.

Physical Measurements. IR spectra were measured with a Perkin-Elmer 983G and a Nicolet 5DX spectrophotometers in KBr pellets. ^{31}P and ^{51}V NMR spectra were measured with a JEOL JNM-EX270 spectrometer operating at 109.36 and 71.04 MHz, respectively. ^{183}W NMR spectra were measured with a JEOL GSX-400 spectrometer operating at 16.625 MHz. ^{31}P, ^{51}V, and ^{183}W NMR parameters: pulse width, 4.7, 5.1, and 80 μs; sweep width, 5400, 60000, and 8000 Hz; number of acquisitions, 500–5000, 200, and 30000, respectively. For all NMR measurements, the cesium, potassium, and tetraalkylammonium salts were dissolved in deuterium oxide (0.003–0.004 mol dm^{-3}), methanol-d_4 (0.01–0.02 mol dm^{-3}), and acetonitrile-d_3 (0.01–0.05 mol dm^{-3}), respectively. ^{31}P, ^{51}V, and ^{183}W NMR chemical shifts were expressed in ppm with negative values upfield from those of 85%H_3PO_4, $VOCl_3$ (neat), and Na_2WO_4 in deuterium oxide (2 mol dm^{-3}), respectively, using the sample replacement method [19].

1.3 Results and Discussion

α-Dodecatungstophosphate, α-$H_3[PW_{12}O_{40}]$, was prepared by the condensation of Na_2WO_4 and Na_2HPO_4 in an acidic solution [20]. Some mixed addenda

molybdotungstophosphates, α-$H_3[PMo_xW_{12-x}O_{40}]$ (x = 1~11), were reported to be conveniently obtained by modification of the above-mentioned, usual method using mixtures of Na_2MoO_4 and Na_2WO_4 in a variety of molar ratios instead of Na_2WO_4 solely [21, 22]. A unique Mo/W composition for these compounds was suggested by their IR spectra; the characteristic bands [23] of the potassium salts of these polyanions were continuously changed according to the Mo/W ratios of starting materials and distinct from those of the mixtures of α-$K_3[PMo_{12}O_{40}]$ and α-$K_3[PW_{12}O_{40}]$ [22]. However, the author found that these mixed addenda compounds were composed of mixtures of a series of anion salts of molybdotungstophosphates, α-$[PMo_xW_{12-x}O_{40}]^{3-}$ (x = 1~10), which was revealed by their ^{31}P NMR spectra as demonstrated in Fig. 1–1 [24]. "α-$(NBu^n_4)_3[PMo_6W_6O_{40}]$" prepared

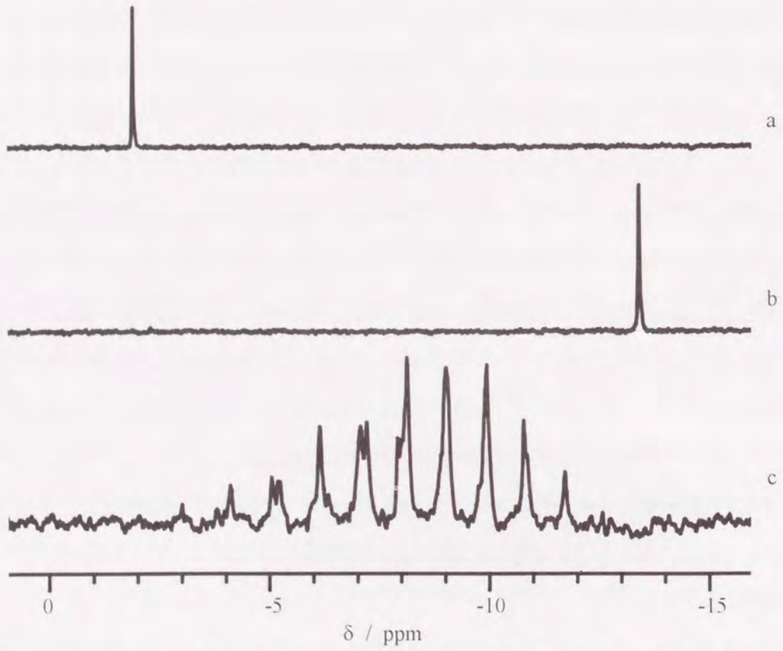

Figure 1–1. ^{31}P NMR spectra of α-$(NBu^n_4)_3[PMo_{12}O_{40}]$ (a), α-$(NBu^n_4)_3[PW_{12}O_{40}]$ (b), and "α-$(NBu^n_4)_3[PMo_6W_6O_{40}]$" prepared by the condensation of Na_2HPO_4, $6Na_2MoO_4$, and $6Na_2WO_4$ (c) measured in acetonitrile-d_3.

by an equimolar mixture of Na_2MoO_4 and Na_2WO_4 shows mainly ten ^{31}P NMR signals observed with about 1 ppm intervals at the region between those of α-$(NBu^n_4)_3[PW_{12}O_{40}]$ and α-$(NBu^n_4)_3[PMo_{12}O_{40}]$. Therefore, each of the eleven signals is considered to be derived from α-$(NBu^n_4)_3[PMo_xW_{12-x}O_{40}]$ (x = 1, 2, 3, ····, 10). Furthermore, in contrast to the single, sharp signals of α-$(NBu^n_4)_3[PW_{12}O_{40}]$ and α-$(NBu^n_4)_3[PMo_{12}O_{40}]$, each signal is broadened and split, which suggests the existence of positional isomers [8, 9] having a unique Mo/W composition. It was pointed out that direct syntheses of mixed addenda heteropolyanions from respective, constitutive oxometalates are liable to lead to mixtures of isomers based on their ^{31}P NMR spectra [6, 7].

All of the vanadium-, niobium-, and molybdenum-trisubstituted dodecatungstophosphate anion salts prepared by using A-$Na_9[PW_9O_{34}]$ as a precursor also showed IR spectral patterns characteristic of the Keggin-type structure. The typical, representative spectra of A-β-$(NBu^n_4)_4H_2[PV_3W_9O_{40}]$ and A-α-$(NBu^n_4)_4H_2[PV_3W_9O_{40}]$ are shown in Fig. 1–2. In the region of 1200–600 cm^{-1}, both the compounds show four major bands: they are assigned to P–O_i (O_i band) [25], M=O_t (terminal oxygen, O_t band, M = V and W), M–O_{bc}–M (corner-sharing oxygen, O_{bc} band), and M–O_{be}–M (edge-sharing oxygen, O_{be} band) stretching modes on the analogy of the assignments of the Keggin-type polyanions [23]. The distinctions between the spectra of these α- and β-isomers are as follows. First, A-α-$(NBu^n_4)_4H_2[PV_3W_9O_{40}]$ develops well-separated O_{bc} (883 cm^{-1}) and O_{be} (805 cm^{-1}) bands, while the O_{bc} band (880 cm^{-1}) of A-β-$(NBu^n_4)_4H_2[PV_3W_9O_{40}]$ is weak and obscured by the broad O_{be} band (805 cm^{-1}). Second, the O_i band of the β-isomer (1077 cm^{-1}) appears in the lower frequency region compared with that of the α-isomer (1086 cm^{-1}). Third, in a lower frequency region (500–300 cm^{-1}), a strong band is observed for the α-isomer (382 cm^{-1}), and three broad ones for the β-isomer (406, 374, and 328 cm^{-1}). These findings are in good agreement with the spectral behavior characteristic of α- and β-isomers of $[XM_{12}O_{40}]^{n-}$ polyanions (X = P, Si, Ge, and As; M = Mo and W) [23]. The other vanadium-, niobium-, and

molybdenum-trisubstituted dodecatungstophosphate anion salts also showed the similar IR spectral patterns characteristic of the α- and β-isomers. The wave numbers of the IR bands of these isomers are summarized in Table 1–1.

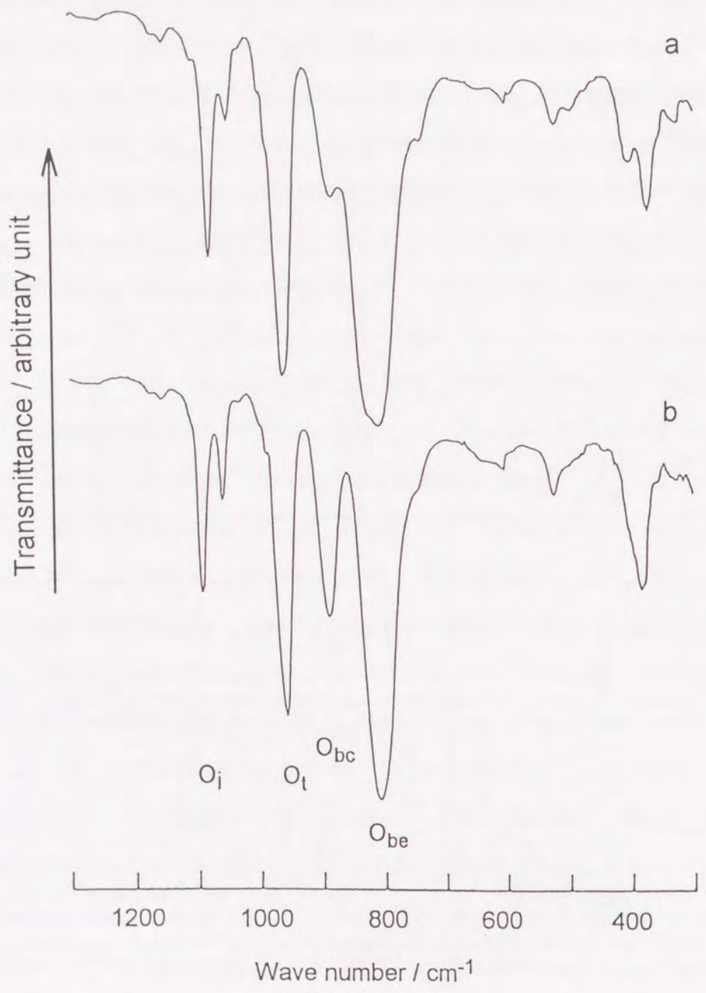

Figure 1–2. IR spectra of A-β-$(NBu^n_4)_4H_2[PV_3W_9O_{40}]$ (a) and A-α-$(NBu^n_4)_4H_2[PV_3W_9O_{40}]$ (b) in KBr pellets.

Table 1–1. Wave Numbers (cm^{-1}) of the Relevant IR Bands[a] of Metal-Trisubstituted Dodecatungstophosphate Anion Salts

Salt	Stretching Mode			
	P–O_i	M=O_t	M–O_{bc}–M	M–O_{be}–M
A-β-$Cs_{5.4}H_{0.6}[PV_3W_9O_{40}]$	1074	962	—[b]	806
A-β-$(NBu^n_4)_4H_2[PV_3W_9O_{40}]$	1077	959	880 (w)	805
A-β-$(NBu^n_4)_6[PV_3W_9O_{40}]$	1077	950	882 (w)	806
A-α-$Cs_6[PV_3W_9O_{40}]$	1086	956	874	801
A-α-$(NBu^n_4)_4H_2[PV_3W_9O_{40}]$	1086	954	883	805
A-β-$Cs_6[PNb_3W_9O_{40}]$	1045	959	—[b]	813
A-β-$(NBu^n_4)_5H[PNb_3W_9O_{40}]$	1045	955	876 (w)	815
A-α-$Cs_6[PNb_3W_9O_{40}]$	1050	964	887	797
A-α-$(NBu^n_4)_5H[PNb_3W_9O_{40}]$	1054	959	890	808
A-β-$K_3[PMo_3W_9O_{40}]$	1070	973	880 (w)	817
A-β-$(NMe_4)_3[PMo_3W_9O_{40}]$	1070	970	882	825
A-β-$(NBu^n_4)_3[PMo_3W_9O_{40}]$	1070	975	875 (sh)	804

a) w, weak; sh, shoulder.
b) Obscured as a shoulder band of the O_{be} band.

All of these metal-trisubstituted dodecatungstophosphate anion salts showed single, sharp ^{31}P NMR signals as summarized in Table 1–2, in contrast to the multiplet signals of "α-$(NBu^n_4)_3[PMo_6W_6O_{40}]$" as shown in Fig. 1–1(c). This indicates these salts consist of a single species of the mixed addenda heteropolyanion, and neither mixtures containing a species with different composition of the addenda atoms or positional isomers of the substituted metal atom. The signals of the α-isomers of vanadium- and niobium-trisubstituted dodecatungstophosphate anion salts are observed at about 1 ppm higher field compared with those of the corresponding β-isomers, suggesting these salts are not mixtures of geometrical isomers. The signal of the α- or β-isomer of $(NBu^n_4)_4H_2[PV_3W_9O_{40}]$ is observed at higher field compared with that of the cesium salt of the corresponding isomer.

Similar differences of the ^{31}P NMR signals are also observed for the α- and β-isomers of $[PNb_3W_9O_{40}]^{6-}$ anion salts. These observations are ascribable to protonation of the $[PM_3W_9O_{40}]^{6-}$ (M = V and Nb) anions, as discussed later.

Table 1–2. ^{31}P NMR Chemical Shifts of Metal-Trisubstituted Dodecatungstophosphate Anion Salts

Salt	Solvent[a)]	Chemical Shift[b)]
A-β-$Cs_{5.4}H_{0.6}[PV_3W_9O_{40}]$	D_2O	−10.98
A-β-$(NBu^n_4)_4H_2[PV_3W_9O_{40}]$	wet CD_3CN	−11.42
A-β-$(NBu^n_4)_6[PV_3W_9O_{40}]$	wet CD_3CN	−10.90
A-α-$Cs_6[PV_3W_9O_{40}]$	D_2O	−11.66
A-α-$(NBu^n_4)_4H_2[PV_3W_9O_{40}]$	wet CD_3CN	−12.64
A-β-$Cs_6[PNb_3W_9O_{40}]$	D_2O	−7.07
A-β-$(NBu^n_4)_5H[PNb_3W_9O_{40}]$	wet CD_3CN	−7.95
A-α-$Cs_6[PNb_3W_9O_{40}]$	D_2O	−8.22
A-α-$(NBu^n_4)_5H[PNb_3W_9O_{40}]$	wet CD_3CN	−9.01
A-β-$K_3[PMo_3W_9O_{40}]$	CD_3OD	−11.43
A-β-$(NMe_4)_3[PMo_3W_9O_{40}]$	CD_3CN	−10.03
A-β-$(NBu^n_4)_3[PMo_3W_9O_{40}]$	CD_3CN	−10.03

a) About 100 equivalent amounts of H_2O to the salt were added in the wet acetonitrile-d_3.
b) Negative values in ppm upfield from 85%H_3PO_4.

The ^{183}W NMR spectrum of A-β-$K_3[PMo_3W_9O_{40}]$ in methanol-d_4 shows two sharp peaks at −93.9 and −105.2 ppm with integrated intensities in the ratio 1:2, as depicted in Fig. 1–3. Both of them are observed as doublets by the spin-spin coupling with the ^{31}P nucleus ($^2J_{W-O-P}$ = 1.5 and 1.0 Hz, respectively). Furthermore, both the signals have satellites due to the reciprocal $^2J_{W-O-W}$ coupling of 21.0 and 15.6 Hz, respectively. It was reported that the magnitude of the $^2J_{W-O-W}$ coupling constant varied with the W–O–W

bond angle [26]. The $W-O_{be}-W$ angles within the same W_3O_{13} triplet are smaller than the $W-O_{bc}-W$ angles between the different W_3O_{13} triplets, therefore, $^2J_{W-O_{be}-W}$ coupling constants (5–12 Hz) are distinguishably smaller than $^2J_{W-O_{bc}-W}$ ones (15–30 Hz) [11, 13]. These findings were applied to the structural characterization of some polyoxotungstate anions [27–29], especially, A- and B-type positional isomers of metal-trisubstituted dodecatungsto heteropolyanions [11, 13]. The present compound exhibits the larger $^2J_{W-O-W}$ coupling constants, which suggests that two kinds of W atoms are linked together through the corner-sharing O_{bc} atoms, that is, this molybdenum-trisubstituted dodecatungstophosphate anion is an A-type positional isomer. Consequently, the signal at the lower field in Fig. 1–3 can be assigned to the three "cap" W atoms in the rotated, trigonal edge-shared W_3O_{13} triplet and the other to the six "belt" W atoms adjacent to both the "cap"

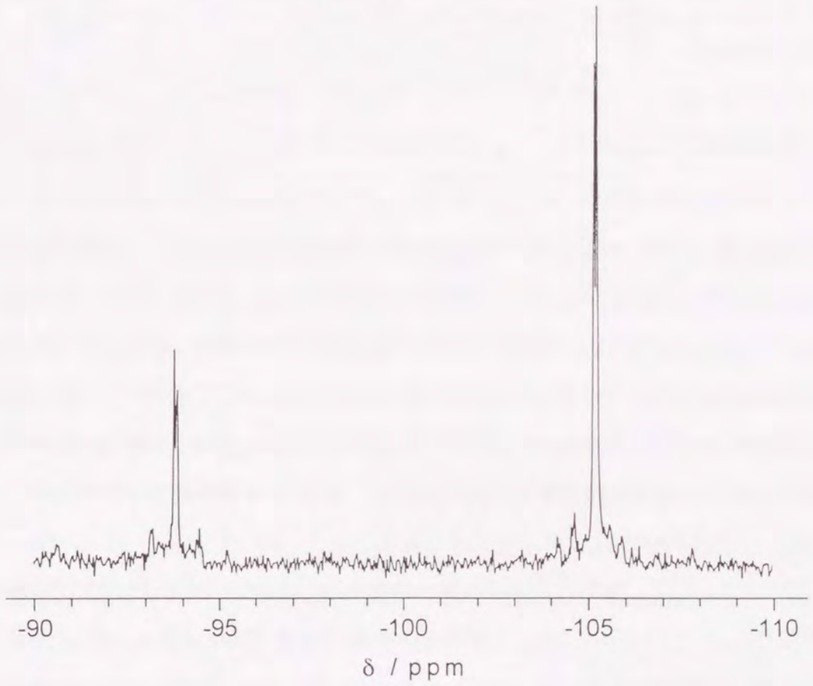

Figure 1–3. ^{183}W NMR spectrum of A-β-$K_3[PMo_3W_9O_{40}]$ in methanol-d_4.

W and Mo atoms. A-β-$(NMe_4)_3[PMo_3W_9O_{40}]$ and A-β-$(NBu^n_4)_3[PMo_3W_9O_{40}]$ in acetonitrile-d_3 showed the similar ^{183}W NMR spectral patterns, although the satellites due to the $^2J_{W-O-W}$ coupling were obscured. The parameters are summarized in Table 1–3.

Table 1–3. ^{183}W NMR Parameters of A-β-$[PMo_3W_9O_{40}]^{3-}$ Anion Salts

Salt	Solvent	δ (ppm)	$^2J_{W-O-P}$ (Hz)	$^2J_{W-O-W}$ (Hz)
A-β-$K_3[PMo_3W_9O_{40}]$	CD_3OD	−93.9	1.5	21.0
		−105.2	1.0	15.6
A-β-$(NMe_4)_3[PMo_3W_9O_{40}]$	CD_3CN	−91.4	1.5	—a)
		−101.5	1.0	—a)
A-β-$(NBu^n_4)_3[PMo_3W_9O_{40}]$	CD_3CN	−91.1	1.5	—a)
		−101.3	1.5	—a)

a) Not resolved.

The reaction solution for the condensation of $NaVO_3$ and A-$Na_9[PW_9O_{34}]$ as described for the preparation of A-β-$Cs_{5.4}H_{0.6}[PV_3W_9O_{40}]$ in the experimental section using deuterium oxide instead of water showed only a single, sharp ^{31}P NMR signal at −11.65 ppm and two ^{183}W NMR signals at −106.7 and −117.9 ppm with integrated intensities in the ratio 1:2. The ^{183}W NMR spectral pattern was similar to that of A-β-$K_3[PMo_3W_9O_{40}]$ described above. The lower field signal assignable to the three "cap" W atoms showed satellites due to the spin-spin coupling ($^2J_{W-O_{bc}-W}$ = ca. 16 Hz), although the higher field signal assignable to the six "belt" W atoms was broadened by the quadrupolar influence of the ^{51}V nuclei.

The ^{31}P, ^{51}V, and ^{183}W NMR spectra of A-β-$(NBu^n_4)_4H_2[PV_3W_9O_{40}]$ in acetonitrile-d_3 vary with amounts of added water, as demonstrated in Fig. 1–4. The broad ^{183}W NMR resonance in dry acetonitrile-d_3 is gradually transformed to the two peaks with addition of water. With 100 equivalent amounts of water, two sharp signals are observed at −99.4 and −107.6 ppm with integrated intensities in the ratio 1:2, which are similar to the

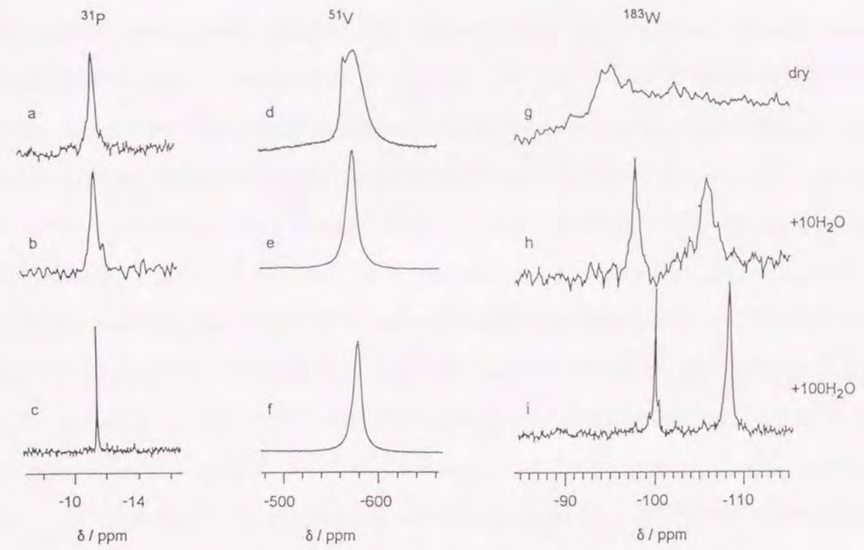

Figure 1–4. ^{31}P (a, b, c), ^{51}V (d, e, f), and ^{183}W NMR spectra (g, h, i) of A-β-$(NBu^n_4)_4H_2[PV_3W_9O_{40}]$ in acetonitrile-d_3. The amount of added water is 0 (a, d, g), 10 (b, e, h), and 100 equivalent (c, f, i) of water to the salt.

signals observed for the reaction solution. The lower field signal shows unambiguous spin-spin coupling satellites ($^2J_{W-O_{bc}-W}$ = 18.1 Hz). The value of the coupling constant agrees with those observed for pairs of tungsten atoms via the corner-sharing oxygen atom as described above. Concomitantly, the broad ^{51}V NMR resonance consisting of two or more components in dry acetonitrile-d_3 is transformed to a single, broad signal (−574.6 ppm) with 10 equivalent amounts of water. In the ^{31}P NMR spectra, the broad signal (−11.64 ppm) in dry acetonitrile-d_3 is also sharpened and shifted to a lower field with addition of water. These results indicate that the bridging oxygen atoms of A-β-$(NBu^n_4)_4H_2[PV_3W_9O_{40}]$ are protonated, as observed for A-β-$(NBu^n_4)_4H_3[SiV_3W_9O_{40}]$ [13]. In dry acetonitrile-d_3, the protonation site is rather localized on the NMR time scales and the C_{3V} symmetry for the naked A-β-$[PV_3W_9O_{40}]^{6-}$ anion is lowered, leading to broadening of ^{31}P, ^{51}V, and ^{183}W

NMR signals of A-β-$(NBu^n_4)_4H_2[PV_3W_9O_{40}]$. The presence of water accelerates the exchange process between the protonation sites of the bridging oxygen atoms. Hence, the A-β-$[H_2PV_3W_9O_{40}]^{4-}$ anion is observed as a species having overall average C_{3v} symmetry.

A-β-$(NBu^n_4)_4H_2[PV_3W_9O_{40}]$ was deprotonated in acetonitrile by addition of two equivalent amounts of NBu^n_4OH. The obtained salt of A-β-$(NBu^n_4)_6[PV_3W_9O_{40}]$ afforded a single, sharp ^{31}P NMR signal at −10.90 ppm in wet acetonitrile-d_3 (about 100 equivalent amounts of water to the salt added). Furthermore, upon the reaction of A-β-$(NBu^n_4)_4H_2[PV_3W_9O_{40}]$ with three equivalent amounts of NBu^n_4OH, the product gave the same ^{31}P NMR signal as that of A-β-$(NBu^n_4)_6[PV_3W_9O_{40}]$. Therefore, the fully deprotonated A-β-$(NBu^n_4)_6[PV_3W_9O_{40}]$ salt did not decompose in the presence of additional OH^-. The distinction between the ^{31}P NMR resonances of A-β-$(NBu^n_4)_4H_2[PV_3W_9O_{40}]$ (−11.42 ppm) and of A-β-$(NBu^n_4)_6[PV_3W_9O_{40}]$ (−10.90 ppm) is assumed to reflect the structural difference between these polyanions; the polyanion moiety of A-β-$(NBu^n_4)_4H_2[PV_3W_9O_{40}]$ is protonated.

1.4 Conclusion

The vanadium-, niobium-, and molybdenum-trisubstituted dodecatungstophosphate anion salts were prepared by using A-$Na_9[PW_9O_{34}]$ as a precursor and they were found to be single species of the α- or β-isomers of A-type metal-trisubstituted ones, A-$[PM_3W_9O_{40}]^{n-}$ (M = V and Nb, n = 6; M = Mo, n = 3), by their IR, ^{31}P and ^{183}W NMR spectroscopic properties. The protonation of the $[PM_3W_9O_{40}]^{6-}$ (M = V and Nb) anions was also suggested by their NMR spectral behavior.

The present compounds are the first examples containing a β-isomer of an A-type PW_9 unit. To obtain these β-isomers the addition of 1,4-dioxane to the condensation solution is indispensable, because the isomerization of the mixed addenda polyanion from a β-form to an α-one would be depressed in a mixture of aqueous and organic solutions, as described for the synthesis of β-$[SiW_{12}O_{40}]^{4-}$ anion [30]. In contrast, by using the same precursor and the

different conditions of condensation, the corresponding α-isomers, A-α-$[PM_3W_9O_{40}]^{6-}$ (M = V and Nb) anion salts, were successfully obtained. Taking into consideration that the β-isomer of the Keggin-type polyanion is generally unstable and tends to isomerize to the corresponding α-one as described in chapter 3, the present A-type trivacant lacunary precursor, A-$Na_9[PW_9O_{34}]$, is suggested to be a β-isomer.

1.5 References

1 M. Misono, *Proc. Int. Conf. Chem. Uses Molybdenum, 4th*, **1982**, 289.

2 K. Nomiya, H. Saijoh, and M. Miwa, *Bull. Chem. Soc. Jpn.*, **53**, 3719 (1980).

3 R. G. Finke, B. Rapko, and T. J. R. Weakley, *Inorg. Chem.*, **28**, 1573 (1989), and references therein.

4 J. K. Burdett and C. K. Nguyen, *J. Am. Chem. Soc.*, **112**, 5366 (1990), and references therein.

5 E. Cadot, R. Thouvenot, A. Tézé, and G. Hervé, *Inorg. Chem.*, **31**, 4128 (1992).

6 W. H. Knoth, *J. Am. Chem. Soc.*, **101**, 759 (1979).

7 J. Canny, A. Tézé, R. Thouvenot, and G. Hervé, *Inorg. Chem.*, **25**, 2114 (1986).

8 M. T. Pope, "Heteropoly and Isopoly Oxometalates", Springer-Verlag, Berlin, p.27 (1983).

9 M. T. Pope and T. F. Scully, *Inorg. Chem.*, **14**, 953 (1975).

10 L. C. W. Baker and J. S. Figgis, *J. Am. Chem. Soc.*, **92**, 3794 (1970).

11 P. J. Domaille, *J. Am. Chem. Soc.*, **106**, 7677 (1984).

12 R. G. Finke and M. W. Droege, *J. Am. Chem. Soc.*, **106**, 7274 (1984).

13 R. G. Finke, B. Rapko, R. J. Saxton, and P. J. Domaille, *J. Am. Chem. Soc.*, **108**, 2947 (1986).

14 M. M. Mossoba, C. J. O'Connor, M. T. Pope, E. Sinn, G. Hervé, and A. Tézé, *J. Am. Chem. Soc.*, **102**, 6866 (1980).

15 F. Robert and A. Tézé, *Acta Crystallogr., Sect. B*, **37B**, 318 (1981).

16 P. J. Domaille and G. Watunya, *Inorg. Chem.*, **25**, 1239 (1986).

17 R. G. Finke, K. Nomiya, C. A. Green, and M. W. Droege, *Inorg. Synth.*, **29**, 239 (1992).

18 P. J. Domaille, *Inorg. Synth.*, **27**, 96 (1990).

19 M. A. Leparulo-Loftus and M. T. Pope, *Inorg. Chem.*, **26**, 2112 (1987).

20 J. C. Bailar, Jr., *Inorg. Synth.*, **1**, 132 (1939).

21 J. J. Altenau, M. T. Pope, R. A. Prados, and H. So, *Inorg. Chem.*, **14**, 417 (1975).

22 M. Misono, N. Mizuno, K. Katamura, A. Kasai, Y. Konishi, K. Sakata, T. Okuhara, and Y. Yoneda, *Bull. Chem. Soc. Jpn.*, **55**, 400 (1982).

23 C. Rocchiccioli-Deltcheff, R. Thouvenot, and R. Franck, *Spectrochim. Acta, Part A*, **32**, 587 (1976); C. Rocchiccioli-Deltcheff, M. Fournier, R. Franck, and R. Thouvenot, *Inorg. Chem.*, **22**, 207 (1983); R. Thouvenot, M. Fournier, R. Franck, and C. Rocchiccioli-Deltcheff, *Inorg. Chem.*, **23**, 598 (1984).

24 I. Kawafune and G. Matsubayashi, *Kagaku To Kogyo (Osaka)*, **67**, 94 (1993).

25 The oxygen atoms of the Keggin-type anion are classified into four species, O_i, O_t, O_{bc}, and O_{be}, as described in General Introduction.

26 J. Lefebvre, F. Chauveau, P. Doppelt, and C. Brevard, *J. Am. Chem. Soc.*, **103**, 4589 (1981).

27 W. H. Knoth, P. J. Domaille, and D. C. Roe, *Inorg. Chem.*, **22**, 198 (1983).

28 P. J. Domaille and W. H. Knoth, *Inorg. Chem.*, **22**, 818 (1983).

29 C. Brevard, R. Schimpf, G. Tourne, and C. M. Tourne, *J. Am. Chem. Soc.*, **105**, 7059 (1983).

30 K. Yamamura and Y. Sasaki, *J. Chem. Soc., Chem. Commun.*, **1973**, 648; K. Y. Matsumoto, A. Kobayashi, and Y. Sasaki, *Bull. Chem. Soc. Jpn.*, **48**, 3146 (1975).

Chapter 2

Crystal Structures of the β-Isomers of the A-Type Vanadium-, Niobium-, and Molybdenum-Trisubstituted Dodecatungstophosphate Anion Salts

2.1 Introduction

Mixed addenda heteropolyoxometalates have attracted much attention from the viewpoints of catalyst-support materials [1] and magnetic characteristics having interactions between different metals [2], as well as fundamental structural chemistry [3, 4] and their inherent catalytic activities [5–11]. Of primary importance in these fields is an acquisition of the precise structure of the heteropolyanion, including the positional isomerism [12] of the different metal atoms as well as the geometrical isomerism [13], as described in chapter 1. As for the partially substituted heteropolytungstates, their structures in solution, especially the location of the substituted metal atoms, have been confirmed in detail by multinuclear (^{29}Si, ^{31}P, ^{51}V, and ^{183}W) NMR spectroscopies [3, 14–16]. In the solid states, on the other hand, these substituted metal atoms are susceptible to disordered arrangements [17–20] and, hence, only a few mixed addenda heteropolyanions of the Keggin type have been structurally clarified by a single-crystal X-ray analysis, the sites of the different addenda atoms having been determined [21–26].

In this chapter, the structures of vanadium-, niobium-, and molybdenum-trisubstituted dodecatungstophosphate anion salts were clarified by single-crystal X-ray analyses as A-type metal-trisubstituted, geometrical β-isomers, A-β-$Cs_{5.4}H_{0.6}[PV_3W_9O_{40}]$, A-β-$Cs_6[PNb_3W_9O_{40}]$, and A-β-$(NMe_4)_3[PMo_3W_9O_{40}]$. These are the first X-ray structural determinations for a heteropolyanion containing a β-isomer of an A-type PW_9 unit in contrast to an α-isomer of an A-PW_9 unit observed for some tungstodiphosphates [27–31]. The β-isomer of the Keggin-type polyanion is generally unstable compared with the corresponding α-one and structural determinations of the β-isomers by single-crystal X-ray analyses have been limited; β_1-$[SiMoW_{11}O_{40}]^{4-}$ [17], β-$[SiW_{12}O_{40}]^{4-}$ [32, 33], and β-$[PMo_{12}O_{40}]^{7-}$

[34]. Furthermore, the positional parameters of the cesium cations of A-β-$Cs_{5.4}H_{0.6}[PV_3W_9O_{40}]$ afford important information concerning protonation to the $[PV_3W_9O_{40}]^{6-}$ anion.

2.2 Experimental

Materials. Preparations of the crystals of the vanadium-, niobium-, and molybdenum-trisubstituted dodecatungstophosphate anion salts were described in chapter 1.

X-Ray Crystal Structure Determination. A-β-$Cs_{5.4}H_{0.6}[PV_3W_9O_{40}]\cdot 12H_2O$. Intensity data were collected on a Rigaku AFC-7R four-circle diffractometer with graphite-monochromated MoKα (λ = 0.71069 Å) radiation, at the Faculty of Science, Osaka University. The crystallographic data are summarized in Table 2–1. The unit-cell parameters were determined from 18 independent reflections with 2θ over the range of 21.9–27.6°. Three standard reflections were monitored after the collection of 150 reflections. No significant decays in their intensities (maximum 8.2%) were observed throughout the data collection. The reflection data were corrected for Lorentz and polarization effects, together with absorption (transmission factors, 0.273–0.999) [35].

The structure was solved by the direct method (SHELXS86) [36] and refined by a full-matrix least-squares technique. The function $\Sigma w(|F_o|-|F_c|)^2$ with $w = (\sigma^2(F_o) + 0.0009F_o^2)^{-1}$ was minimized for the refinement. All of the non-hydrogen atoms, except for O(13) of the polyanion (see Fig. 2–1) and one oxygen atom (O(30)) of eight water molecules, were refined anisotropically. Although the thermogravimetric analysis determined twelve water molecules for this complex molecule as described in chapter 1, eight oxygen atoms of water were clarified from the D-Fourier maps. The positions of the hydrogen atoms were not determined. Since the Cs(4) atom on a mirror plane afforded a very large B_{eq} (about 15 Å^2) compared with those (3.40–6.79 Å^2) of the other Cs atoms, the occupancy factor was refined to be reduced to 0.2. Thus, the counter cations are considered to be $(Cs^+)_{5.4}(H^+)_{0.6}$. Although numerous large peaks (up to 3.15 e Å^{-3}) near to the Cs

Table 2–1. Crystallographic Data

	A-β-$Cs_{5.4}H_{0.6}$-$[PV_3W_9O_{40}]\cdot 12H_2O$	A-β-Cs_6-$[PNb_3W_9O_{40}]\cdot 14H_2O$	A-β-$(NMe_4)_3$-$[PMo_3W_9O_{40}]$
Formula	$H_{24.6}Cs_{5.4}O_{52}PV_3W_9$	$H_{28}Cs_6O_{54}PNb_3W_9$	$C_{12}H_{36}N_3O_{40}PMo_3W_9$
Formula weight	3412.9	3654.0	2835.9
Crystal size / mm	0.2 × 0.1 × 0.3	0.2 × 0.2 × 0.4	0.4 × 0.45 × 0.7
Crystal system	Orthorhombic	Monoclinic	Orthorhombic
Space group	*Pbcm* (No. 57)	$P2_1/c$ (No.13)	$Pmn2_1$ (No.31)
a / Å	13.648(4)	16.865(4)	13.844(10)
b / Å	21.417(2)	13.577(4)	12.871(10)
c / Å	16.742(2)	22.240(5)	14.687(13)
β / °	——	92.26(2)	——
V / Å^3	4893(1)	5088(2)	2617(3)
Z	4	4	2
D_{calc} / g cm^{-3}	4.632	4.769	3.598
F(000)	5950.4	6376	2512
μ(MoKα) / mm^{-1}	27.0	26.5	20.5
T / °C	23	23	23
Scan range 2θ / °	3–60	3–5	6–55
Scan width Δω / °	1.00 + 0.35tanθ	1.05 + 0.35tanθ	1.63 + 0.30tanθ
Scan speed ω / ° min^{-1}	16 (3° < 2θ < 50°) and 8 (50° ≤ 2θ ≤ 60°)	32	16
Scan mode	ω–2θ	ω–2θ	ω–2θ
Number of unique reflections	7844	9726	3397
Number of reflections with $I > 3\sigma(I)$	4123	5432	2148
R	0.046	0.071	0.091
R_W	0.060	0.079	0.095

and W atoms (0.8–1.2 Å) were contained on the D-Fourier map, they were ignored because they make no chemical sense. Calculations were performed with the TEXSAN structure analysis software [37] on an IRIS INDIGO workstation at the Faculty of Science, Osaka University. The atomic-scattering factors were taken from the usual sources [38]. The

final positional parameters for non-hydrogen atoms are listed in Table 2–2. Figures 2–1 and 2–4 were drawn with a local version of ORTEP II [39].

A-β-$Cs_6[PNb_3W_9O_{40}]\cdot 14H_2O$ Intensity data were collected on a Rigaku AFC-7R four-circle diffractometer with graphite-monochromated MoKα (λ = 0.71069 Å) radiation, at the Faculty of Science, Osaka University. The crystallographic data are also summarized in Table 2–1. The unit-cell parameters were determined from 20 independent reflections with 2θ over the range of 8.47–11.75°. Three standard reflections were monitored after the collection of 150 reflections. No significant decays in their intensities (maximum 12.7%) were observed throughout the data collection. The reflection data were corrected for Lorentz and polarization effects, together with absorption (transmission factors, 0.128–1.000) [35].

The structure was solved by the direct method (SHELXS86) [36] and refined by a full-matrix least-squares technique assuming anisotropic thermal parameters for the P, Nb and W atoms and isotropic ones for the Cs and O atoms. The function $\Sigma w(|F_o|-|F_c|)^2$ with $w = (\sigma^2(F_o) + 0.0009F_o^2)^{-1}$ was minimized for the refinement. Although the thermogravimetric analysis determined fourteen water molecules for this complex molecule as described in chapter 1, eight oxygen atoms of water were clarified from the D-Fourier maps. The positions of the hydrogen atoms were not determined. Calculations were performed with the TEXSAN structure analysis software [37] on an IRIS INDIGO workstation at the Faculty of Science, Osaka University. The atomic-scattering factors were taken from the usual sources [38]. The final positional parameters for non-hydrogen atoms are listed in Table 2–3. The terminal oxygen atoms bound to the Nb atoms were disordered in two positions (O(10)/O(11), O(12)/O(13), and O(14)/O(15)); their occupancy factors were also summarized in Table 2–3. One of the Cs atom was disordered in two positions (Cs(3)/Cs(8)), which were also disordered with the oxygen atoms of water molecules respectively (Cs(3)/O(58) and Cs(8)/O(57)) ; their occupancy factors were also summarized in Table 2–3. Figures 2–2 was drawn with a local version of ORTEP II [39].

Table 2–2. Atomic Coordinates and B_{eq} of A-β-$Cs_{5.4}H_{0.6}[PV_3W_9O_{40}]\cdot 12H_2O$

Atom	x	y	z	B_{eq} / Å^2
W(1)	0.05965(6)	0.03222(3)	0.13790(5)	1.51(1)
W(2)	0.24924(7)	0.08979(3)	0.03766(4)	1.65(1)
W(3)	0.46549(6)	0.15244(3)	0.15019(5)	1.53(1)
W(4)	0.09900(6)	0.20216(3)	0.14820(4)	1.40(1)
W(5)	0.29472(8)	0.26045(4)	0.25	1.38(2)
Cs(1)	0.4821(1)	0.14953(8)	0.59724(10)	3.40(3)
Cs(2)	0.8900(2)	0.1440(1)	0.5013(2)	6.79(6)
Cs(3)	0.2040(2)	0.0355(2)	0.75	5.96(8)
Cs(4)	0.9101(5)	0.1587(3)	0.75	5.2(2)
V(1)	0.2775(2)	−0.0437(1)	0.1424(2)	1.66(6)
V(2)	0.4808(3)	0.0161(2)	0.25	1.63(8)
P(1)	0.2541(5)	0.0979(3)	0.25	1.1(1)
O(1)	−0.055(1)	0.0104(6)	0.1043(9)	2.1(3)
O(2)	0.267(1)	0.1040(7)	−0.0620(9)	2.7(3)
O(3)	0.545(1)	0.1863(7)	0.0847(9)	2.8(3)
O(4)	0.042(1)	0.0231(7)	0.25	1.5(3)
O(5)	0.1166(9)	0.0638(6)	0.0411(8)	1.8(3)
O(6)	0.3709(10)	0.1186(6)	0.0778(8)	1.7(3)
O(7)	0.521(1)	0.1777(9)	0.25	1.6(3)
O(8)	0.2213(9)	0.0618(5)	0.1753(8)	1.4(2)
O(9)	0.365(1)	0.1043(7)	0.25	1.3(3)
O(10)	0.0398(10)	0.1218(5)	0.1539(8)	1.8(2)
O(11)	0.1931(10)	0.1679(5)	0.0769(8)	1.6(2)
O(12)	0.3752(10)	0.2208(6)	0.1724(8)	1.8(2)
O(13)	0.210(1)	0.1633(6)	0.25	0.9(2)
O(14)	0.020(1)	0.2416(6)	0.0870(9)	2.6(3)
O(15)	0.340(1)	0.3337(7)	0.25	1.5(3)
O(16)	0.044(1)	0.2229(7)	0.25	1.0(3)
O(17)	0.195(1)	0.2674(5)	0.1707(8)	1.8(3)
O(18)	0.133(1)	−0.0383(5)	0.1280(8)	1.8(2)
O(19)	0.2869(10)	0.0073(5)	0.0464(8)	1.7(2)
O(20)	0.5209(10)	0.0744(6)	0.1690(8)	1.8(3)
O(21)	0.246(2)	−0.0627(8)	0.25	2.4(4)
O(22)	0.396(1)	−0.0191(6)	0.1747(9)	2.4(3)
O(23)	0.294(1)	−0.1105(6)	0.1028(10)	2.6(3)
O(24)	0.571(1)	−0.0307(8)	0.25	2.4(4)
O(25)	0.345(2)	0.25	0.5	2.9(5)
O(26)	1.069(1)	0.1220(7)	0.632(1)	5.0(5)
O(27)	0.598(2)	0.197(1)	0.75	4.8(7)
O(28)	0.718(1)	0.055(1)	0.112(1)	5.7(6)
O(29)	0.5	0	0	6.4(9)
O(30)	0.839(4)	0.132(2)	0.25	10.5(8)

Table 2–3. Atomic Coordinates and B_{eq} of A-β-$Cs_6[PNb_3W_9O_{40}]\cdot 14H_2O$

Atom	x	y	z	B_{eq} / Å^2	occupancy
W(1)	0.85303(9)	0.4111(1)	0.19489(6)	2.82(3)	
W(2)	0.74872(9)	0.2185(1)	0.24985(6)	2.70(3)	
W(3)	0.65122(9)	0.4175(1)	0.18950(6)	2.79(3)	
W(4)	0.96158(9)	0.2516(1)	0.09328(6)	2.94(3)	
W(5)	0.84235(9)	0.0386(1)	0.15072(6)	2.83(3)	
W(6)	0.64167(9)	0.0488(1)	0.14748(6)	2.81(3)	
W(7)	0.53736(9)	0.2692(1)	0.07824(6)	2.92(3)	
W(8)	0.64334(9)	0.4611(1)	0.02715(6)	2.87(3)	
W(9)	0.86660(9)	0.4476(1)	0.03182(6)	2.78(3)	
Cs(1)	0.3977(2)	0.0470(2)	0.1468(1)	4.70(7)	
Cs(2)	0.0979(2)	0.0181(2)	0.1591(1)	4.81(7)	
Cs(3)	0.5990(3)	0.2280(4)	0.5910(2)	6.10(9)	0.773
Cs(4)	0.4149(2)	0.4761(3)	0.1450(1)	6.38(9)	
Cs(5)	0.0257(3)	0.4131(6)	0.6468(2)	10.8(2)	0.609
Cs(6)	0.2284(4)	0.3025(5)	0.0539(3)	6.9(2)	0.391
Cs(7)	0.8723(6)	0.2167(7)	0.5255(5)	4.8(2)	
Cs(8)	0.5711	0.242	0.7272	6.10	0.227
Nb(1)	0.8596(2)	0.2244(3)	−0.0450(1)	3.05(7)	
Nb(2)	0.7371(2)	0.0196(3)	0.0122(1)	3.10(7)	
Nb(3)	0.6391(2)	0.2426(3)	−0.0541(1)	3.13(7)	
P(1)	0.7480(5)	0.2538(7)	0.0890(4)	2.3(2)	
O(1)	0.916(1)	0.489(2)	0.2325(10)	3.1(5)	
O(2)	0.748(1)	0.180(2)	0.323(1)	3.6(5)	
O(3)	0.588(2)	0.500(2)	0.223(1)	3.7(5)	
O(4)	1.059(2)	0.236(2)	0.112(1)	3.7(5)	
O(5)	0.906(1)	−0.042(2)	0.187(1)	3.4(5)	
O(6)	0.575(1)	−0.025(2)	0.1826(10)	3.4(5)	
O(7)	0.442(2)	0.266(3)	0.089(1)	4.7(6)	
O(8)	0.617(1)	0.577(2)	0.008(1)	3.5(5)	
O(9)	0.906(2)	0.554(3)	0.015(1)	5.5(7)	
O(10)	0.939(5)	0.193(7)	−0.102(3)	5.2	0.403
O(11)	0.869(3)	0.214(4)	−0.131(2)	5.2	0.597
O(12)	0.764(3)	−0.066(4)	−0.052(2)	4.5	0.571
O(13)	0.705(4)	−0.106(6)	−0.018(3)	4.5	0.429
O(14)	0.594(3)	0.181(5)	−0.126(2)	4.1	0.510
O(15)	0.584(3)	0.277(5)	−0.129(2)	4.1	0.490

continued

O(16)	0.827(1)	0.314(2)	0.2561(10)	3.0(5)	
O(17)	0.671(1)	0.327(2)	0.2499(10)	3.1(5)	
O(18)	0.751(1)	0.472(2)	0.2117(9)	2.8(4)	
O(19)	0.915(1)	0.129(2)	0.1214(10)	3.0(5)	
O(20)	0.739(1)	−0.008(2)	0.1742(10)	3.1(5)	
O(21)	0.575(1)	0.145(2)	0.1121(10)	3.2(5)	
O(22)	0.546(1)	0.401(2)	0.053(1)	3.5(5)	
O(23)	0.755(1)	0.467(2)	0.0189(10)	3.0(5)	
O(24)	0.958(1)	0.386(2)	0.066(1)	3.4(5)	
O(25)	0.823(1)	0.104(2)	−0.018(1)	3.4(5)	
O(26)	0.668(1)	0.109(2)	−0.023(1)	3.6(5)	
O(27)	0.746(1)	0.262(2)	−0.065(1)	3.3(5)	
O(28)	0.920(1)	0.313(2)	0.1661(9)	2.9(5)	
O(29)	0.579(1)	0.324(2)	0.1538(9)	2.5(4)	
O(30)	0.749(1)	0.303(2)	0.1521(9)	2.2(4)	
O(31)	0.956(1)	0.215(2)	0.0144(10)	3.2(5)	
O(32)	0.875(1)	0.373(2)	−0.037(1)	3.6(5)	
O(33)	0.629(2)	0.394(2)	−0.043(1)	3.6(5)	
O(34)	0.541(1)	0.236(2)	0.0004(10)	3.3(5)	
O(35)	0.822(1)	0.280(2)	0.0567(9)	2.5(4)	
O(36)	0.675(1)	0.287(2)	0.0496(9)	2.8(4)	
O(37)	0.744(1)	0.142(2)	0.0944(9)	2.5(4)	
O(38)	0.824(1)	0.137(2)	0.2124(10)	3.2(5)	
O(39)	0.667(1)	0.148(2)	0.2086(10)	3.0(5)	
O(40)	0.846(1)	0.468(2)	0.1179(10)	3.0(5)	
O(41)	0.662(2)	0.470(2)	0.112(1)	4.1(6)	
O(42)	0.658(2)	−0.012(2)	0.075(1)	4.5(6)	
O(43)	0.822(1)	−0.020(2)	0.0770(10)	3.0(5)	
O(51)	0.764(2)	0.330(4)	0.618(2)	8(1)	
O(52)	0.122(2)	0.554(3)	0.632(1)	5.8(7)	
O(53)	0.111(2)	0.221(3)	−0.048(1)	2.7(8)	
O(54)	1	0.161(4)	0.25	5.2(10)	1/2
O(55)	0.5	0.184(3)	0.25	4.5(8)	1/2
O(56)	0.264(2)	0.086(3)	0.706(2)	7.1(9)	
O(57)	0.5711(8)	0.242(1)	0.7272(5)	14(1)	0.945
O(58)	0.5990	0.2280	0.5910	14	0.055
O(59)	0.246(3)	0.412(4)	0.658(2)	9(1)	
O(60)	0.236(4)	0.297(6)	0.745(3)	14(1)	

Table 2–4. Atomic Coordinates and B_{eq} of A-β-$(NMe_4)_3[PMo_3W_9O_{40}]$

Atom	x	y	z	B_{eq} / Å^2
W(1)	0.3642(1)	0.4706(1)	0.2681(1)	3.40(3)
W(2)	0.24349(9)	0.3581(1)	0.4396(1)	3.35(3)
W(3)	0.3785(1)	0.2336(1)	0.6313(1)	2.98(3)
W(4)	0.3757(1)	0.5929(1)	0.4897(1)	4.21(4)
W(5)	0.5	0.4798(2)	0.6642(2)	3.51(5)
Mo(1)	0.3691(2)	0.2029(2)	0.2843(2)	1.13(4)
Mo(2)	0.5	0.0816(3)	0.4687(3)	1.78(7)
P(1)	0.5	0.3549(10)	0.448(1)	2.4(2)
O(1)	0.408(2)	0.336(2)	0.384(2)	5.2(6)
O(2)	0.5	0.468(2)	0.499(2)	2.2(6)
O(3)	0.5	0.256(2)	0.505(2)	3.1(6)
O(4)	0.327(3)	0.128(3)	0.205(3)	12(1)
O(5)	0.5	−0.056(2)	0.468(4)	9(1)
O(6)	0.320(2)	0.540(2)	0.178(2)	5.8(7)
O(7)	0.126(2)	0.335(2)	0.465(2)	5.6(6)
O(8)	0.304(2)	0.704(2)	0.494(2)	4.5(6)
O(9)	0.5	0.525(3)	0.771(3)	4.0(7)
O(10)	0.316(2)	0.194(2)	0.706(2)	6.2(7)
O(11)	0.354(2)	0.332(2)	0.211(2)	6.3(7)
O(12)	0.261(2)	0.240(2)	0.357(2)	4.4(6)
O(13)	0.253(2)	0.431(2)	0.334(2)	4.7(6)
O(14)	0.399(1)	0.556(1)	0.602(1)	2.6(4)
O(15)	0.5	0.653(3)	0.456(3)	4.7(8)
O(16)	0.404(3)	0.114(2)	0.553(2)	8.5(9)
O(17)	0.5	0.203(3)	0.679(2)	4.0(8)
O(18)	0.421(3)	0.114(3)	0.390(2)	11(1)
O(19)	0.5	0.218(3)	0.260(3)	5.1(8)
O(20)	0.306(2)	0.280(2)	0.540(2)	4.0(5)
O(21)	0.5	0.452(4)	0.259(4)	10(1)
O(22)	0.380(2)	0.570(2)	0.355(2)	5.1(6)
O(23)	0.285(2)	0.484(2)	0.494(2)	3.7(5)
O(24)	0.403(2)	0.377(2)	0.662(2)	3.8(5)
N(1)	0	0.196(6)	0.793(6)	12.5(8)
N(2)	0.5	0.843(3)	0.735(3)	2.7(7)
N(3)	0.5	0.329(4)	0.981(4)	7(1)

A-β-$(NMe_4)_3[PMo_3W_9O_{40}]$. Intensity data were collected on a Rigaku AFC-5R four-circle diffractometer with graphite-monochromated MoKα (λ = 0.71069 Å) radiation, at the Faculty of Engineering, Osaka University. The crystallographic data are also summarized in Table 2–1. The unit-cell parameters were determined from 13 independent reflections with 2θ over the range of 29.0–30.0°. Three standard reflections were monitored after the collection of 150 reflections. No significant decays in their intensities (maximum 2.5%) were observed throughout the data collection. The reflection data were corrected for Lorentz and polarization effects, together with absorption (transmission factors, 0.214–1.000) [35].

The structure was solved by the direct methods [40]. All the calculations were performed using the TEXAN Crystallographic Software Package of Molecular Structure Corporation [41]. The positions of the N atoms of three tetramethylammonium groups could be determined from D-Fourier maps. However, no C atoms of methyl groups were found. The positions of the hydrogen atoms were not determined. The full-matrix least-squares refinements were carried out by assuming anisotropic thermal parameters for the W atoms and isotropic ones for the Mo, N, O, and P atoms. The final positional parameters for the atoms except for H and C atoms are listed in Table 2–4.

2.3 Results and Discussion

Crystal Structures of the Heteropolyanions. Perspective views of the anions of A-β-$Cs_{5.4}H_{0.6}[PV_3W_9O_{40}]$, A-β-$Cs_6[PNb_3W_9O_{40}]$, and A-β-$(NMe_4)_3[PMo_3W_9O_{40}]$ are illustrated in Figs. 2–1, 2–2, and 2–3, respectively, together with the atom-labeling scheme. Every anion is a geometrical β-isomer [13], which results from a 60° rotation about the threefold axis of one trigonal edge-shared W_3O_{13} unit of the Keggin structure (α-isomer), as described in General Introduction. It belongs to an A-type metal-trisubstituted dodecatungstophosphate anion in which three W atoms of three different W_3O_{13} units are replaced by three V, Nb, or Mo atoms [3]. The bond distances of these anions are

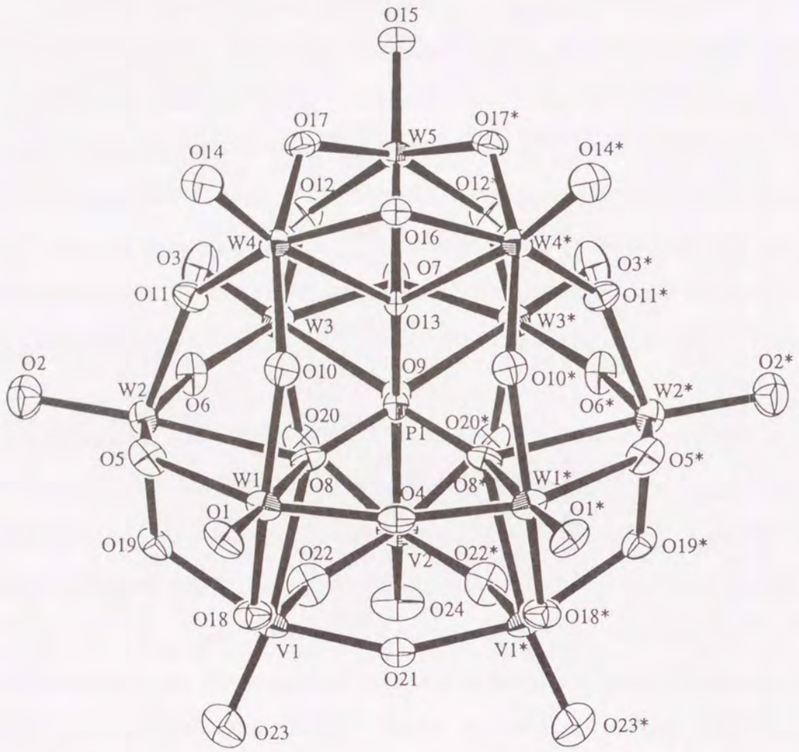

Figure 2–1. Structure of the anion of A-β-$Cs_{5.4}H_{0.6}[PV_3W_9O_{40}]\cdot 12H_2O$. Thermal ellipsoids are shown at the 50% probability level. Atoms are related to starred ones by a mirror symmetry.

summarized in Tables 2–5, 2–6, and 2–7. The M–O and P–O distances and the O–M–O and O–P–O angles classified by the bonding type of the oxygen atoms [42] are summarized in Tables 2–8 and 2–9, respectively. The MO_6 (M = W, V, Nb, and Mo) octahedra have geometries elongated in the direction of the internal oxygen atoms (O_i) coordinated to the P atom, whereas the terminal M–O_t bonds opposite to the internal M–O_i ones are appreciably short in the octahedron. The O_b atoms of each MO_6 octahedron share those of the adjacent octahedra so as to construct the longitudinal and latitudinal framework of the anion like a ball.

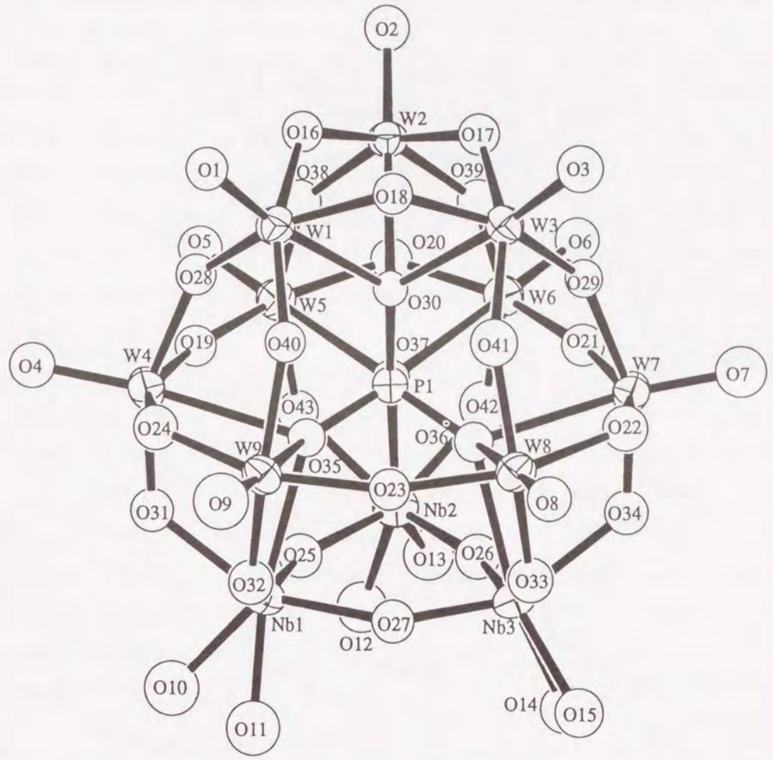

Figure 2–2. Structure of the anion of A-β-$Cs_6[PNb_3W_9O_{40}]\cdot 14H_2O$. Thermal ellipsoids are shown at the 50% probability level.

The V–O_{bc} distances (1.79(2)–1.896(7) Å) are appreciably short compared with the other M–O_b (M = W and V) ones (1.82(1)–1.99(1) Å) in A-β-$Cs_{5.4}H_{0.6}[PV_3W_9O_{40}]$ and the Nb–O_{be} ones (2.03(3)–2.09(2) Å) are appreciably long compared with the other M–O_b (M = W and Nb) ones (1.79(2)–2.01(3) Å) in A-β-$Cs_6[PNb_3W_9O_{40}]$. These findings are ascribable to the facts that the ion radius [43] of W^{6+} (coordination number 6), 0.74 Å, is longer than that of V^{5+} (coordination number 6), 0.68 Å, and shorter than that of Nb^{5+} (coordination number 6), 0.78 Å, and that three substituted metals form the corner-shared M_3O_{13} (M = V or Nb) unit of the A-type through the three O_{bc} atoms. In contrast, no

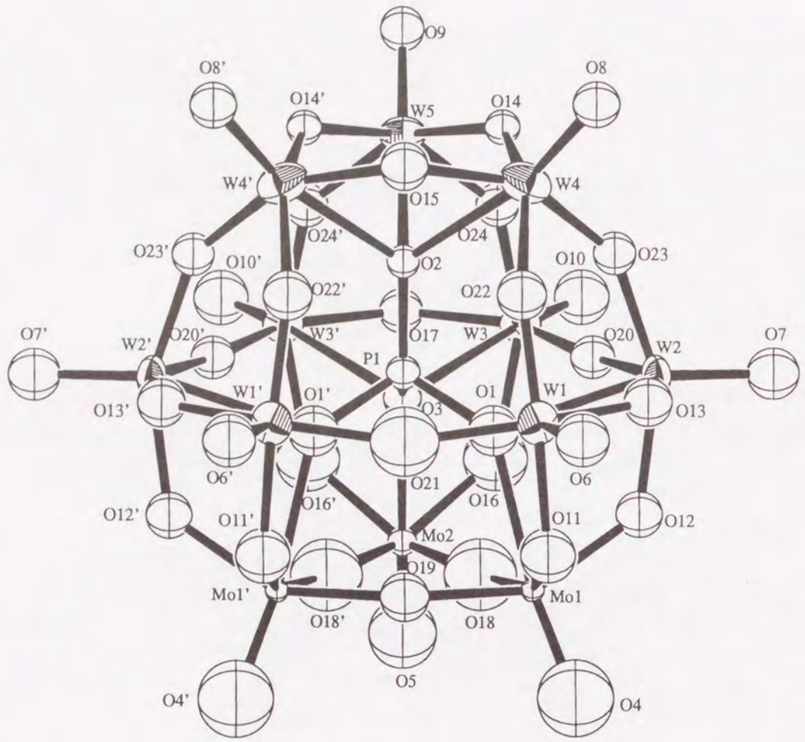

Figure 2–3. Structure of the anion of A-β-$(NMe_4)_3[PMo_3W_9O_{40}]$. Thermal ellipsoids are shown at the 40% probability level. Atoms are related to starred ones by a mirror symmetry.

appreciable difference is observed between the W–O_b (1.74(3)–2.01(5) Å) and Mo–O_b distances (1.64(5)–2.06(4) Å), which is ascribed to the fact that the ion radius [43] of Mo^{6+} (coordination number 6), 0.73 Å, is almost equal to that of W^{6+} (coordination number 6), 0.74 Å.

The bond angles surrounding the metal atoms and heteroatom (P) in A-β-$(NMe_4)_3[PMo_3W_9O_{40}]$ vary widely compared with those in A-β-$Cs_{5.4}H_{0.6}[PV_3W_9O_{40}]$ and in A-β-$Cs_6[PNb_3W_9O_{40}]$ (Table 2–9). The sum of the four O_b–M–O_b (M = W, V, Nb, and Mo) angles of each MO_6 octahedron is considerably smaller than 360° for a perfect

Table 2–5. Bond Distances (Å) of the Anion of A-β-$Cs_{5.4}H_{0.6}[PV_3W_9O_{40}]\cdot 12H_2O$

Atom	Atom	Distance	Atom	Atom	Distance	Atom	Atom	Distance
W(1)	O(1)	1.73(1)	W(3)	O(7)	1.915(9)	V(1)	O(8)	2.45(1)
W(1)	O(4)	1.901(3)	W(3)	O(9)	2.40(1)	V(1)	O(18)	1.99(1)
W(1)	O(5)	1.92(1)	W(3)	O(12)	1.95(1)	V(1)	O(19)	1.95(1)
W(1)	O(8)	2.38(1)	W(3)	O(20)	1.86(1)	V(1)	O(21)	1.896(7)
W(1)	O(10)	1.96(1)	W(4)	O(10)	1.90(1)	V(1)	O(22)	1.79(2)
W(1)	O(18)	1.82(1)	W(4)	O(11)	1.90(1)	V(1)	O(23)	1.59(1)
W(2)	O(2)	1.71(1)	W(4)	O(13)	2.43(1)	V(2)	O(9)	2.46(2)
W(2)	O(5)	1.90(1)	W(4)	O(14)	1.71(2)	V(2)	O(20)	1.92(1)
W(2)	O(6)	1.90(1)	W(4)	O(16)	1.913(7)	V(2)	O(22)	1.87(2)
W(2)	O(8)	2.41(1)	W(4)	O(17)	1.95(1)	V(2)	O(24)	1.59(2)
W(2)	O(11)	1.95(1)	W(5)	O(12)	1.90(1)	P(1)	O(8)	1.54(1)
W(2)	O(19)	1.85(1)	W(5)	O(13)	2.38(1)	P(1)	O(9)	1.52(2)
W(3)	O(3)	1.71(2)	W(5)	O(15)	1.69(2)	P(1)	O(13)	1.53(2)
W(3)	O(6)	1.91(1)	W(5)	O(17)	1.91(1)			

octahedron: 350.2–351.2° in A-β-$Cs_{5.4}H_{0.6}[PV_3W_9O_{40}]$, 346–351° in A-β-$Cs_6[PNb_3W_9O_{40}]$, and 342–346° in A-β-$(NMe_4)_3[PMo_3W_9O_{40}]$. The O_t–M–O_b angles are apparently larger than the O_i–M–O_b ones in each compound. These values indicate that the metal atoms deviate from the planes formed by four O_b atoms to the outside of the anion in order to construct the framework.

The central PO_4 moieties of A-β-$Cs_{5.4}H_{0.6}[PV_3W_9O_{40}]$ and A-β-$Cs_6[PNb_3W_9O_{40}]$ adopt almost a regular tetrahedral arrangement having P–O_i distances of 1.52(2)–1.54(1) and 1.51(2)–1.55(2) Å and O_i–P–O_i angles of 108.1(9)–110.2(6) and 107(1)–111(1)°, respectively. In contrast, the PO_4 tetrahedron in A-β-$(NMe_4)_3[PMo_3W_9O_{40}]$ is largely distorted (P–O_i, 1.52(5)–1.63(5) Å; O_i–P–O_i, 101(2)–119(2)°), as was observed for other β-isomers of dodecatungstosilicate anions, β-$K_4[SiW_{12}O_{40}]$ (Si–O_i, 1.37–1.83 Å; O_i–Si–O_i, 99–117°) [32] and β-$(NBu^n_4)_4[SiW_{12}O_{40}]$ (Si–O_i, 1.63–1.86 Å; O_i–Si–O_i, 103–117°) [33].

Table 2–6. Bond Distances (Å) of the Anion of A-β-$Cs_6[PNb_3W_9O_{40}]\cdot 14H_2O$

Atom	Atom	Distance	Atom	Atom	Distance	Atom	Atom	Distance
W(1)	O(1)	1.70(3)	W(5)	O(37)	2.47(2)	Nb(1)	O(10)	1.93(7)
W(1)	O(16)	1.96(2)	W(5)	O(38)	1.95(2)	Nb(1)	O(11)	1.92(5)
W(1)	O(18)	1.95(2)	W(5)	O(43)	1.84(2)	Nb(1)	O(25)	1.85(3)
W(1)	O(28)	1.87(2)	W(6)	O(6)	1.71(3)	Nb(1)	O(27)	2.01(3)
W(1)	O(30)	2.46(2)	W(6)	O(20)	1.89(2)	Nb(1)	O(31)	2.06(2)
W(1)	O(40)	1.88(2)	W(6)	O(21)	1.87(3)	Nb(1)	O(32)	2.04(3)
W(2)	O(2)	1.71(2)	W(6)	O(37)	2.47(2)	Nb(1)	O(35)	2.49(2)
W(2)	O(16)	1.85(3)	W(6)	O(39)	1.95(2)	Nb(2)	O(12)	1.90(5)
W(2)	O(17)	1.97(3)	W(6)	O(42)	1.83(3)	Nb(2)	O(13)	1.91(8)
W(2)	O(30)	2.46(2)	W(7)	O(7)	1.64(3)	Nb(2)	O(25)	1.99(3)
W(2)	O(38)	1.90(2)	W(7)	O(21)	1.95(3)	Nb(2)	O(26)	1.84(3)
W(2)	O(39)	1.88(2)	W(7)	O(22)	1.88(3)	Nb(2)	O(37)	2.47(2)
W(3)	O(3)	1.74(3)	W(7)	O(29)	1.95(2)	Nb(2)	O(42)	2.03(3)
W(3)	O(17)	1.85(2)	W(7)	O(34)	1.79(2)	Nb(2)	O(43)	2.06(2)
W(3)	O(18)	1.89(2)	W(7)	O(36)	2.45(2)	Nb(3)	O(14)	1.93(5)
W(3)	O(29)	1.90(2)	W(8)	O(8)	1.68(3)	Nb(3)	O(15)	1.94(6)
W(3)	O(30)	2.43(2)	W(8)	O(22)	1.94(3)	Nb(3)	O(26)	1.99(3)
W(3)	O(41)	1.88(3)	W(8)	O(23)	1.90(2)	Nb(3)	O(27)	1.86(2)
W(4)	O(4)	1.70(3)	W(8)	O(33)	1.82(3)	Nb(3)	O(33)	2.07(3)
W(4)	O(19)	1.95(3)	W(8)	O(36)	2.47(3)	Nb(3)	O(34)	2.09(2)
W(4)	O(24)	1.93(3)	W(8)	O(41)	1.91(2)	Nb(3)	O(36)	2.44(2)
W(4)	O(28)	1.98(2)	W(9)	O(9)	1.64(4)	P(1)	O(30)	1.55(2)
W(4)	O(31)	1.82(2)	W(9)	O(23)	1.91(2)	P(1)	O(35)	1.51(2)
W(4)	O(35)	2.48(2)	W(9)	O(24)	1.88(3)	P(1)	O(36)	1.54(2)
W(5)	O(5)	1.71(3)	W(9)	O(32)	1.85(3)	P(1)	O(37)	1.53(3)
W(5)	O(19)	1.88(2)	W(9)	O(35)	2.46(2)			
W(5)	O(20)	1.94(2)	W(9)	O(40)	1.98(2)			

Table 2–7. Bond Distances (Å) of the Anion of A-β-$(NMe_4)_3[PMo_3W_9O_{40}]$

Atom	Atom	Distance	Atom	Atom	Distance	Atom	Atom	Distance
W(1)	O(1)	2.51(4)	W(3)	O(16)	1.95(4)	Mo(1)	O(1)	2.31(3)
W(1)	O(6)	1.71(5)	W(3)	O(17)	1.87(2)	Mo(1)	O(4)	1.62(4)
W(1)	O(11)	1.97(4)	W(3)	O(20)	1.78(4)	Mo(1)	O(11)	1.99(5)
W(1)	O(13)	1.89(4)	W(3)	O(24)	1.93(4)	Mo(1)	O(12)	1.90(4)
W(1)	O(21)	1.90(1)	W(4)	O(2)	2.36(3)	Mo(1)	O(18)	2.06(4)
W(1)	O(22)	1.82(4)	W(4)	O(8)	1.73(4)	Mo(1)	O(19)	1.86(1)
W(2)	O(1)	2.44(4)	W(4)	O(14)	1.74(3)	Mo(2)	O(3)	2.31(5)
W(2)	O(7)	1.70(4)	W(4)	O(15)	1.95(3)	Mo(2)	O(5)	1.77(4)
W(2)	O(12)	1.97(4)	W(4)	O(22)	2.01(5)	Mo(2)	O(16)	1.86(5)
W(2)	O(13)	1.82(4)	W(4)	O(23)	1.88(4)	Mo(2)	O(18)	1.64(5)
W(2)	O(20)	1.98(4)	W(5)	O(2)	2.44(5)	P(1)	O(1)	1.60(4)
W(2)	O(23)	1.89(4)	W(5)	O(9)	1.67(6)	P(1)	O(2)	1.63(5)
W(3)	O(3)	2.52(4)	W(5)	O(14)	1.94(3)	P(1)	O(3)	1.52(5)
W(3)	O(10)	1.49(5)	W(5)	O(24)	1.89(4)			

Consequently, it is noteworthy that the present β-isomers, A-β-$Cs_{5.4}H_{0.6}[PV_3W_9O_{40}]$ and A-β-$Cs_6[PNb_3W_9O_{40}]$, have almost regular tetrahedra of the central PO_4 moieties.

The non-bonded metal–metal distances between neighboring MO_6 (M = W, V, Nb, and Mo) octahedra in the present A-β-$[PM_3W_9O_{40}]^{n-}$ (M = V and Nb, n = 6; M = Mo, n = 3) anion salts are summarized in Table 2–10, 2–11, and 2–12, respectively, and their averaged values are summarized in Table 2–13. The W–W distances in these compounds are almost identical. Since the spatial locations of the W_{cap} [44] atoms are closer to those of the W_{belt} atoms in the β-isomer compared with in the α-isomer, the corner-shared W_{belt}–W_{cap} distances (av. 3.62–3.68 Å) are obviously shorter than the corner-shared W_{belt}–W_{belt} ones (av. 3.75–3.77 Å). Accordingly, the edge-shared W_3O_{13} unit comprising the W_{cap} atoms is distorted and the edge-shared W_{cap}–W_{cap} distances (av. 3.41–3.42 Å) are apparently longer than the edge-shared W_{belt}–W_{belt} ones (av. 3.33–3.38 Å).

Table 2–8. M–O and P–O Distances (Å) Classified by the Bonding Types [42] of the Oxygen Atoms

A-β-$Cs_{5.4}H_{0.6}[PV_3W_9O_{40}]\cdot 12H_2O$		A-β-$Cs_6[PNb_3W_9O_{40}]\cdot 14H_2O$		A-β-$(NMe_4)_3[PMo_3W_9O_{40}]$	
W–O_{bc}	V–O_{bc}	W–O_{bc}	Nb–O_{bc}	W–O_{bc}	Mo–O_{bc}
1.90(1)–1.96(1)	1.79(2)–1.896(7)	1.87(2)–1.98(2)	1.84(3)–2.01(3)	1.78(4)–2.01(5)	1.64(5)–2.06(4)
W–O_{be}	V–O_{be}	W–O_{be}	Nb–O_{be}	W–O_{be}	Mo–O_{be}
1.82(1)–1.95(1)	1.92(1)–1.99(1)	1.79(2)–1.97(3)	2.03(3)–2.09(2)	1.74(3)–1.97(4)	1.86(5)–1.99(5)
W–O_t	V–O_t	W–O_t	Nb–O_t	W–O_t	Mo–O_t
1.69(2)–1.73(1)	1.59(1)–1.59(2)	1.64(3)–1.74(3)	1.90(5)–1.94(6)	1.49(5)–1.73(4)	1.62(4)–1.77(4)
W–O_i	V–O_i	W–O_i	Nb–O_i	W–O_i	Mo–O_i
2.38(1)–2.43(1)	2.45(1)–2.46(2)	2.43(2)–2.48(2)	2.44(2)–2.49(2)	2.36(3)–2.52(4)	2.31(3)–2.31(5)
P–O_i		P–O_i		P–O_i	
1.52(2)–1.54(1)		1.51(2)–1.55(2)		1.52(5)–1.63(5)	

Table 2–9. O–M–O and O–P–O Angles (°) Classified by the Bonding Types [42] of the Oxygen Atoms[a)]

	A-β-$Cs_{5.4}H_{0.6}[PV_3W_9O_{40}]\cdot 12H_2O$	A-β-$Cs_6[PNb_3W_9O_{40}]\cdot 14H_2O$	A-β-$(NMe_4)_3[PMo_3W_9O_{40}]$
O_b–M–O_b	80.0(5)–94.2(7)	81(1)–98(1)	77(2)–100(2)
O_t–M–O_b	98.1(7)–105.2(7)	99(1)–108(1)	94(2)–111(3)
O_i–M–O_b	70.3(5)–86.8(5)	68.7(9)–83.6(9)	62(2)–89(1)
O_i–P–O_i	108.1(9)–110.2(6)	107(1)–111(1)	101(2)–119(2)

a) M = W, V, Nb, and Mo.

Table 2–10. Non-Bonded Metal–Metal Distances (Å) of A-β-$Cs_{5.4}H_{0.6}[PV_3W_9O_{40}]\cdot 12H_2O$

	Atom	Atom	Distance	Average
Edge-shared W_{belt}–W_{belt}				3.33
	W(1)	W(2)	3.321(1)	
	W(3)	W(3*)	3.342(2)	
Edge-shared W_{belt}–V				3.38
	W(3)	V(2)	3.371(4)	
	W(2)	V(1)	3.377(3)	
	W(1)	V(1)	3.390(3)	
Edge-shared W_{cap}–W_{cap}				3.41
	W(4)	W(5)	3.406(1)	
	W(4)	W(4*)	3.409(1)	
Corner-shared V–V				3.57
	V(1)	V(2)	3.548(5)	
	V(1)	V(1*)	3.604(7)	
Corner-shared W_{belt}–W_{cap}				3.68
	W(2)	W(4)	3.663(1)	
	W(1)	W(4)	3.6829(9)	
	W(3)	W(5)	3.685(1)	
Corner-shared W_{belt}–W_{belt}				3.75
	W(2)	W(3)	3.750(1)	
	W(1)	W(1*)	3.754(2)	

Table 2–11. Non-Bonded Metal–Metal Distances (Å) of A-β-$Cs_6[PNb_3W_9O_{40}]\cdot 14H_2O$

	Atom	Atom	Distance	Average
Edge-shared W_{belt}–W_{belt}				3.38
	W(4)	W(9)	3.368(2)	
	W(7)	W(8)	3.382(2)	
	W(5)	W(6)	3.385(2)	
Edge-shared W_{belt}–Nb				3.49
	W(8)	Nb(3)	3.473(4)	
	W(9)	Nb(1)	3.478(4)	
	W(4)	Nb(1)	3.483(4)	
	W(7)	Nb(3)	3.483(4)	
	W(6)	Nb(2)	3.491(4)	
	W(5)	Nb(2)	3.505(4)	
Edge-shared W_{cap}–W_{cap}				3.41
	W(1)	W(3)	3.402(2)	
	W(1)	W(2)	3.405(2)	
	W(2)	W(3)	3.411(2)	
Corner-shared Nb–Nb				3.72
	Nb(1)	Nb(2)	3.718(5)	
	Nb(1)	Nb(3)	3.724(5)	
	Nb(2)	Nb(3)	3.725(5)	
Corner-shared W_{belt}–W_{cap}				3.67
	W(8)	W(3)	3.656(2)	
	W(6)	W(2)	3.664(2)	
	W(4)	W(1)	3.670(2)	
	W(7)	W(3)	3.673(2)	
	W(9)	W(1)	3.676(2)	
	W(5)	W(2)	3.687(2)	
Corner-shared W_{belt}–W_{belt}				3.77
	W(8)	W(9)	3.767(2)	
	W(6)	W(7)	3.769(2)	
	W(4)	W(5)	3.775(2)	

Table 2–12. Non-Bonded Metal–Metal Distances (Å) of A-β-$(NMe_4)_3[PMo_3W_9O_{40}]$

	Atom	Atom	Distance	Average
Edge-shared W_{belt}–W_{belt}				3.36
	W(1)	W(2)	3.352(4)	
	W(3)	W(3*)	3.365(6)	
Edge-shared W_{belt}–Mo				3.49
	W(1)	Mo(1)	3.455(4)	
	W(2)	Mo(1)	3.497(4)	
	W(3)	Mo(2)	3.516(6)	
Edge-shared W_{cap}–W_{cap}				3.42
	W(4)	W(5)	3.414(4)	
	W(4)	W(4*)	3.441(7)	
Corner-shared Mo–Mo				3.62
	Mo(1)	Mo(1*)	3.624(8)	
	Mo(1)	Mo(2)	3.614(7)	
Corner-shared W_{belt}–W_{cap}				3.62
	W(2)	W(4)	3.609(4)	
	W(1)	W(4)	3.619(4)	
	W(3)	W(5)	3.620(4)	
Corner-shared W_{belt}–W_{belt}				3.75
	W(2)	W(3)	3.740(4)	
	W(1)	W(1*)	3.761(6)	

On the other hand, the M_{bottom}–M_{bottom} (M_{bottom} = V, Nb, and Mo) distances are distinguishable from one another depending on the ion radii [43] of these metals as described above ($V^{5+} < Mo^{6+} \approx W^{6+} < Nb^{5+}$). The corner-shared V_3O_{13} unit is contracted, which results in the shorter corner-shared V–V distances (av. 3.57 Å) compared with the corner-shared W_{belt}–W_{cap} ones (av. 3.68 Å). In contrast, the corner-shared Nb_3O_{13} unit is spread out, which results in the longer corner-shared Nb–Nb distances (av. 3.72 Å) compared

Table 2–13. Averaged Non-Bonded Metal–Metal Distances (Å) of the Metal-Trisubstituted Dodecatungstophosphate Anion Salts

Salt	Edge-shared W_{cap}–W_{cap}	Corner-shared W_{belt}–W_{cap}	Edge-shared W_{belt}–W_{belt}	Corner-shared W_{belt}–W_{belt}	Edge-shared W_{belt}–M_{bottom}[a)]	Corner-shared M_{bottom}–M_{bottom}[a)]
A-β-$Cs_{5.4}H_{0.6}[PV_3W_9O_{40}]$	3.41	3.68	3.33	3.75	3.38	3.57
A-β-$Cs_6[PNb_3W_9O_{40}]$	3.41	3.67	3.38	3.77	3.49	3.72
A-β-$(NMe_4)_3[PMo_3W_9O_{40}]$	3.42	3.62	3.36	3.75	3.49	3.62

a) M_{bottom} = V, Nb, and Mo.

with the corner-shared W_{belt}–W_{cap} ones (av. 3.67 Å). The corner-shared Mo–Mo distances (av. 3.62 Å) are quite equal to the corner-shared W_{belt}–W_{cap} ones (av. 3.62 Å).

Protonation Site of the Heteropolyanion. In A-β-$Cs_{5.4}H_{0.6}[PV_3W_9O_{40}]$, the cesium cations were surrounded by six to nine oxygen atoms of the polyanion and of water molecules with the Cs–O contacts of 2.96(2)–3.50(1) Å, although all water molecules were not found in the structure determination. Non-bonded contact (2.96(2) Å) between Cs(4) and O(21) bridging V(1) to V(1*) was the shortest among them, as illustrated in the packing diagram of the compound (Fig. 2–4). The other non-bonded contacts between the Cs atoms and the oxygen atoms of the polyanion were 3.07(2)–3.50(1) Å. As described in the experimental section, the occupancy factor of the Cs(4) atom on the mirror in the symmetry operation was reduced to 0.2, indicating the disordered arrangement of Cs(4) and a proton in the fractions of 0.4 and 0.6, respectively. The short Cs(4)–O(21) distance is, therefore,

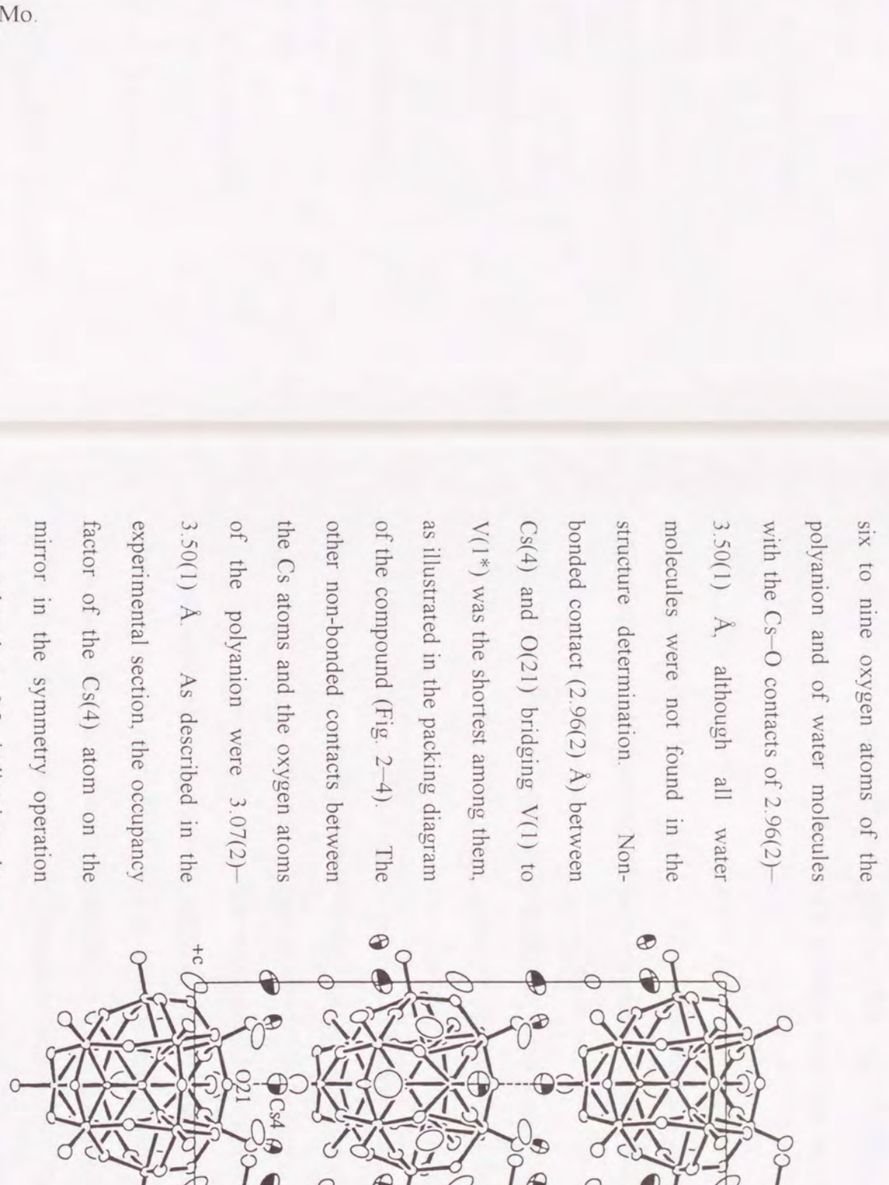

Figure 2–4. Crystal structure of A-β-$Cs_{5.4}H_{0.6}[PV_3W_9O_{40}]\cdot 12H_2O$. Shaded and plain ellipsoids indicate cesium and water-oxygen atoms, respectively. Dashed lines represent the shortest non-bonded contact between Cs(4) and O(21) (2.96(2) Å).

considered to be due to the contribution of binding of the proton to the O(21) atom. In accordance with this, the V(1)–O(21) distance (1.896(7) Å) was appreciably longer than the V(1)–O(22) one (1.79(2) Å), which supported protonation of the O(21) atom. The lengthened distance between a metal atom and a protonated oxygen atom was also observed for α-$K_{3.5}[H_{4.5}PtMo_6O_{24}]$ [45]. In A-β-$Cs_6[PNb_3W_9O_{40}]$, such short non-bonded contacts between the Cs atoms and the oxygen atoms bound to the Nb atoms were not observed (> 3.12(3) Å).

In chapter 1, protonation at the bridging oxygen atom in A-β-$(NBu^n_4)_4H_2[PV_3W_9O_{40}]$ was also indicated by its ^{31}P, ^{51}V and ^{183}W NMR spectral behavior. The most probable protonation site was thought to be the bridging oxygen atom in the V–O–V bond, since this atom was suggested to be the most basic one among the oxygen atoms in the polyanion, as previously described for the A-β-$[HSiV_3W_9O_{40}]^{6-}$ anion [3]. Thus, the present finding concerning protonation at the O(21) atom in the V–O–V bond accords with the previously estimated protonation site.

The bond-valence sums (BVS) [46] of the oxygen atoms of A-β-$Cs_{5.4}H_{0.6}[PV_3W_9O_{40}]$ are summarized in Table 2–14. The BVS value of the O(21) atom, 1.56, is apparently smaller compared with those of the other bridging oxygen atoms (O_{bc}, O_{be}, and O_i), 1.87–2.09, which are in good agreement with their formal charges of 2. Since the O(21) atom is expected to be protonated as described above, a reduction in the BVS value for this oxygen atom may be compensated by O–H bond formation, as previously reported for some heteropolyanions [23, 47]. Valences of the terminal M–O_t bonds are in the range of 1.66–1.85, which are comparable to those of the terminal W–O_t bonds calculated for $[H_2PTi_2W_{10}O_{40}]^{5-}$ [23]. The BVS values of the P, V, and W atoms of the present heteropolyanion were calculated to be 5.03, 5.04–5.07, and 6.02–6.27, respectively, which were also consistent with these formal charges of 5, 5, and 6.

Table 2–14. Bond-Valence Sums (BVS) of the Oxygen Atoms of A-β-$Cs_{5.4}H_{0.6}[PV_3W_9O_{40}]$

Oxygen atom	BVS
Corner-sharing oxygen atom (O_{bc})	
O(21)	1.56
O(22)	1.87
O(10)	1.94
O(11)	1.96
O(12)	1.96
O(6)	2.07
O(4)	2.09
Edge-sharing oxygen atom (O_{be})	
O(19)	1.87
O(20)	1.90
O(18)	1.90
O(17)	1.93
O(7)	2.01
O(16)	2.02
O(5)	2.04
Internal oxygen atom (O_i)	
O(8)	1.96
O(9)	2.01
O(13)	2.05
Terminal oxygen atom (O_t)	
O(1)	1.66
O(2)	1.75
O(3)	1.75
O(14)	1.75
O(23)	1.79
O(24)	1.79
O(15)	1.85

2.4 Conclusion

The structures of vanadium-, niobium-, and molybdenum-trisubstituted dodecatungstophosphate anion salts were clarified by single-crystal X-ray analyses as A-type metal-trisubstituted, geometrical β-isomers of the Keggin type, A-β-$Cs_{5.4}H_{0.6}[PV_3W_9O_{40}]$, A-β-$Cs_6[PNb_3W_9O_{40}]$, and A-β-$(NMe_4)_3[PMo_3W_9O_{40}]$, in which three substituted metals formed the corner-shared M_3O_{13} unit of the A-type through the three corner-sharing oxygen atoms. The structural characteristics of these polyanions were reflected in the differences between the ion radii of the substituted metals. The positional parameters of the cesium cations of A-β-$Cs_{5.4}H_{0.6}[PV_3W_9O_{40}]$ afforded structural information concerning protonation to the oxygen atom of the $[PV_3W_9O_{40}]^{6-}$ anion.

2.5 References

1 B. Rapko, M. Pohl, and R. G. Finke, *Inorg. Chem.*, **33**, 3625 (1994), and references therein.

2 C. J. Gómez-Garcia, E. Coronado, P. Gómez-Romero, and N. Casañ-Pastor, *Inorg. Chem.*, **32**, 89 (1993).

3 R. G. Finke, B. Rapko, R. J. Saxton, and P. J. Domaille, *J. Am. Chem. Soc.*, **108**, 2947 (1986).

4 E. Cadot, R. Thouvenot, A. Tézé, and G. Hervé, *Inorg. Chem.*, **31**, 4128 (1992).

5 K. Nomiya, H. Saijoh, and M. Miwa, *Bull. Chem. Soc. Jpn.*, **53**, 3719 (1980).

6 E. G. Zhizhina, L. I. Kuznetsova, R. I. Maksimovskaya, S. N. Pavlova, and K. I. Matveev, *J. Mol. Catal.*, **38**, 345 (1986).

7 H. Furukawa, T. Nakamura, H. Inagaki, E. Nishikawa, C. Imai, and M. Misono, *Chem. Lett.*, **1988**, 877.

8 J. K. Burdett and C. K. Nguyen, *J. Am. Chem. Soc.*, **112**, 5366 (1990).

9 R. Neumann and M. Levin, *J. Org. Chem.*, **56**, 5707 (1991); R. Neumann and M. Levin, *J. Am. Chem. Soc.*, **114**, 7278 (1992).

10 Y. Izumi, Y. Satoh, H. Kondoh, and K. Urabe, *J. Mol. Catal.*, **72**, 37 (1992).

11 E. Cadot, M. Fournier, A. Tézé, and G. Hervé, *Inorg. Chem.*, **35**, 282 (1996).

12 M. T. Pope and T. F. Scully, *Inorg. Chem.*, **14**, 953 (1975).

13 L. C. W. Baker and J. S. Figgis, *J. Am. Chem. Soc.*, **92**, 3794 (1970).

14 P. J. Domaille, *J. Am. Chem. Soc.*, **106**, 7677 (1984).

15 P. J. Domaille and G. Watunya, *Inorg. Chem.*, **25**, 1239 (1986).

16 R. G. Finke and M. W. Droege, *J. Am. Chem. Soc.*, **106**, 7274 (1984).

17 B. F. Robert, A. Tézé, G. Hervé, and Y. Jeannin, *Acta Crystallogr., Sect. B*, **36B**, 11 (1980).

18 B. A. Björnberg and B. Hedman, *Acta Crystallogr., Sect. B*, **36B**, 1018 (1980).

19 T. Yamase, T. Ozeki, and S. Motomura, *Bull. Chem. Soc. Jpn.*, **65**, 1453 (1992).

20 M. Cindric, B. Kamenar, N. Strukan, and Z. Veksli, *Polyhedron*, **14**, 1045 (1995).

21 T. J. R. Weakley, *J. Chem. Soc., Chem. Commun.*, **1984**, 1406.

22 P. J. Domaille and R. L. Harlow, *J. Am. Chem. Soc.*, **108**, 2108 (1986).

23 T. Ozeki and T. Yamase, *Acta Crystallogr., Sect. C*, **47C**, 693 (1991).

24 K. Wassermann, H. Lunk, R. Pałm, and J. Fuchs, *Acta Crystallogr., Sect. C*, **50C**, 348 (1994).

25 X. Zhang, C. J. O'Connor, G. B. Jameson, and M. T. Pope, *Inorg. Chem.*, **35**, 30 (1996).

26 F. Xin, M. T. Pope, G. J. Long, and U. Russo, *Inorg. Chem.*, **35**, 1207 (1996).

27 B. Dawson, *Acta Crystallogr.*, **6**, 113 (1953).

28 H. D'Amour, *Acta Crystallogr., Sect. B*, **32B**, 729 (1976).

29 J. Fuchs and R. Palm, *Z. Naturforsch., B*, **39B**, 757 (1984).

30 W. H. Knoth, P. J. Domaille, and R. L. Harlow, *Inorg. Chem.*, **25**, 1577 (1986).

31 C. M. Tourné G. F. Tourné and T. J. R. Weakley, *J. Chem. Soc., Dalton Trans.*, **1986**, 2237.

32 K. Yamamura and Y. Sasaki, *J. Chem. Soc., Chem. Commun.*, **1973**, 648; K. Y. Matsumoto, A. Kobayashi, and Y. Sasaki, *Bull. Chem. Soc. Jpn.*, **48**, 3146 (1975).

33 J. Fuchs, A. Thiele, and R. Palm, *Z. Naturforsch., B*, **36B**, 161 (1981).

34 J. N. Barrows, G. B. Jameson, and M. T. Pope, *J. Am. Chem. Soc.*, **107**, 1771 (1985).

35 A. C. T. North, D. C. Phillips, and F. C. Matheus, *Acta Crystallogr.*, **24A**, 351 (1968).

36 G. M. Sheldrick, SHELXS86, A computer program for the solution of crystal structures, University of Göttingen, Germany (1985).

37 TEXSAN, Crystal structure analysis software, Molecular Structure Corporation, The Woodlands, TX (1992).

38 International Tables for X-Ray Crystallography, Vol. 4, Kynoch Press, Birmingham (1974).

39 C. K. Johnson, ORTEP II, Report ORNL-5138, Oak Ridge National Laboratory, Oak Ridge, TN (1976).

40 C. J. Gilmore, MITHRIL, an integrated direct methods computer program, *J. Appl. Crystallogr.*, **17**, 42 (1984); P. T. Beurskens, DIRDIF, direct methods for difference structures–an automatic procedure for phase extension and refinement of difference structure factors, Technical Report 1984/1, Crystallography Laboratory, Toernooiveld, Nijmegen (1984).

41 TEXSAN, Structure Analysis Package, Molecular Structure Corporation, College Station, TX (1985).

42 The oxygen atoms of the Keggin-type anion are classified into four species, O_i, O_t, and O_b (O_{bc} and O_{be}), as described in General Introduction.

43 R. D. Shannon and C. T. Prewitt, *Acta Crystallogr., Sect. B*, **25B**, 925 (1969); R. D. Shannon, *Acta Crystallogr., Sect. A*, **32A**, 751 (1976).

44 The metal atoms of the β-isomer of the Keggin-type heteropolyanion are classified into three species represented by the subscripts as follows: the three (M_{cap}) in the rotated, trigonal edge-shared M_3O_{13} unit, the three (M_{bottom}) on the opposite side of the M_{cap} unit, and the six (M_{belt}) in octahedra adjacent to both M_{cap} and M_{bottom} atoms.

45 U. Lee and Y. Sasaki, *Chem. Lett.*, **1984**, 1297; U. Lee and Y. Sasaki, *Bull. Korean Chem. Soc.*, **15**, 37 (1994).

46 Bond-valence sums are the sum of the bond valence at each atom. Bond valence (s) is calculated by the equation, $s = \exp[(r_O - r)/B]$, where r is the observed bond distance (Å) and r_O and B are empirical parameters; r_O for P^{5+}–O^{2-}, V^{5+}–O^{2-}, and W^{6+}–O^{2-} bonds are 1.617, 1.803, and 1.917 Å, respectively, and B is 0.37: I. D. Brown and D. Altermatt, *Acta Crystallogr., Sect. B*, **41B**, 244 (1985).

47 F. Xin and M. T. Pope, *Organometallics*, **13**, 4881 (1994).

Chapter 3

Isomerization of the β-Isomers of the A-Type Vanadium-Trisubstituted Dodecatungstophosphate Anion Salts to the Corresponding α-Isomers

3.1 Introduction

The β-isomers of the Keggin-type polyanions are generally unstable compared with the corresponding α-ones and tend to isomerize to the α-form in an aqueous solution [1]. The stability of β-$[XM_{12}O_{40}]^{n-}$ anions, that is, the rate of the β-to-α isomerization of them, depends on the kind of both X (heteroatom) and M (metal atom). The β-forms of the polyanions involving P or As as a heteroatom were reported to isomerize to the corresponding α-ones much easily and, therefore, such β-isomers were much difficult to be isolated [1–3]. The β-isomers of $[SiW_{12}O_{40}]^{4-}$ anion salts were found to be relatively stable even in an aqueous solution [1]. In contrast, isomerization of β-$H_4[XMo_{12}O_{40}]$ (X = Si and Ge) occurred readily in aqueous solutions and their kinetic studies were undertaken by polarography [2, 4] and by absorptiometry [5], in which the rates of isomerization were found to depend on pH of the solutions. Consequently, the β-to-α isomerization is quite of interest, because it provides useful information about the formation and isolation of β-isomers. However, only a few studies on β-to-α isomerization of β-dodecamolybdosilicate and β-dodecamolybdogermanate acids have been reported as described above [2, 4, 5] and little is known about the mechanism of the isomerization.

In a series of β-isomers of A-type metal-trisubstituted dodecatungstophosphate anion salts, A-β-$[PM_3W_9O_{40}]^{n-}$ (M = V and Nb, n = 6; M = Mo, n = 3), as described in chapter 1, A-β-$(NBu^n_4)_4H_2[PV_3W_9O_{40}]$ was found to isomerize to the α-form with moderate rate both in the solid state and in solution under mild conditions, in contrast to A-β-$Cs_{5.4}H_{0.6}[PV_3W_9O_{40}]$ and A-β-$(NBu^n_4)_6[PV_3W_9O_{40}]$, which were stable in the β-form. In this chapter, the β-to-α isomerization of A-β-$(NBu^n_4)_4H_2[PV_3W_9O_{40}]$ was directly followed by Fourier transform-IR (FT-IR) and ^{31}P NMR spectroscopies, which afforded its

kinetics as the first example of the β-to-α isomerization in the solid state and its mechanism concerning the protonation to the polyanion moiety.

3.2 Experimental

Materials. Preparations of the vanadium-, niobium-, and molybdenum-trisubstituted dodecatungstophosphate anion salts were described in chapter 1.

Physical Measurements. Measurements of IR and ^{31}P NMR spectra were described in chapter 1. FT-IR spectra in solution were measured with a Nicolet 5DX spectrophotometer using a KRS-6 cell with a 0.1-mm light path.

3.3 Results and Discussion

A-β-$(NBu^n_4)_4H_2[PV_3W_9O_{40}]$ was heated at 80°C for 160 h, which had the same IR spectral patterns as those of A-α-$(NBu^n_4)_4H_2[PV_3W_9O_{40}]$ depicted in Fig. 1–2 in chapter 1. This indicates the isomerization of the β-form to the α-one in the solid state. Figure 3–1 shows the ^{31}P NMR spectra of the wet acetonitrile-d_3

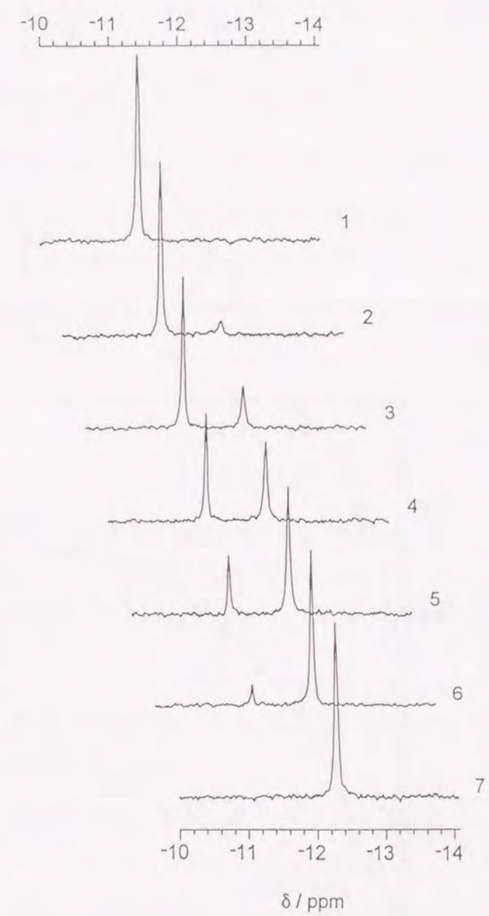

Figure 3–1. ^{31}P NMR spectra of the wet acetonitrile-d_3 solutions of A-β-$(NBu^n_4)_4H_2[PV_3W_9O_{40}]$ heated at 80°C in the solid state: heating time: 0(1), 2(2), 8(3), 19(4), 39(5), 94(6), and 160 h(7).

solutions [6] of the β-isomer heated at 80°C in the solid state. The sharp signal observed at −11.42 ppm for the unheated β-isomer decreases in the intensity with the heating time and, concomitantly, a new signal develops at −12.28 ppm; the chemical shift is corresponding to that observed for the α-isomer. These findings indicate the β-to-α isomerization according to the reaction (Eq. 3–1).

$$\text{A-}\beta\text{-}(\text{NBu}^{n}_4)_4\text{H}_2[\text{PV}_3\text{W}_9\text{O}_{40}] \rightarrow \text{A-}\alpha\text{-}(\text{NBu}^{n}_4)_4\text{H}_2[\text{PV}_3\text{W}_9\text{O}_{40}] \quad (3\text{–}1)$$

Figure 3–2 shows the progress of the isomerization of A-β-$(\text{NBu}^{n}_4)_4\text{H}_2[\text{PV}_3\text{W}_9\text{O}_{40}]$ to the α-isomer at 40, 60, 80, and 100°C in the solid state, which is evaluated by the intensity ratios of their ^{31}P NMR signals measured in wet acetonitrile-d_3 (Fig. 3–1). The first-order rate law (Eq. 3–2) was applied to the kinetics of this isomerization;

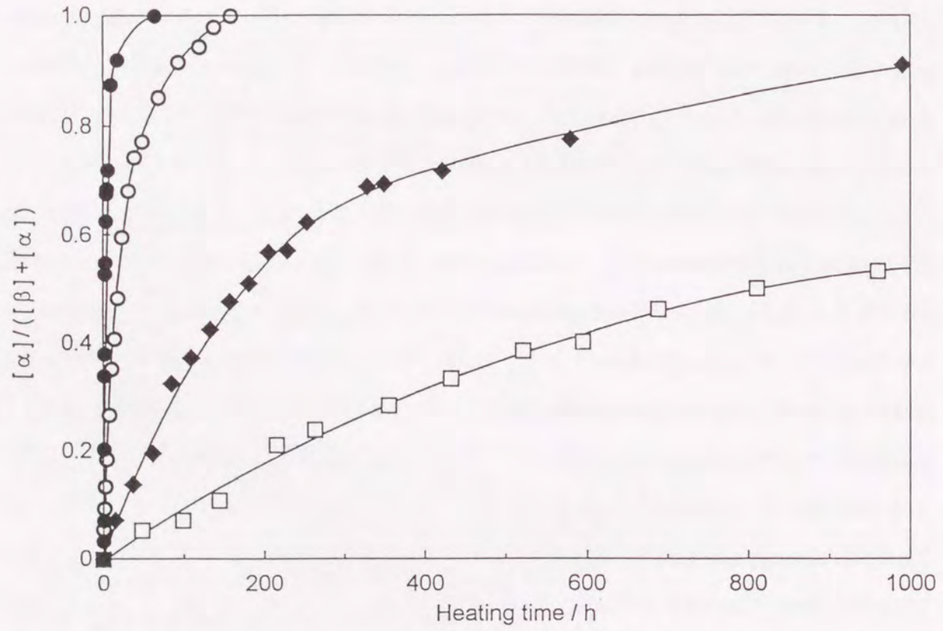

Figure 3–2. Progress of the isomerization of A-β-$(\text{NBu}^{n}_4)_4\text{H}_2[\text{PV}_3\text{W}_9\text{O}_{40}]$ to the α-isomer heated at 40(□), 60(◆), 80(○), and 100°C(●) in the solid state.

$$\ln(1-[\alpha]/([\beta]+[\alpha])) = \ln([\beta]/([\beta]+[\alpha])) = -k_1 t \quad (3\text{–}2)$$

where [α] and [β] are the concentration of the α- and β-isomers, respectively. Plots of ln([β]/([β]+[α])) vs. time for the isomerization at each temperature are shown in Fig. 3–3. Linear correlations between them are observed up to 60–70% completion of the isomerization. From the slopes of their plots the first-order rate constants, k_1, were evaluated to be 2.19×10^{-7} (s^{-1}) at 40°C, 1.02×10^{-6} (s^{-1}) at 60°C, 9.64×10^{-6} (s^{-1}) at 80°C, and 7.94×10^{-5} (s^{-1}) at 100°C. Figure 3–4 shows Eyring plots for the rate constants. The activation parameters were calculated using the Eyring equation: $\Delta H^{\ddagger} = 93.3$ (kJ mol^{-1}) and $\Delta S^{\ddagger} = -77.3$ (J K^{-1} mol^{-1}).

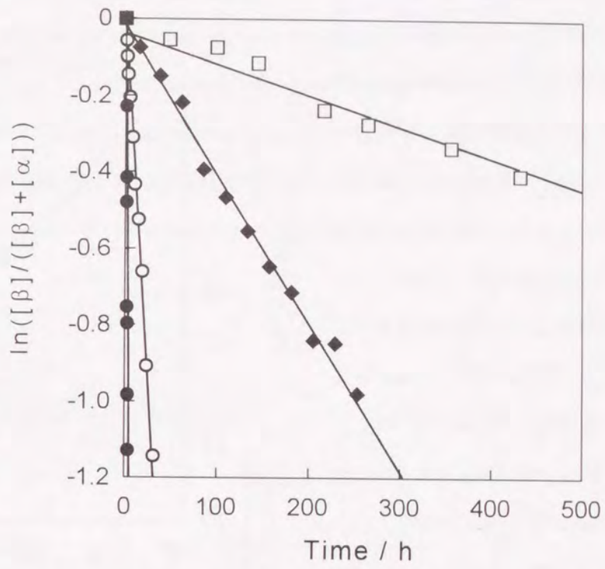

Figure 3–3. Plots of ln([β]/([β]+[α])) vs. time for the isomerization of A-β-$(\text{NBu}^{n}_4)_4\text{H}_2[\text{PV}_3\text{W}_9\text{O}_{40}]$ to the α-isomer heated at 40(□), 60(◆), 80(○), and 100°C(●) in the solid state.

The other β-isomers, A-β-$\text{Cs}_{5.4}\text{H}_{0.6}[\text{PV}_3\text{W}_9\text{O}_{40}]$, A-β-$(\text{NBu}^{n}_4)_6[\text{PV}_3\text{W}_9\text{O}_{40}]$, and A-β-$[\text{PM}_3\text{W}_9\text{O}_{40}]^{n-}$ anion salts (M = Nb, n = 6; M = Mo, n = 3), were also heated at 100°C in the solid state for several hours. However, the ^{31}P NMR spectra of them measured in deuterium oxide or wet acetonitrile-d_3 were identical with those of the respective unheated β-isomers, indicating no isomerization to the α-isomers. The difference between these β-isomers and A-β-$(\text{NBu}^{n}_4)_4\text{H}_2[\text{PV}_3\text{W}_9\text{O}_{40}]$ is that the number of protons in their cation parts is up to one for the former and two for the latter. These results suggest that protonation to

the polyanion of A-β-$(NBu^n_4)_4H_2[PV_3W_9O_{40}]$ promotes the β-to-α isomerization in the solid state.

Figure 3–5 shows the FT-IR spectral changes of an acetonitrile solution containing A-β-$(NBu^n_4)_4H_2[PV_3W_9O_{40}]$ at 60°C. In the region of 1200–600 cm^{-1}, there occur four major bands characteristic of the Keggin-type structure. They are assigned to P–O_i [7], M=O_t (M = V and W), M–O_{bc}–M, and M–O_{be}–M stretching modes, as described in chapter 1 [8]. In the region of the obscured O_{bc} band, a new one develops at 885 cm^{-1} with time. Concomitantly, the O_i band (1078 cm^{-1}) decreases, while a new one in the higher frequency (1088 cm^{-1}) increases. The final spectrum in Fig. 3–5 was changed no more by further heating of the solution at 60°C and agreed well with that of the A-α-$(NBu^n_4)_4H_2[PV_3W_9O_{40}]$.

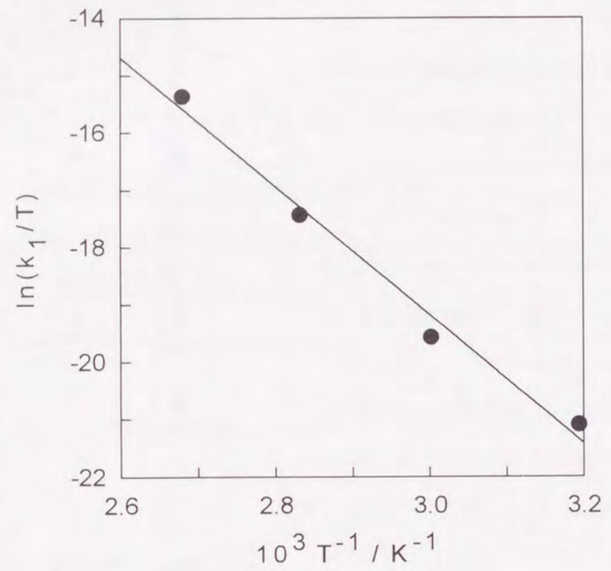

Figure 3–4. Eyring plots of the rate constants for the isomerization of A-β-$(NBu^n_4)_4H_2[PV_3W_9O_{40}]$ to the α-isomer in the solid state.

The ^{31}P NMR spectrum of an acetonitrile-d_3 solution containing A-β-$(NBu^n_4)_4H_2[PV_3W_9O_{40}]$ showed the spectral changes similar to those observed for the compound heated in the solid state depicted in Fig. 3–1. These findings indicate that the β-form also isomerizes to the α-one in solution. The progress of the isomerization in acetonitrile-d_3 was examined in the presence of some kinds of proton sources. It was

evaluated by the intensity ratios of the ^{31}P NMR signals of the β- and α-isomers, as depicted in Fig. 3–6. The rate of the isomerization increases by the addition of HCl. Furthermore, the presence of DCl instead of HCl appreciably decreases the rate, indicating a deuterium effect. These results indicate that the appreciable increase of proton concentration in the solution promotes the protonation to the polyanion and consequently accelerates the β-to-α isomerization. On the other hand, in the presence of a large amount of H_2O the rate of the isomerization decreases compared with that in dry acetonitrile-d_3. This is presumably due to the depression of the protonation caused by the addition of H_2O to the solution.

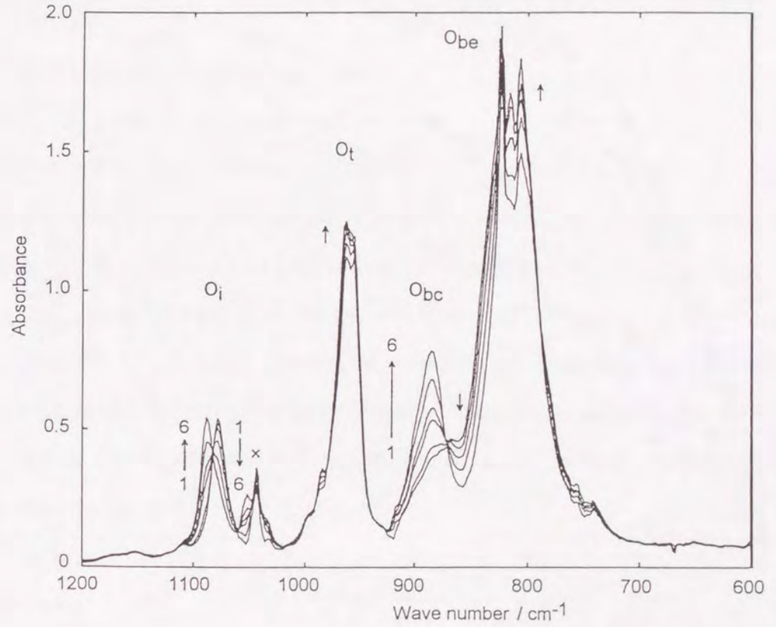

Figure 3–5. FT-IR spectral changes of an acetonitrile solution containing A-β-$(NBu^n_4)_4H_2[PV_3W_9O_{40}]$ (2.40×10^{-2} mol dm^{-3}): reaction time at 60°C: 0(1), 20(2), 98(3), 164(4), 315(5), and 644 h(6). ×: peak of the solvent.

A-β-$(NBu^n_4)_4H_2[PV_3W_9O_{40}]$ has two protons. One of them is probably bound to the bridging oxygen atom (O_{bc}) in the V–O–V bond, because it is the most basic one among the oxygen atoms in the polyanion, as previously described for the A-β-$[HSiV_3W_9O_{40}]^{6-}$ anion [9]. The other protonation site is considered to be the bridging oxygen atom (O_{bc}) between the W_{cap} and W_{belt} atoms [10], as illustrated in Fig. 3–7, on the basis of the finding that the protonation to the A-β-$[PV_3W_9O_{40}]^{6-}$ anion promotes the β-to-α isomerization. On the other hand, A-β-$Cs_{5.4}H_{0.6}[PV_3W_9O_{40}]$ and A-β-$(NBu^n_4)_5H[PNb_3W_9O_{40}]$ did not isomerize under the same conditions as described above, although they had one proton or less in the cation parts. The protonation to the bridging oxygen atom (O_{bc}) in the V–O–V bond of A-β-$Cs_{5.4}H_{0.6}[PV_3W_9O_{40}]$ is suggested by the structural determination as

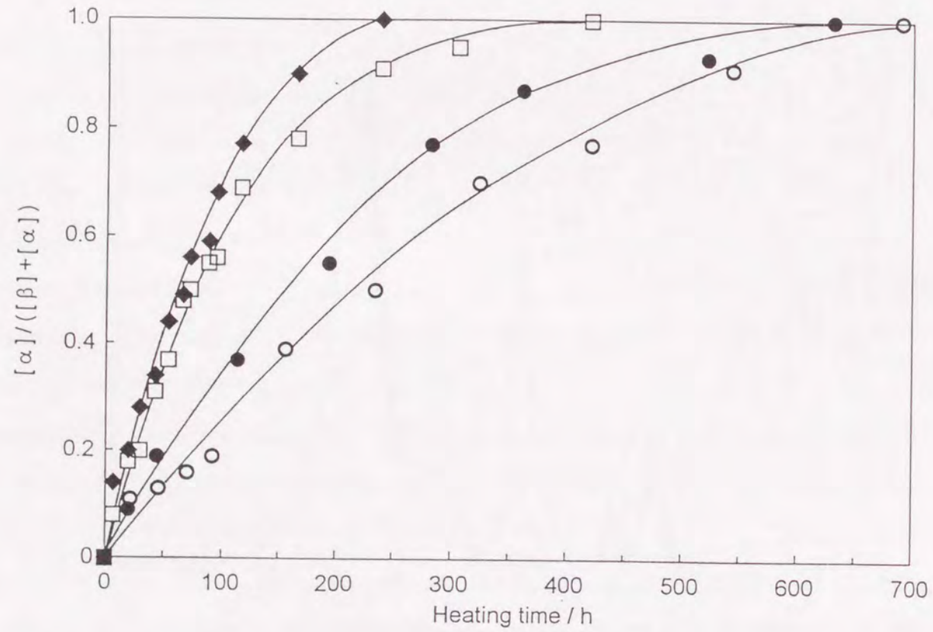

Figure 3–6. Progress of the isomerization of A-β-$(NBu^n_4)_4H_2[PV_3W_9O_{40}]$ to the α-isomer in dry acetonitrile-d_3(●) at 60°C, and in the presence of H_2O(○), 0.1M HCl(◆), and 0.1M DCl(□), where 100 equivalent amounts of the additive to the salt were used.

described in chapter 2. The proton in A-β-$(NBu^n_4)_5H[PNb_3W_9O_{40}]$ is also considered to be bound to the bridging oxygen atom (O_{bc}) in the Nb–O–Nb bond, because it is the most basic one among the oxygen atoms in the polyanion, as previously described for the A-β-$[SiNb_3W_9O_{40}]^{7-}$ anion [11]. It is, therefore, suggested that protonation to the bridging oxygen atom (O_{bc}) in the M–O–M (M = V and Nb) bond is not responsible for the β-to-α isomerization.

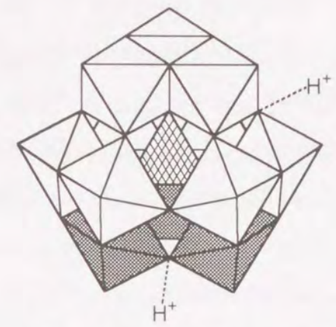

Figure 3–7. Polyhedral representation of the A-β-$[H_2PV_3W_9O_{40}]^{4-}$ anion together with probable protonation sites. Hatched, plain, and shaded parts indicate the central PO_4 tetrahedron, WO_6 octahedra, and VO_6 octahedra, respectively.

3.4 Conclusion

A-β-$(NBu^n_4)_4H_2[PV_3W_9O_{40}]$ isomerized to A-α-$(NBu^n_4)_4H_2[PV_3W_9O_{40}]$ both in the solid state and in solution under mild conditions.

The isomerization process was directly followed by FT-IR and ^{31}P NMR spectroscopies, which afforded its kinetics as a first-order reaction in the β-isomer. In contrast, the other β-isomers of A-type metal-trisubstituted dodecatungsto-phosphate anion salts, A-β-$[PM_3W_9O_{40}]^{n-}$ (M = V and Nb, n = 6; M = Mo, n = 3), containing one proton or less in their cation parts did not isomerize under the same conditions. It was suggested that the β-to-α isomerization was promoted by protonation to the bridging oxygen atom in the W–O–W bond of the polyanion.

3.5 References

1 K. Y. Matsumoto, A. Kobayashi, and Y. Sasaki, *Bull. Chem. Soc. Jpn.*, **48**, 3146 (1975), and references therein.

2 V. F. Umland, F. Pottkamp, and F. Alt, *Z. Anorg. Allg. Chem.*, **395**, 320 (1973); V. M.

Plöger, F. Pottkamp, and V. F. Umland, *Z. Anorg. Allg. Chem.*, **407**, 211 (1974).

3 M. T. Pope, "Heteropoly and Isopoly Oxometalates", Springer-Verlag, Berlin, p.65 (1983).

4 R. Massart, *Ann. Chim.*, **3**, 507 (1968).

5 V. W. Truesdale, C. J. Smith, and P. J. Smith, *Analyst*, **102**, 73 (1977).

6 About 100 equivalent amounts of H_2O to the salt were added in the wet acetonitrile-d_3, as described in chapter 1.

7 The oxygen atoms of the Keggin-type anion are classified into four species, O_i, O_t, O_{bc}, and O_{be}, as described in General Introduction.

8 C. Rocchiccioli-Deltcheff, R. Thouvenot, and R. Franck, *Spectrochim. Acta, Part A*, **32**, 587 (1976); C. Rocchiccioli-Deltcheff, M. Fournier, R. Franck, and R. Thouvenot, *Inorg. Chem.*, **22**, 207 (1983); R. Thouvenot, M. Fournier, R. Franck, and C. Rocchiccioli-Deltcheff, *Inorg. Chem.*, **23**, 598 (1984).

9 R. G. Finke, B. Rapko, R. J. Saxton, and P. J. Domaille, *J. Am. Chem. Soc.*, **108**, 2947 (1986).

10 The metal atoms of the β-isomer of the Keggin-type heteropolyanion are classified into three species: M_{cap}, M_{belt}, and M_{bottom} as described in reference 44 in chapter 2.

11 R. G. Finke and M. W. Droege, *J. Am. Chem. Soc.*, **106**, 7274 (1984).

Chapter 4

Reductions of the α-Dodecamolybdophosphate Anion Salt and of the A-Type Molybdenum-Trisubstituted Dodecatungstophosphate Anion Salt with Triphenylphosphine, and Spectroscopic Properties of the Isolated Oxygen-Deficient Reduced Species

4.1 Introduction

α-Dodecamolybdophosphate (α-$H_3[PMo_{12}O_{40}]$) and related compounds are known as practical oxidation catalysts and their redox mechanisms have systematically been studied in relation to their catalytic functions [1–7]. In heterogeneous (vapor/solid phase) redox processes, behavior of the lattice oxygen atoms of the polyanion attracted much attention and it was well clarified that the α-dodecamolybdophosphate anion was reduced by hydrogen or organic substrates (methacrolein, cyclohexane, and isobutyric acid) accompanied by elimination of the bridging oxygen atom in the Mo–O–Mo bond [1–4]. In addition, the electronic structure calculation for the polyanion revealed that the bridging oxygen atoms in the Mo–O–Mo bonds were exclusively reactive among the oxygen species [5]. However, only a few studies were reported on the characterization of the oxygen-deficient reduced forms, which were isolated by the heterogeneous reduction of the polyanion with hydrogen or organic substrates at elevated temperature [4, 6]. Under these conditions, the polyanion reduced in the solid state was liable to decompose [7] and to be reduced with some heterogeneity [4]. Although the polyanion can be characterized as a structurally well-defined oxomolybdenum complex [1, 7], an oxygen-transfer reaction of the polyanion in a homogeneous system has not been reported so far. It is therefore of interest to investigate a stoichiometric reduction of the polyanion under rather mild conditions and to characterize properties and geometries of the oxygen-deficient reduced polyanion species.

The bridging oxygen atoms in the Mo–O–Mo bonds of the α-dodecamolybdophosphate anion are classified into two species, the corner-sharing one (O_{bc}) and the edge-sharing one

(O_{be}) [8]. However, no investigations have been done to clarify the difference in the reactivity between these two bridging oxygen atoms so far. A structurally designed mixed addenda heteropolyanion, A-β-$[PMo_3W_9O_{40}]^{3-}$ is advantageous to evaluate the individual reactivity of each bridging oxygen atom, because three Mo atoms in this polyanion are linked to each other through only the O_{bc} atoms, and three MoO_6 octahedra are coordinated to the "unreactive" PW_9O_{34} unit.

In this chapter, triphenylphosphine (PPh_3) was used as a reducing agent, which was known to abstract an oxygen atom from oxomolybdenum complexes [9], and reductions of α-$(NBu^n_4)_3[PMo_{12}O_{40}]$ and of A-β-$(NBu^n_4)_3[PMo_3W_9O_{40}]$ with PPh_3 were investigated in a non-aqueous solution. In this system, the polyanions were homogeneously reduced without hydrolytic decomposition. The reduction processes were directly followed by FT-IR and ^{31}P NMR spectroscopies. The oxygen-deficient reduced species were isolated and characterized by X-ray diffractometry, IR, ^{31}P NMR, and X-ray photoelectron spectroscopies. Behavior of the lattice oxygen atoms of the polyanions upon reduction was also discussed. This is the first study on the reactivity of the O_{bc} atom in the Mo–O–Mo bond of the Keggin-type polyanion in the absence of the corresponding O_{be} atom.

4.2 Experimental

Materials. Tetrabutylammonium α-dodecamolybdophosphate(3–), α-$(NBu^n_4)_3[PMo_{12}O_{40}]$, was prepared by the cation-exchange reaction of commercially available α-dodecamolybdophosphoric acid triacontahydrate, α-$H_3[PMo_{12}O_{40}]\cdot 30H_2O$, with an excess amount of NBu^n_4Br in methanol. The precipitates were filtered and recrystallized from acetonitrile to give yellow crystals. Anal. Found: C, 22.57; H, 4.26; N, 1.59%. Calcd for $C_{48}H_{108}N_3O_{40}PMo_{12}$: C, 22.61; H, 4.27; N, 1.65%. Tetrabutylammonium α-dodecatungstophosphate(3–), α-$(NBu^n_4)_3[PW_{12}O_{40}]$, was prepared in the same manner. Preparation of tetrabutylammonium A-β-trimolybdononatungstophosphate(3–), A-β-$(NBu^n_4)_3[PMo_3W_9O_{40}]$, was described in

chapter 1. Tetrabutylammonium α-monomolybdoundecatungstophosphate(3–), α-$(NBu^n_4)_3[PMoW_{11}O_{40}]$, was prepared according to the procedures in the literature [10].

Reactions of the Tetrabutylammonium Salts with PPh_3. Reactions of the tetrabutylammonium salts with one or two equimolar amounts of PPh_3 were homogeneously carried out in acetonitrile under a nitrogen atmosphere. The progress of the reactions was followed by the amount of triphenylphosphine oxide ($OPPh_3$) formed in the solution. The concentration of $OPPh_3$ was determined from the intensities of the FT-IR bands at 1194 and 544 cm^{-1}, since a linear relationship between them was obtained independent of the coexistence of the other species in the solution. The same reactions were done in acetonitrile-d_3 degassed by the freeze-thaw cycle method. The ^{31}P NMR spectra of the solutions contained in a sealed NMR tube were measured at different times.

Neither α-$(NBu^n_4)_3[PW_{12}O_{40}]$ nor α-$(NBu^n_4)_3[PMoW_{11}O_{40}]$ reacted with PPh_3 under similar conditions, which was confirmed by the FT-IR spectra of the reaction solutions.

Isolation of the Reduced Species. An acetonitrile (200 cm^3) solution containing α-$(NBu^n_4)_3[PMo_{12}O_{40}]$ (4.00 g, 1.57 mmol) and an equimolar amount of PPh_3 (0.412 g, 1.57 mmol) was refluxed under a nitrogen atmosphere. After all amounts of PPh_3 were oxidized to $OPPh_3$, the solvent was evaporated to dryness under reduced pressure. A residue was washed with methanol to remove $OPPh_3$ and dried in vacuo to afford the dark blue, two-electron reduced compound, α-$(NBu^n_4)_3[PMo_{12}O_{39}]$, (3.31 g, 83% yield). Anal. Found: C, 22.86; H, 4.28; N, 1.59; Mo, 45; P, 1.3. Calcd for $C_{48}H_{108}N_3Mo_{12}O_{39}P$: C, 22.76; H, 4.30; N, 1.66; Mo, 45.4; P, 1.22%.

A reaction of α-$(NBu^n_4)_3[PMo_{12}O_{40}]$ (4.00 g, 1.57 mmol) with two equimolar amounts of PPh_3 (0.824 g, 3.14 mmol) was done in the same manner, affording the dark-blue, four-electron reduced compound, α-$(NBu^n_4)_3[PMo_{12}O_{38}]$, (3.24 g, 82% yield). Anal. Found: C, 22.71; H, 4.20; N, 1.62; Mo, 46; P, 1.3. Calcd for $C_{48}H_{108}N_3Mo_{12}O_{38}P$: C, 22.90; H, 4.32; N, 1.67; Mo, 45.7; P, 1.23%.

A reaction of A-β-$(NBu^n_4)_3[PMo_3W_9O_{40}]$ (1.77 g, 0.530 mmol) with an equimolar

amount of PPh_3 (0.139 g, 0.530 mmol) was done in acetonitrile (100 cm^3) at 60°C under a nitrogen atmosphere. According to the same procedure described above, was obtained the dark-blue, two-electron reduced compound, A-β-$(NBu^n_4)_3[PMo_3W_9O_{39}]$ (1.46 g, 83% yield). Found: C, 17.37; H, 3.15; N, 1.26; Mo, 8.6; P, 0.97; W, 48%. Calcd for $C_{48}H_{108}N_3Mo_3O_{39}PW_9$: C, 17.34; H, 3.27; N, 1.26; Mo, 8.66; P, 0.93; W, 49.77%.

Reoxidation of the Reduced Compounds. These reduced compounds were heated at 200°C in the air for half an hour to change from dark-blue to bluish-green. The bluish-green powders were dissolved in acetonitrile and oxygen gas was bubbled through the solution. After the solution turned pale greenish-yellow, it was evaporated to dryness under reduced pressure to afford the reoxidized compounds.

Physical measurements. Measurements of FT-IR spectra were described in chapter 3. Electronic absorption spectra were measured with a Hitachi 340 spectrophotometer using a quartz cell with a 1-mm light path. Both the measurements were carried out under a nitrogen atmosphere. X-ray photoelectron spectra were measured for compressed pellet samples with a Shimadzu ESCA-750 spectrometer employing MgKα radiation at 5 kV and 30 mA. All the spectra were referenced to the C $1s_{1/2}$ signal of the tetrabutylammonium cation at 285.0 eV for correction of the charge effect. Deconvolution of the spectra was carried out with a Shimadzu ESCAPAC-760 data system employing a Gaussian-Lorentzian shape fit. X-ray diffraction patterns were measured with a Rigaku Denki roterflex X-ray diffractometer RAD-rA employing CuKα radiation at 40 kV and 100 mA. ^{31}P NMR spectra of the reaction solution of α-$(NBu^n_4)_3[PMo_{12}O_{40}]$ were measured with a JEOL JNM-FX90Q spectrometer operating at 36.23 MHz. The sample was dissolved in acetonitrile-d_3 (ca. 0.01 mol dm^{-3}) degassed by the freeze-thaw cycle method and sealed. Chemical shifts were determined by using the sample replacement method [11] externally referenced to 30%H_3PO_4 and reported in ppm with negative value upfield from the standard. NMR parameters: 30° pulse width, 6 μs; sweep width, 400, 1000, and 2500 Hz; relaxation delay, 20 s; number of acquisition, 100–300. Measurements

of ^{31}P NMR spectra of the reaction solution of A-β-$(NBu^n_4)_3[PMo_3W_9O_{40}]$ were the same as those described in chapter 1.

4.3 Results and discussion

Reactions of α-$(NBu^n_4)_3[PMo_{12}O_{40}]$ with PPh_3. A yellow acetonitrile solution containing α-$(NBu^n_4)_3[PMo_{12}O_{40}]$ and an equimolar amount of PPh_3 gradually turned green and finally dark-blue. The FT-IR spectral changes of the solution at 23°C are shown in Fig. 4–1. The absorption band ascribed to PPh_3 at 505 cm^{-1} decreases in intensity with time. Concomitantly, the bands ascribed to $OPPh_3$ arise at 1194 (ν(P=O)) [12] and 544 cm^{-1}. These findings indicate that PPh_3 reduces α-$(NBu^n_4)_3[PMo_{12}O_{40}]$

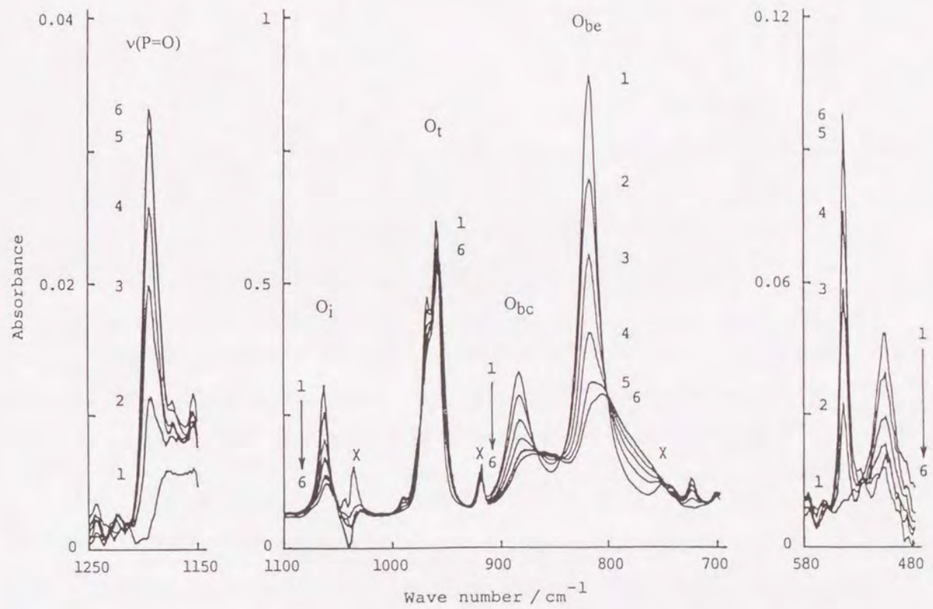

Figure 4–1. FT-IR spectral changes of an acetonitrile solution containing α-$(NBu^n_4)_3[PMo_{12}O_{40}]$ (6.00×10^{-3} mol dm^{-3}) and an equimolar amount of PPh_3: reaction time at 23°C: 0.1(1), 24(2), 73(3), 174(4), 506(5), and 1039 h(6). ×: peaks of the solvent.

accompanying the oxygen atom transfer from the polyanion to PPh_3. The progress of the reduction was followed by the amount of $OPPh_3$ formed in the solution. As shown in Fig. 4–2, all amounts of PPh_3 are finally oxidized to $OPPh_3$ in the reaction.

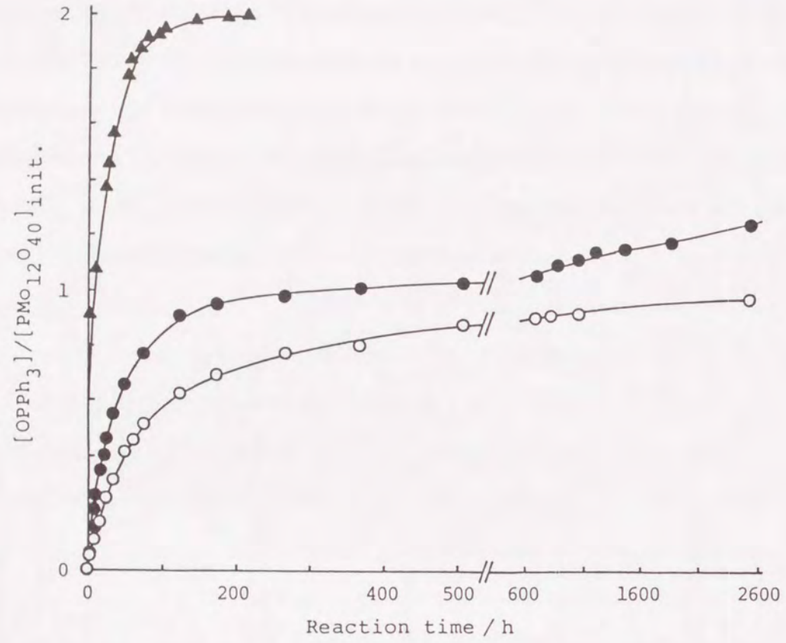

Figure 4–2. Amounts of $OPPh_3$ formed in reactions of α-$(NBu^n_4)_3[PMo_{12}O_{40}]$ with an equimolar amount of PPh_3 at 23°C (○), and two equimolar amounts of PPh_3 at 23°C (●) and at the reflux temperature (▲) in acetonitrile: $[PMo_{12}O_{40}]_{init.}$: the initial concentration of α-$(NBu^n_4)_3[PMo_{12}O_{40}]$.

In the region of 1100–700 cm^{-1} (Fig. 4–1), there are four major bands (O_i, O_t, O_{bc}, and O_{be} bands [13]) characteristic of the Keggin-anion structure. During the reaction, the O_i and two O_b bands drastically decrease in their intensities and gradually shift to lower frequencies, whereas the O_t band is appreciably broadened. The absorbances of the O_i and

two O_b bands decrease quite linearly with the degree of the reduction progress. Although the O_t band apparently decreases in absorbance, its band area is almost unchanged during the reaction, as illustrated in Fig. 4–3.

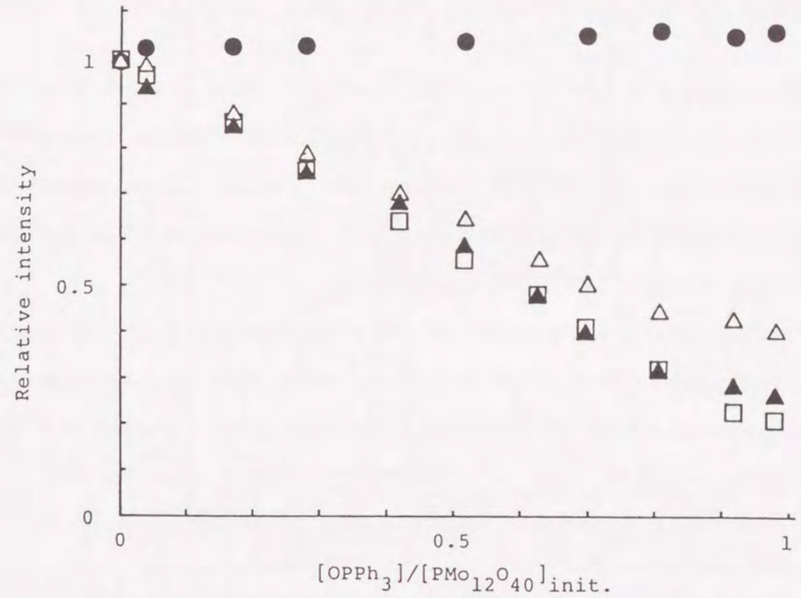

Figure 4–3. The variation in intensity of the FT-IR bands of α-$(NBu^n_4)_3[PMo_{12}O_{40}]$ during the reaction with an equimolar amount of PPh_3 in acetonitrile at 23°C. Relative intensity is based on the absorbance for the O_i(□), O_{bc}(△), and O_{be}(▲) bands and on the band area for the O_t band(●).

These findings suggest that the bridging oxygen atom in the Mo–O–Mo bond is eliminated in the reduction of the polyanion, which results in the depress of the symmetry of the polyanion and the weakened O_i and two O_b bands. The similar spectral behavior was also observed for the reduction of the α-dodecamolybdophosphate anion in a heterogeneous (vapor/solid phase) system [1–4]. Furthermore, the electronic structure calculation for the α-dodecamolybdophosphate anion revealed that the bridging oxygen atoms in the Mo–O–Mo

bonds were exclusively reactive among the oxygen species [5]. Consequently, in the present reaction, two-electron reduction of α-$(NBu^n_4)_3[PMo_{12}O_{40}]$ by PPh_3 homogeneously proceeds according to the reaction (Eq. 4–1), accompanied by the transfer of

$$\alpha\text{-}(NBu^n_4)_3[PMo_{12}O_{40}] + PPh_3 \rightarrow \alpha\text{-}(NBu^n_4)_3[PMo_{12}O_{39}] + OPPh_3 \qquad (4\text{–}1)$$

one bridging oxygen atom in the Mo–O–Mo bond to PPh_3. However, the difference in the reactivity between the O_{bc} and O_{be} atoms was equivocal, since even the reduction of the Keggin-type polyanion without any elimination of the lattice oxygen atom resulted in the symmetry depression of the polyanion to weaken the O_i, O_{bc}, and O_{be} bands, as reported for the electrochemical reduction of $H_3[PMo_{12}O_{40}]$ [2, 4].

As shown in Fig. 4–2, the reaction of α-$(NBu^n_4)_3[PMo_{12}O_{40}]$ with two equimolar amounts of PPh_3 in acetonitrile at 23°C proceeds very slowly in the reduction process of the two-electron reduced species, whereas at the reflux temperature all amounts of PPh_3 are finally oxidized to $OPPh_3$; that is, α-$(NBu^n_4)_3[PMo_{12}O_{40}]$ undergoes four-electron reduction by two equimolar amounts of PPh_3 according to the reaction (Eq. 4–2).

$$\alpha\text{-}(NBu^n_4)_3[PMo_{12}O_{40}] + 2\ PPh_3 \rightarrow \alpha\text{-}(NBu^n_4)_3[PMo_{12}O_{38}] + 2\ OPPh_3 \qquad (4\text{–}2)$$

The FT-IR spectral changes of the reaction (Eq. 4–2) in acetonitrile at the reflux temperature showed considerable decreases of O_i and two O_b bands in absorbance, while the band area of the O_t band was almost unchanged during the reaction. Figure 4–4 shows the FT-IR spectra of the isolated two- and four-electron reduced compounds in acetonitrile together with that of α-$(NBu^n_4)_3[PMo_{12}O_{40}]$. The similar features were observed for the spectra of them measured in KBr pellets. This spectral behavior indicates that the second oxygen atom eliminated from α-$(NBu^n_4)_3[PMo_{12}O_{39}]$ is also ascribed to the bridging oxygen atom in the Mo–O–Mo bond.

Spectroscopic Properties of the Reduced Compounds of α-$(NBu^n_4)_3[PMo_{12}O_{40}]$. The X-ray photoelectron spectra of the Mo 3d electrons of α-$(NBu^n_4)_3[PMo_{12}O_{40}]$ and the

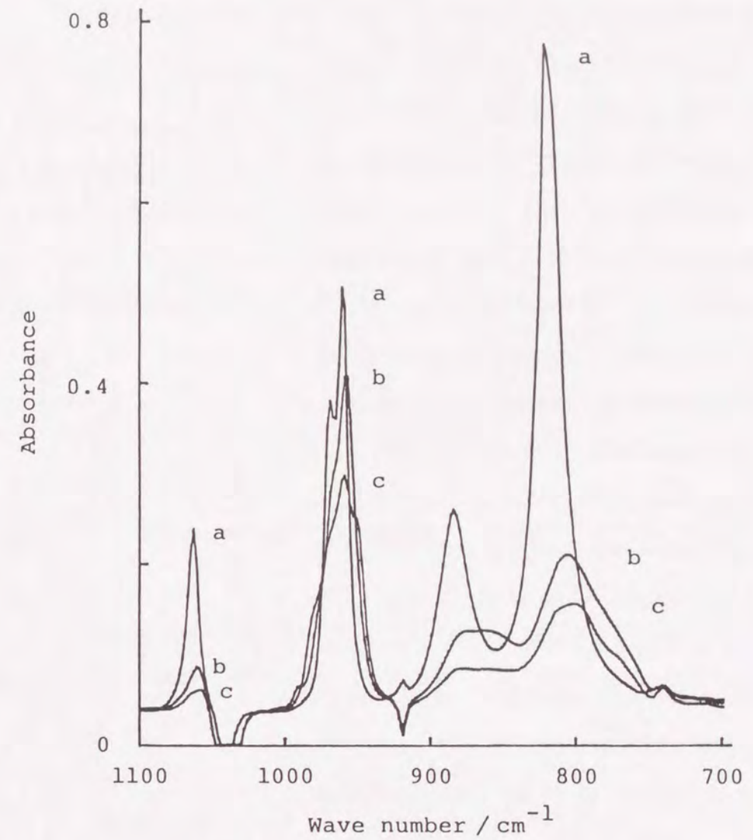

Figure 4–4. FT-IR spectra of α-$(NBu^n_4)_3[PMo_{12}O_{40}]$ (a), α-$(NBu^n_4)_3[PMo_{12}O_{39}]$ (b), and α-$(NBu^n_4)_3[PMo_{12}O_{38}]$ (c) (5.00×10^{-3} mol dm^{-3}) in acetonitrile.

reduced compounds are shown in Fig. 4–5. The spectrum of α-$(NBu^n_4)_3[PMo_{12}O_{40}]$ exhibits the characteristic doublet due to Mo(VI) $3d_{5/2}$ and Mo(VI) $3d_{3/2}$ electrons, which is caused by the spin-orbit coupling [14]. The doublet observed for α-$(NBu^n_4)_3[PMo_{12}O_{39}]$ is broadened on the lower binding energy sides and that for α-$(NBu^n_4)_3[PMo_{12}O_{38}]$ further broadened. The parameters for deconvolution of these spectra are summarized in Table 4–1.

The separation between $3d_{5/2}$ and $3d_{3/2}$ bands is found to be 3.2 eV and the intensity ratio of them to be 1.2–1.4 for all the deconvoluted curves; these values are in good agreement with those reported for molybdenum oxides [14, 15]. The new doublet which appears at a 1.2–1.3 eV lower energy region compared with that of the Mo(VI) ion can be assigned to the Mo(V) 3d electrons, based on the binding energies for the Mo(V) 3d electrons in α-dodecamolybdophosphate anions [4, 6] and molybdenum oxides [14, 15]. No signals due to Mo(IV) and further reduced molybdenum ions were observed in a lower binding energy region. The contents of Mo(VI) and Mo(V) ions in the reduced compounds estimated from peak areas of the deconvoluted curves are also given in Table 4–1. These results indicate that the two- and four-electron reduced anions are constituted by $[PMo(VI)_{10}Mo(V)_2O_{39}]^{3-}$ and $[PMo(VI)_8Mo(V)_4O_{38}]^{3-}$, respectively. On the other hand, the binding energies of the P 2p electrons of the reduced compounds are almost the same as that of α-$(NBu^n_4)_3[PMo_{12}O_{40}]$ (Table 4–1). This indicates that no internal oxygen atoms (O_i) ligating the phosphorus atom are eliminated during the reduction, the valence state of P(V) being preserved. Therefore, the elimination of one oxygen atom in the

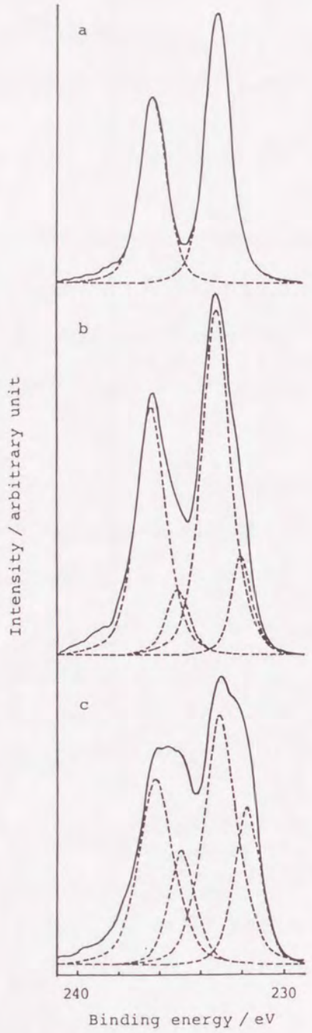

Figure 4–5. X-ray photoelectron spectra of α-$(NBu^n_4)_3[PMo_{12}O_{40}]$ (a), α-$(NBu^n_4)_3[PMo_{12}O_{39}]$ (b), and α-$(NBu^n_4)_3[PMo_{12}O_{38}]$ (c). Dashed lines represent deconvoluted curves.

Table 4–1. Binding Energies (eV) for Deconvoluted Curves[a)]

Compound	Mo(VI) $3d_{3/2}$	Mo(V) $3d_{3/2}$	Mo(VI) $3d_{5/2}$	Mo(V) $3d_{5/2}$	P[b)] 2p
α-$(NBu^n_4)_3[PMo_{12}O_{40}]$	236.1	—	232.9	—	134.4
α-$(NBu^n_4)_3[PMo_{12}O_{39}]$	236.3	235.1	233.1	231.9	135.1
		(0.20)		(0.20)	
α-$(NBu^n_4)_3[PMo_{12}O_{38}]$	236.2	234.9	233.0	231.7	134.6
		(0.47)		(0.50)	

a) Ratio of the peak area of Mo(V) to that of the corresponding Mo(VI) in parentheses.
b) For the original measured peak.

Mo(VI)–O–Mo(VI) bond is reasonably concluded to produce two Mo(V) ions in the polyanion.

The reduced compounds exhibit an intense band in the visible and near infrared regions, as depicted in Fig. 4–6, which is assigned to the intervalence charge transfer

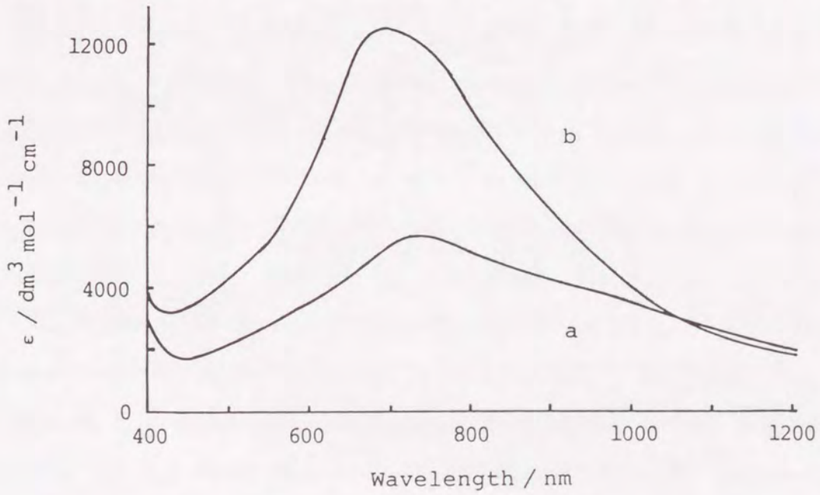

Figure 4–6. Electronic absorption spectra of α-$(NBu^n_4)_3[PMo_{12}O_{39}]$ (a) and α-$(NBu^n_4)_3[PMo_{12}O_{38}]$ (b) in acetonitrile.

(Mo(V)→Mo(VI)) band as was observed for reduced α-dodecamolybdophosphate anions, "heteropoly blues" [16]. The intensity of the band was reported to be proportional to the number of electrons introduced to the polyanion [16, 17]. The intensity of α-$(NBu^n_4)_3[PMo_{12}O_{38}]$ (ε_{max} = 12500 dm^3 mol^{-1} cm^{-1}) is about twice that of α-$(NBu^n_4)_3[PMo_{12}O_{39}]$ (ε_{max} = 5800 dm^3 mol^{-1} cm^{-1}), indicating that the anion structure of the Keggin type is retained in the present two- and four-electron reduced compounds.

The FT-IR spectra of reoxidized compounds of α-$(NBu^n_4)_3[PMo_{12}O_{39}]$ and α-$(NBu^n_4)_3[PMo_{12}O_{38}]$ were essentially identical with that of α-$(NBu^n_4)_3[PMo_{12}O_{40}]$; the O_i, O_t, and two O_b bands were regenerated in intensity and in shape. Furthermore, the X-ray diffraction patterns of the reoxidized compounds are very close to that of α-$(NBu^n_4)_3[PMo_{12}O_{40}]$, although the patterns of the reduced compounds are entirely different from that of α-$(NBu^n_4)_3[PMo_{12}O_{40}]$, as depicted in Fig. 4–7. These observations indicate that no decomposition occurs on the anion structure of the oxygen-deficient reduced compounds.

^{31}P NMR Spectra of the Reduced Compounds of α-$(NBu^n_4)_3[PMo_{12}O_{40}]$. Figure 4–8 shows ^{31}P NMR spectra of an acetonitrile-d_3 solution containing α-$(NBu^n_4)_3[PMo_{12}O_{40}]$ and an equimolar amount of PPh_3 at 23°C. As the reaction proceeds, the signals observed at +0.24 and −1.76 ppm due to α-$(NBu^n_4)_3[PMo_{12}O_{40}]$ and PPh_3, respectively, decrease in their intensities and two new signals develop at +30.6 and −2.36 ppm which are ascribed to $OPPh_3$ and α-$(NBu^n_4)_3[PMo_{12}O_{39}]$, respectively.

Both the ^{31}P NMR spectra of the isolated reduced compounds, α-$(NBu^n_4)_3[PMo_{12}O_{39}]$ and α-$(NBu^n_4)_3[PMo_{12}O_{38}]$, showed a single peak at −2.31 and −2.60 ppm, respectively. Upfield shifts of the signals of these reduced compounds compared with that of α-$(NBu^n_4)_3[PMo_{12}O_{40}]$ were also the same as those of the electrochemically reduced α-dodecamolybdophosphate anion species [18, 19]. No other signals were observed besides those of these reduced compounds, indicating that essentially no other oxidation states of the polyanion were present. In addition, the narrow line

widths ($\Delta\nu_{1/2}$ < 1 Hz) of the observed signals suggest a single anion structure of the Keggin type for each reduced compound.

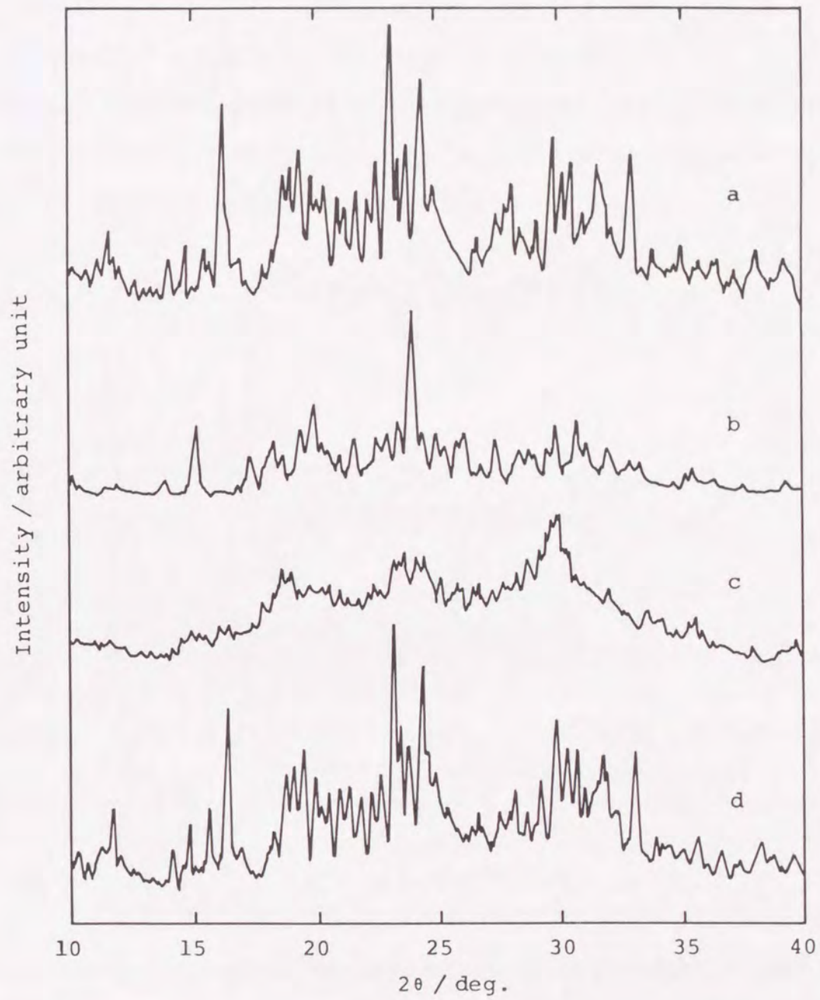

Figure 4–7. X-ray diffraction patterns of α-$(NBu^n_4)_3[PMo_{12}O_{40}]$ (a), α-$(NBu^n_4)_3[PMo_{12}O_{39}]$ (b), α-$(NBu^n_4)_3[PMo_{12}O_{38}]$ (c), and the reoxidized compound of α-$(NBu^n_4)_3[PMo_{12}O_{38}]$ (d).

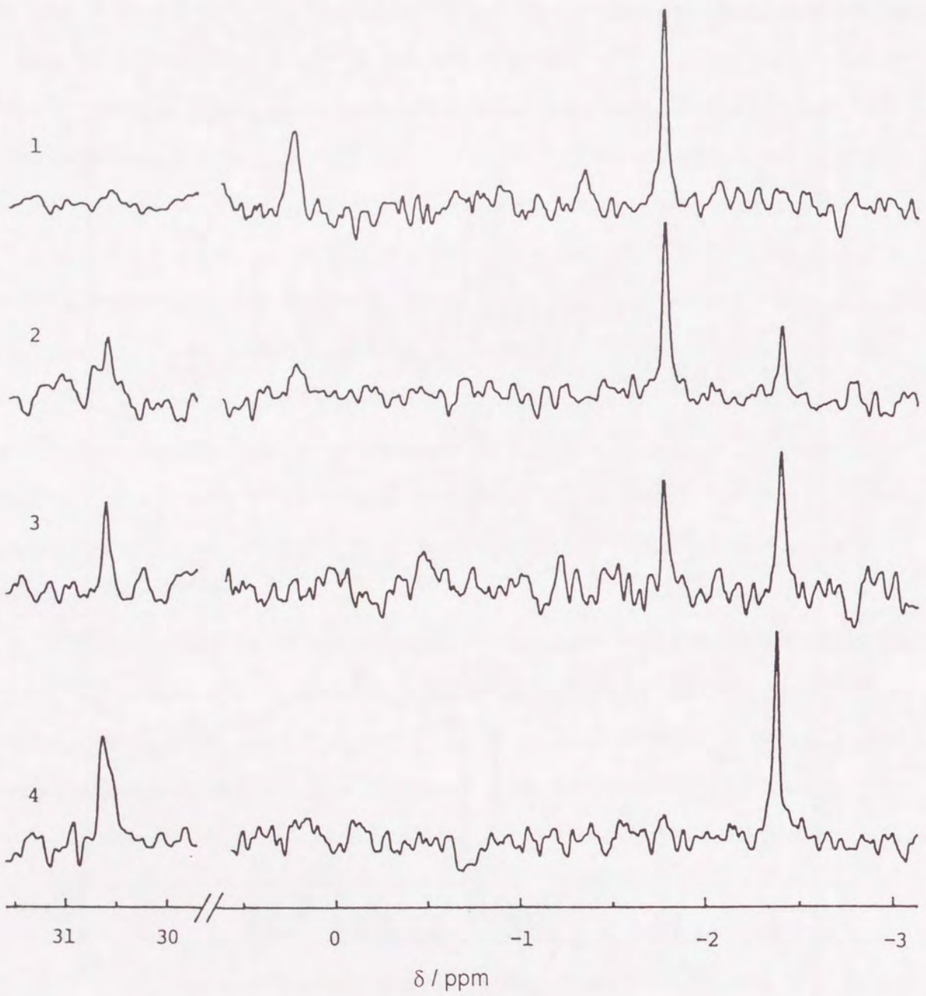

Figure 4–8. ^{31}P NMR spectral changes of an acetonitrile-d_3 solution containing α-$(NBu^n_4)_3[PMo_{12}O_{40}]$ and an equimolar amount of PPh_3: reaction time at 74°C: 0(1), 1.5(2), 2.3(3), and 23 h(4).

Figure 4–9(a) shows the ^{31}P NMR spectrum of an equimolar mixture of α-$(NBu^n_4)_3[PMo_{12}O_{40}]$ and α-$(NBu^n_4)_3[PMo_{12}O_{39}]$ in acetonitrile-d_3. Signals occur at +0.23 ppm (α-$(NBu^n_4)_3[PMo_{12}O_{40}]$, $\Delta\nu_{1/2} < 1$ Hz) and at −2.31 ppm (α-$(NBu^n_4)_3[PMo_{12}O_{39}]$, $\Delta\nu_{1/2} < 1$ Hz) with integrated intensities in the ratio 1:1. An equimolar mixture of α-$(NBu^n_4)_3[PMo_{12}O_{40}]$ and α-$(NBu^n_4)_3[PMo_{12}O_{38}]$ in the same solvent also gives the signals at +0.22 ppm (α-$(NBu^n_4)_3[PMo_{12}O_{40}]$, $\Delta\nu_{1/2} = 2.9$ Hz) and −2.58 ppm (α-$(NBu^n_4)_3[PMo_{12}O_{38}]$, $\Delta\nu_{1/2} = 1.4$ Hz) with integrated intensities in the ratio 1:0.9, although they are somewhat broad (Fig. 4–9(b)). These findings indicate that the

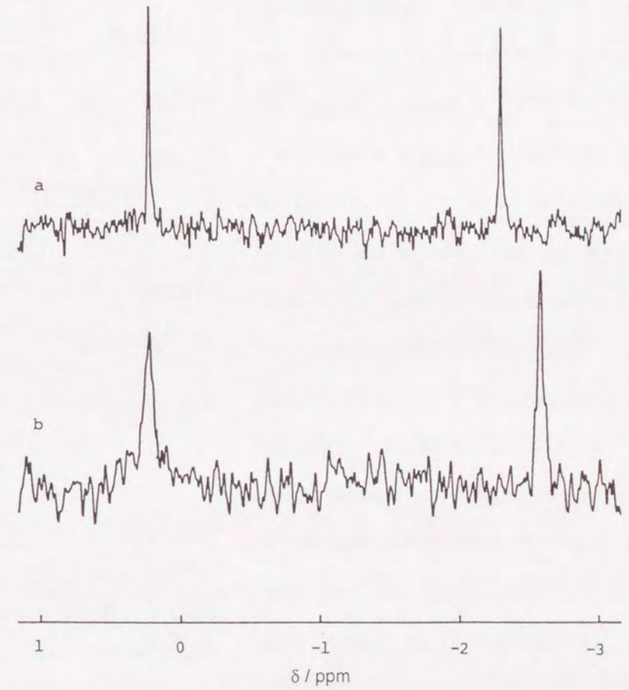

Figure 4–9. ^{31}P NMR spectra of equimolar mixtures of α-$(NBu^n_4)_3[PMo_{12}O_{40}]$ and α-$(NBu^n_4)_3[PMo_{12}O_{39}]$ (a), and α-$(NBu^n_4)_3[PMo_{12}O_{40}]$ and α-$(NBu^n_4)_3[PMo_{12}O_{38}]$ (b) in acetonitrile-d_3.

anion structures of α-$(NBu^n_4)_3[PMo_{12}O_{39}]$ and α-$(NBu^n_4)_3[PMo_{12}O_{38}]$ are not affected by α-$(NBu^n_4)_3[PMo_{12}O_{40}]$ in solution.

On the other hand, a mixture of the two reduced compounds, α-$(NBu^n_4)_3[PMo_{12}O_{39}]$ and α-$(NBu^n_4)_3[PMo_{12}O_{38}]$, in acetonitrile-$d_3$ exhibits a new single resonance at the averaged position between those of α-$(NBu^n_4)_3[PMo_{12}O_{39}]$ and α-$(NBu^n_4)_3[PMo_{12}O_{38}]$ according to their relative amounts, as shown in Fig. 4–10. In the reduction process of α-$(NBu^n_4)_3[PMo_{12}O_{39}]$ with an equimolar amount of PPh_3 in acetonitrile-d_3, the signal of α-$(NBu^n_4)_3[PMo_{12}O_{39}]$ was continuously shifted to a higher field and finally to the position of α-$(NBu^n_4)_3[PMo_{12}O_{38}]$, the intensity and the line width of the peak being almost unchanged. These findings support some interaction between α-$(NBu^n_4)_3[PMo_{12}O_{39}]$ and α-$(NBu^n_4)_3[PMo_{12}O_{38}]$ in the solution. Thus, a pair of Mo(V) ions in α-$(NBu^n_4)_3[PMo_{12}O_{38}]$ is suggested to interact with a bridging oxygen atom of the Mo(VI)–O–Mo(VI) bond in α-$(NBu^n_4)_3[PMo_{12}O_{39}]$ in solution, accompanied by the transfer of an oxygen atom between them within the NMR time scale, as depicted in Scheme 4–1.

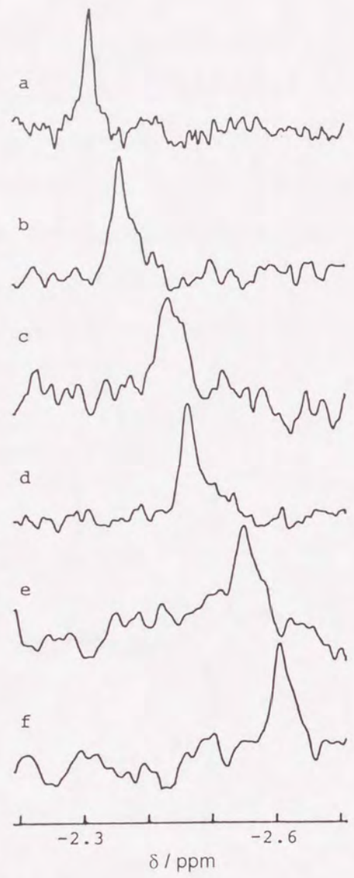

Figure 4–10. ^{31}P NMR spectra of mixtures of α-$(NBu^n_4)_3[PMo_{12}O_{39}]$ and α-$(NBu^n_4)_3[PMo_{12}O_{38}]$ in acetonitrile-d_3: mole fraction of α-$(NBu^n_4)_3[PMo_{12}O_{38}]$: 0(a), 0.34(b), 0.50(c), 0.66(d), 0.89(e), and 1(f).

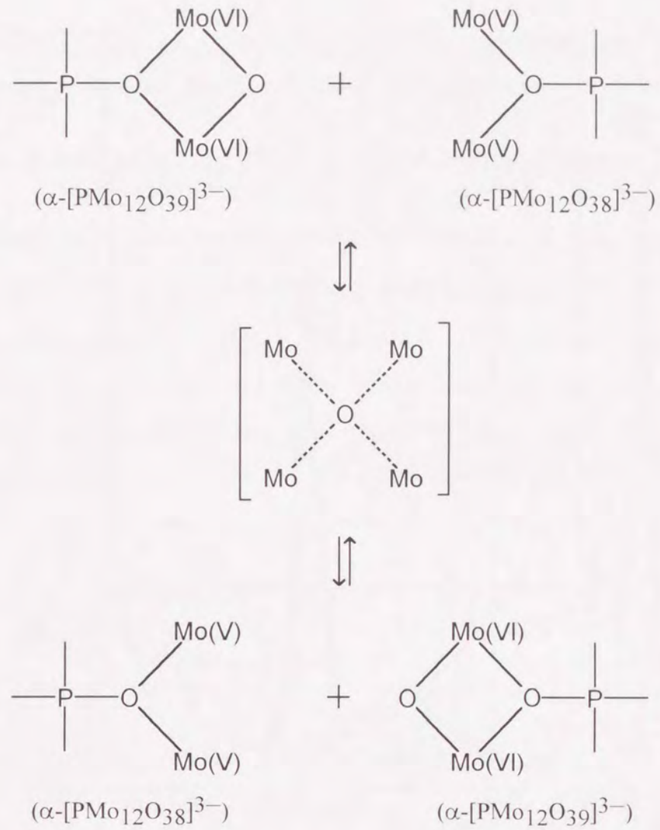

Scheme 4–1.

Reaction of A-β-$(NBu^n_4)_3[PMo_3W_9O_{40}]$ with PPh_3. FT-IR spectral changes of a yellow acetonitrile solution containing A-β-$(NBu^n_4)_3[PMo_3W_9O_{40}]$ and an equimolar amount of PPh_3 at 60°C are shown in Fig. 4–11. Decrease of the PPh_3 band intensities and increase of the $OPPh_3$ ones are observed similar to those for the reaction of α-$(NBu^n_4)_3[PMo_{12}O_{40}]$ with PPh_3 (Fig. 4–1), which also indicates that PPh_3 reduces A-β-$(NBu^n_4)_3[PMo_3W_9O_{40}]$, accompanied with an oxygen atom transfer from the polyanion to PPh_3. The progress of the reduction has been estimated by the IR band of $OPPh_3$ (see the experimental section).

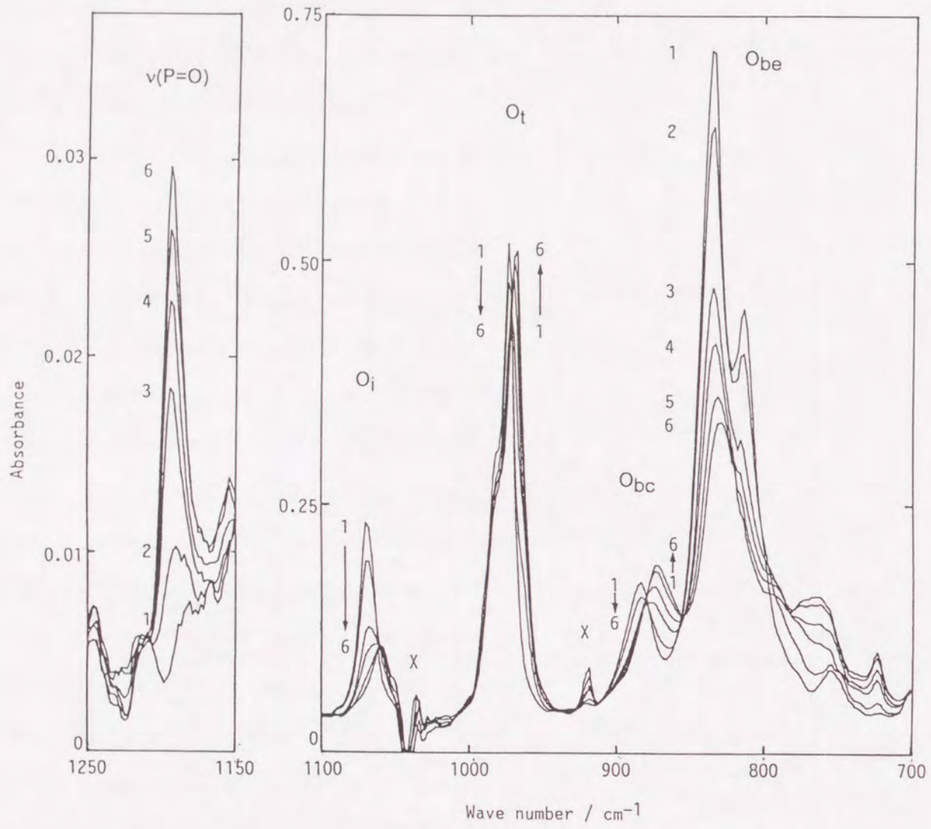

Figure 4–11. FT-IR spectral changes of an acetonitrile solution containing A-β-$(NBu^n_4)_3[PMo_3W_9O_{40}]$ (5.30×10^{-3} mol dm^{-3}) and an equimolar amount of PPh_3: reaction time at 60°C: 0(1), 24(2), 97(3), 151(4), 241(5), and 465 h(6). ×: peaks of the solvent.

In the region of 1100–700 cm^{-1}, the spectral changes of the four major bands (O_i, O_t, O_{bc}, and O_{be} bands [13]) characteristic of the Keggin-anion structure are essentially similar to those observed for the reduction of α-$(NBu^n_4)_3[PMo_{12}O_{40}]$ with PPh_3 (Fig. 4–1). Taking into consideration that neither α-$(NBu^n_4)_3[PW_{12}O_{40}]$ nor α-$(NBu^n_4)_3[PMoW_{11}O_{40}]$ reacts with PPh_3 as described in the experimental section, it is suggested that the corner-sharing bridging oxygen atom in the Mo–O–Mo bond of A-β-

$(NBu^n_4)_3[PMo_3W_9O_{40}]$ is also eliminated during the reduction and the two-electron reduced species, A-β-$(NBu^n_4)_3[PMo_3W_9O_{39}]$, is formed according to the reaction (Eq. 4–3).

$$\text{A-β-}(NBu^n_4)_3[PMo_3W_9O_{40}] + PPh_3 \rightarrow \text{A-β-}(NBu^n_4)_3[PMo_3W_9O_{39}] + OPPh_3 \quad (4\text{–}3)$$

As shown in Fig. 4–12, all amounts of PPh_3 are found to be finally oxidized to $OPPh_3$ in the reaction. The rate of reduction of A-β-$(NBu^n_4)_3[PMo_3W_9O_{40}]$ with PPh_3 is much smaller than that of α-$(NBu^n_4)_3[PMo_{12}O_{40}]$, which may be ascribed to the number of the bridging oxygen atoms in the Mo–O–Mo bonds; only three O_{bc} atoms exist in A-β-$(NBu^n_4)_3[PMo_3W_9O_{40}]$, but there are twelve O_{bc} and twelve O_{be} atoms in α-$(NBu^n_4)_3[PMo_{12}O_{40}]$.

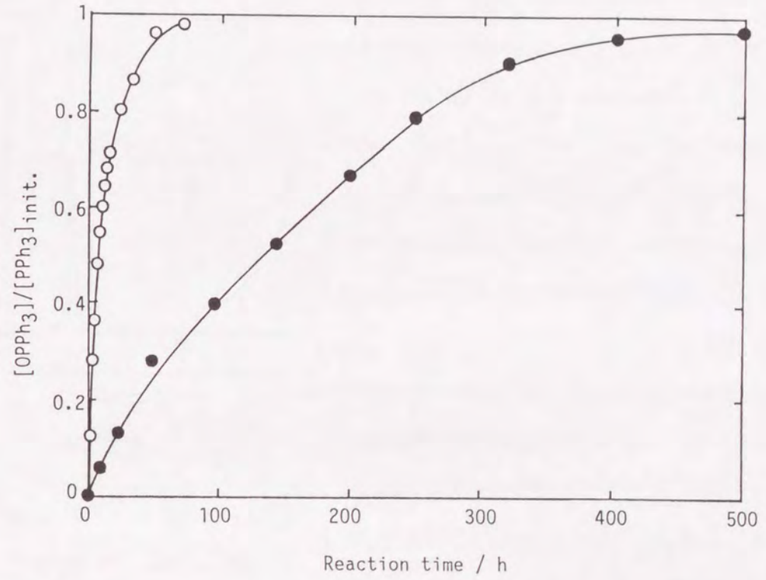

Figure 4–12. Amounts of $OPPh_3$ formed in reactions of α-$(NBu^n_4)_3[PMo_{12}O_{40}]$ (○) and of A-β-$(NBu^n_4)_3[PMo_3W_9O_{40}]$ (●) with an equimolar amount of PPh_3 in acetonitrile at 60°C: $[PPh_3]_{init.}$: the initial concentration of PPh_3.

The reaction was also followed by ^{31}P NMR spectral changes of an acetonitrile-d_3 solution containing A-β-$(NBu^n_4)_3[PMo_3W_9O_{40}]$ and PPh_3. The solution had two signals at −3.93 and −10.05 ppm ascribed to PPh_3 and A-β-$(NBu^n_4)_3[PMo_3W_9O_{40}]$, respectively. The former signal decreased in intensity with time and, concomitantly, the new broad signal ascribable to $OPPh_3$ developed at +28.6 ppm. In accordance with this, a new signal ascribed to A-β-$(NBu^n_4)_3[PMo_3W_9O_{39}]$ occurred at a higher field (−10.11 ppm) than that of A-β-$(NBu^n_4)_3[PMo_3W_9O_{40}]$, as depicted in Fig. 4–13. However, it is noteworthy that the upfield shift (0.06 ppm) of the ^{31}P signal of A-β-$(NBu^n_4)_3[PMo_3W_9O_{40}]$ upon the reduction is very slight compared with that observed for the reduction of α-$(NBu^n_4)_3[PMo_{12}O_{40}]$ (the upfield shift; 2.60 ppm).

Spectroscopic Properties of the Reduced Compound of A-β-$(NBu^n_4)_3[PMo_3W_9O_{40}]$. The IR spectra of A-β-$(NBu^n_4)_3[PMo_3W_9O_{40}]$ and A-β-$(NBu^n_4)_3[PMo_3W_9O_{39}]$ measured in KBr pellets are illustrated in Fig. 4–14. Although the O_i, O_{bc}, and O_{be} bands decreased in their intensities upon the reduction, the entire spectral pattern of A-β-$(NBu^n_4)_3[PMo_3W_9O_{39}]$

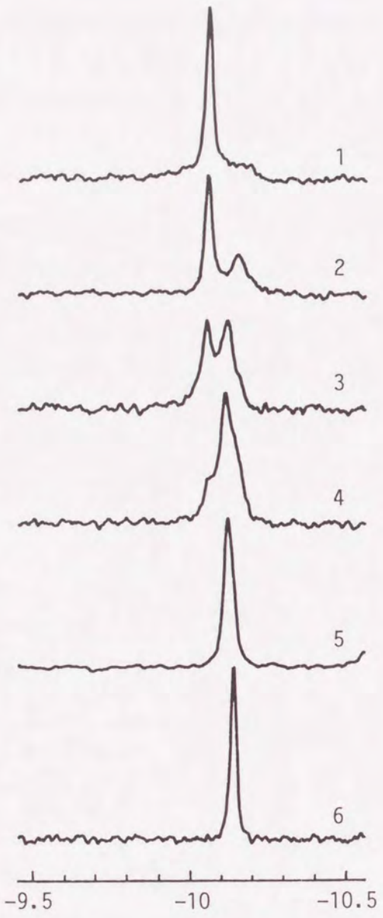

Figure 4–13. ^{31}P NMR spectral changes of an acetonitrile-d_3 solution containing A-β-$(NBu^n_4)_3[PMo_3W_9O_{40}]$ and an equimolar amount of PPh_3: reaction time at 60°C: 0(1), 18(2), 44(3), 64(4), 204(5), and 424 h(6).

was similar to that of A-β-$(NBu^n_4)_3[PMo_3W_9O_{40}]$. Therefore, the geometry of the β-isomer of the Keggin-type polyanion is essentially retained for both the species. The ^{31}P NMR spectrum of A-β-$(NBu^n_4)_3[PMo_3W_9O_{39}]$ in acetonitrile-d_3 showed only a single, sharp signal at −10.12 ppm, confirming a single species of the oxygen-deficient reduced polyanion salt.

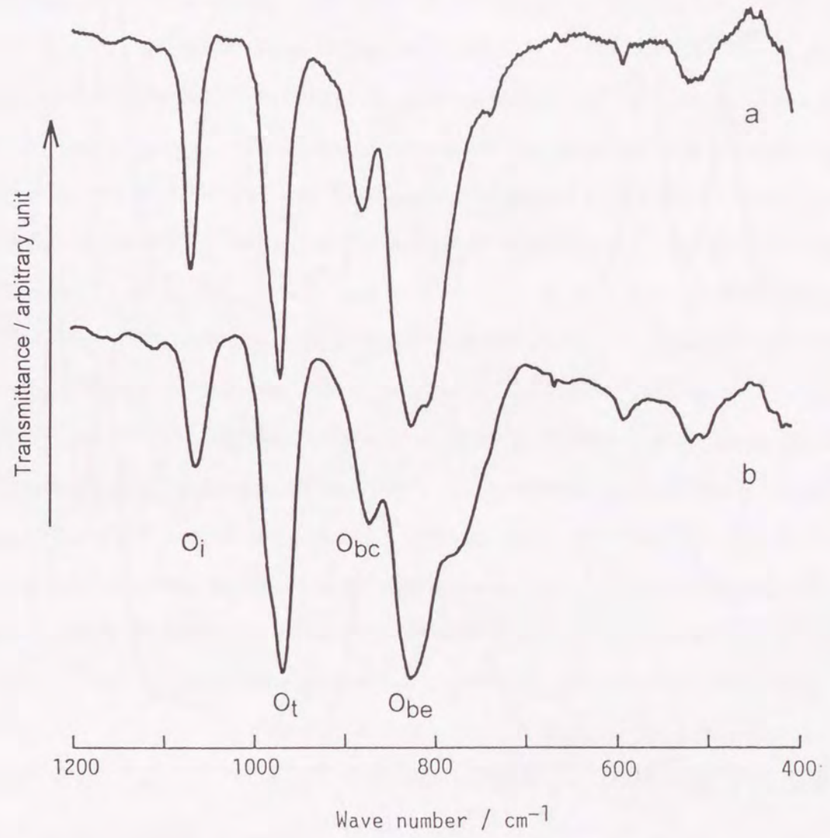

Figure 4–14. IR spectra of A-β-$(NBu^n_4)_3[PMo_3W_9O_{40}]$ (a) and A-β-$(NBu^n_4)_3[PMo_3W_9O_{39}]$ (b) in KBr pellets.

Figure 4–15 shows the X-ray photoelectron spectra of the Mo 3d, P 2p, and W 4f electrons of both A-β-$(NBu^n_4)_3[PMo_3W_9O_{40}]$ and A-β-$(NBu^n_4)_3[PMo_3W_9O_{39}]$. The reduced compound exhibits bands due to P(V) 2p, W(VI) $4f_{5/2}$ and $4f_{7/2}$ electrons which are

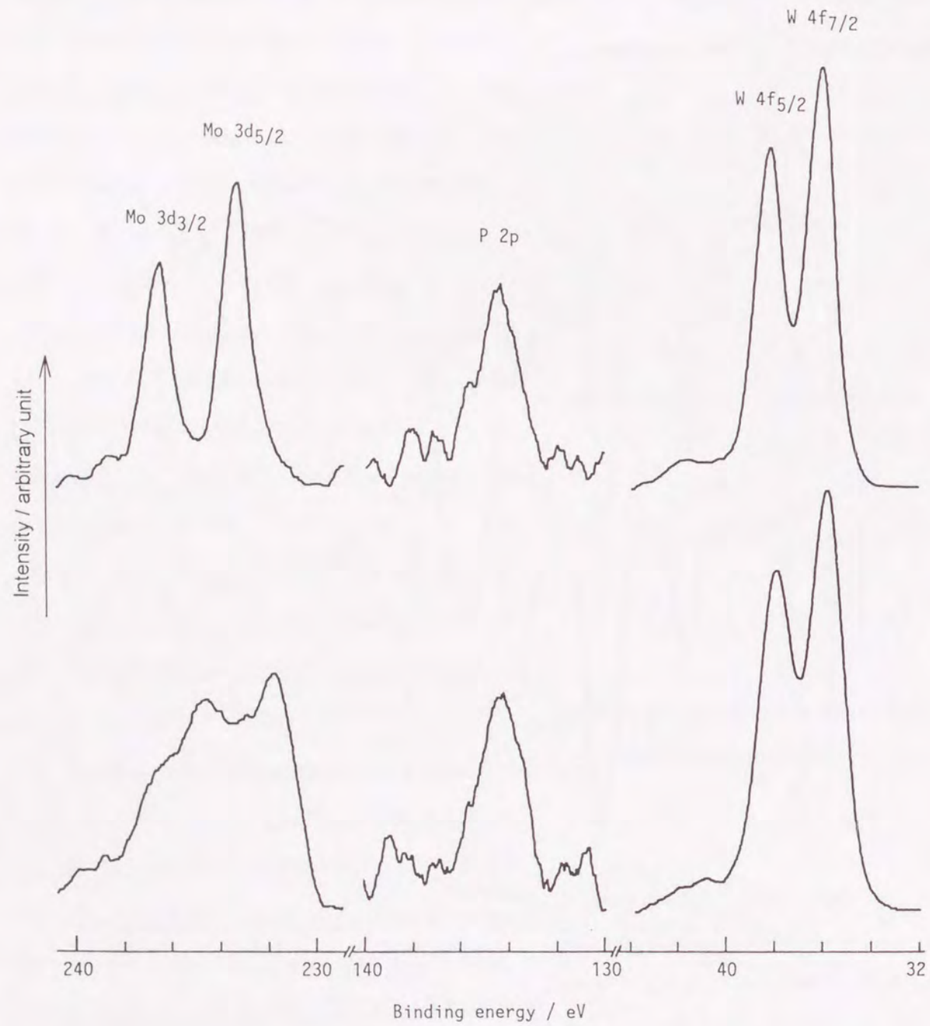

Figure 4–15. X-ray photoelectron spectra of A-β-$(NBu^n_4)_3[PMo_3W_9O_{40}]$ (upper) and A-β-$(NBu^n_4)_3[PMo_3W_9O_{39}]$ (lower).

very close to those observed for A-β-$(NBu^n_4)_3[PMo_3W_9O_{40}]$. On the other hand, the characteristic doublet band due to Mo(VI) $3d_{3/2}$ and $3d_{5/2}$ electrons, which is appreciably observed for A-β-$(NBu^n_4)_3[PMo_3W_9O_{40}]$, is obscured for the reduced compound by the new bands at the lower energy sides. This indicates the formation of an Mo species in a lower valence in the reduced compound. This broad band is deconvoluted into four bands, as depicted in Fig. 4–16. The bands at the first and the third highest binding energies are ascribed to Mo(VI) $3d_{3/2}$ and $3d_{5/2}$ electrons, respectively, because the binding energies are almost identical to those for A-β-$(NBu^n_4)_3[PMo_3W_9O_{40}]$. The other two bands which occur at a 1.6–1.8 eV lower energy region compared with those of the Mo(VI) ion can be assigned to the doublet due to the Mo(V) 3d electrons, as described for the reduced species of α-$(NBu^n_4)_3[PMo_{12}O_{40}]$. For both the doublets, the separations between $3d_{3/2}$ and $3d_{5/2}$ bands are found to be 3.1–3.3 eV and the intensity ratio of them to be about 1.1, which agrees with those reported for the reduced species of α-$(NBu^n_4)_3[PMo_{12}O_{40}]$ as described above. Binding energies of the Mo 3d, P 2p, and W 4f electrons of A-β-$(NBu^n_4)_3[PMo_3W_9O_{40}]$ and A-β-$(NBu^n_4)_3[PMo_3W_9O_{39}]$ are summarized in Table 4–2. No bands due to Mo(IV) and further reduced molybdenum ions were observed in a lower binding energy region. The ratio of the Mo(VI) and Mo(V) ions in A-β-$(NBu^n_4)_3[PMo_3W_9O_{39}]$ was evaluated to be 1:2 from the areas of the deconvoluted bands. These results indicate that the reduction of A-β-$(NBu^n_4)_3[PMo_3W_9O_{40}]$ with PPh_3 does not occur on P(V) or W(VI) atoms but occurs on Mo(VI) atoms, accompanied by elimination of one of the corner-sharing bridging oxygen atoms in the Mo(VI)–O–Mo(VI) bonds and formation of two Mo(V) ions in the polyanion. Furthermore, these findings are consistent with the fact that neither α-$(NBu^n_4)_3[PW_{12}O_{40}]$ nor α-$(NBu^n_4)_3[PMoW_{11}O_{40}]$ is reduced by PPh_3, that is, the bridging oxygen atoms in the W–O–W and Mo–O–W bonds are not transferred to PPh_3 under the conditions used.

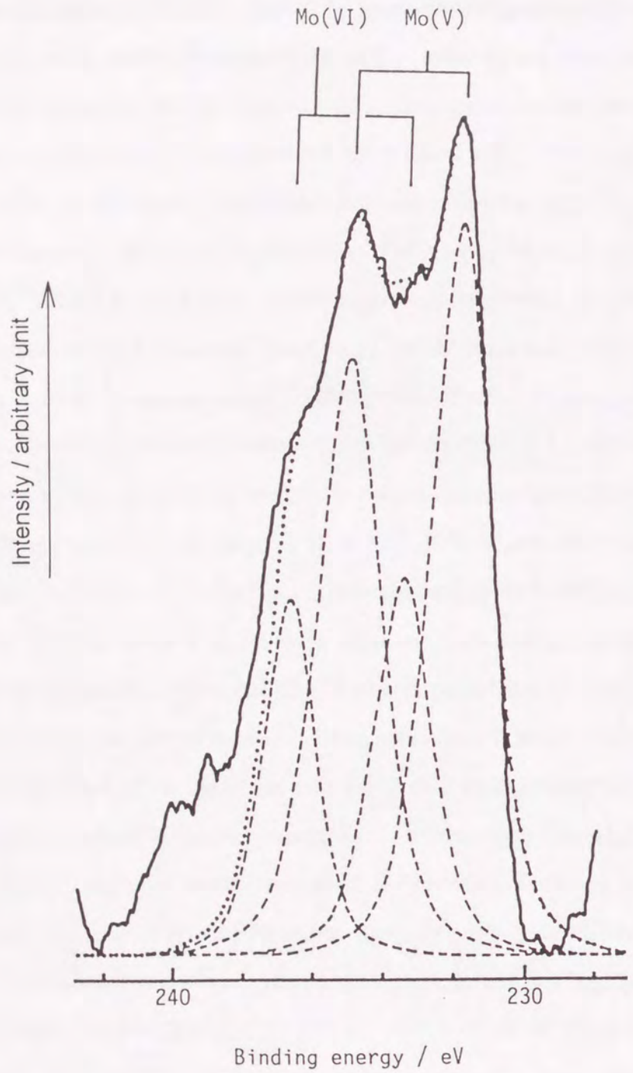

Figure 4–16. X-ray photoelectron spectrum of Mo 3d electrons for A-β-$(NBu^n_4)_3[PMo_3W_9O_{39}]$. Dashed and dotted lines represent deconvoluted and synthesized curves, respectively.

Table 4–2. Binding Energies (eV) of the Mo 3d, P 2p, and W 4f Electrons of the Mixed Addenda Heteropolyanion Salts[a)]

Compound	Mo(VI) $3d_{3/2}$	Mo(V) $3d_{3/2}$	Mo(VI) $3d_{5/2}$	Mo(V) $3d_{5/2}$	P(V) 2p	W(VI) $4f_{5/2}$	W(VI) $4f_{7/2}$
A-β-$(NBu^n_4)_3[PMo_3W_9O_{40}]$	236.6	–	233.4	–	134.3	38.2	36.0
	(1.4)		(1.4)		(2.0)	(1.4)	(1.4)
A-β-$(NBu^n_4)_3[PMo_3W_9O_{39}]$	236.6	234.8	233.3	231.7	134.2	37.8	35.7
	(1.8)	(2.1)	(1.9)	(1.9)	(2.3)	(1.6)	(1.6)

a) Peak width (eV) for deconvoluted bands in parentheses.

4.4 Conclusion

Reductions of α-$(NBu^n_4)_3[PMo_{12}O_{40}]$ and of A-β-$(NBu^n_4)_3[PMo_3W_9O_{40}]$ with PPh_3 in acetonitrile homogeneously proceeded, accompanied by the transfer of the bridging oxygen atoms in the Mo–O–Mo bonds to PPh_3. The ^{31}P NMR and X-ray photoelectron spectra of the isolated reduced species revealed that they were single species of oxygen-deficient reduced forms of α-$(NBu^n_4)_3[PMo(VI)_{10}Mo(V)_2O_{39}]$, α-$(NBu^n_4)_3[PMo(VI)_8Mo(V)_4O_{38}]$, and A-β-$(NBu^n_4)_3[PMo(VI)Mo(V)_2W_9O_{39}]$. Among the bridging oxygen atoms in the Keggin-type polyanion, it was demonstrated that the corner-sharing one in the Mo–O–Mo bond was reactive for the oxygen-transfer reaction upon the reduction of the polyanion.

4.5 References

1 M. Misono, *Proc. Int. Conf. Chem. Uses Molybdenum, 4th*, **1982**, 289, and references therein.

2 H. Tsuneki, H. Niiyama, and E. Echigoya, *Chem. Lett.*, **1978**, 645 and 1183; M. Akimoto and E. Echigoya, *Chem. Lett.*, **1981**, 1759; S. Yoshida, H. Niiyama, and E. Echigoya, *J. Phys. Chem.*, **86**, 3150 (1982).

3 K. Katamura, T. Nakamura, K. Sakata, M. Misono, and Y. Yoneda, *Chem. Lett.*, **1981**,

89; N. Mizuno, K. Katamura, Y. Yoneda, and M. Misono, *J. Catal.*, **83**, 384 (1983); N. Mizuno, T. Watanabe, and M. Misono, *J. Phys. Chem.*, **89**, 80 (1985).

4 K. Eguchi, Y. Toyozawa, K. Furuta, N. Yamazoe, and T. Seiyama, *Chem. Lett.*, **1981**, 1253; K. Eguchi, N. Yamazoe, and T. Seiyama, *Chem. Lett.*, **1982**, 1341; K. Eguchi, Y. Toyozawa, N. Yamazoe, and T. Seiyama, *J. Catal.*, **83**, 32 (1983).

5 H. Taketa, S. Katsuki, K. Eguchi, T. Seiyama, and N. Yamazoe, *J. Phys. Chem.*, **90**, 2959 (1986).

6 M. Akimoto, K. Shima, and E. Echigoya, *J. Chem. Soc., Faraday Trans. 1*, **79**, 2467 (1983); M. Akimoto, K. Shima, H. Ikeda and E. Echigoya, *J. Catal.*, **86**, 173 (1984).

7 Y. Konishi, K. Sakata, M. Misono, and Y. Yoneda, *J. Catal.*, **77**, 169 (1982).

8 C. Rocchiccioli-Deltcheff, R. Thouvenot, and R. Franck, *Spectrochim. Acta, Part A*, **32**, 587 (1976); C. Rocchiccioli-Deltcheff, M. Fournier, R. Franck, and R. Thouvenot, *Inorg. Chem.*, **22**, 207 (1983); R. Thouvenot, M. Fournier, R. Franck, and C. Rocchiccioli-Deltcheff, *Inorg. Chem.*, **23**, 598 (1984).

9 R. Barral, C. Bocard, I. Seree de Roch, and L. Sajus, *Tetrahedron Letters*, **1972**, 1693.

10 P. T. Meiklejohn, M. T. Pope, and R. A. Prados, *J. Am. Chem. Soc.*, **96**, 6779 (1974).

11 M. A. Leparulo-Loftus and M. T. Pope, *Inorg. Chem.*, **26**, 2112 (1987).

12 L. J. Bellamy, *The Infra-red Spectra of Complex Molecules*, Methuen, London, 1958, p. 311.

13 The oxygen atoms of the Keggin-type anion are classified into four species, O_i, O_t, and O_b (O_{bc} and O_{be}), as described in General Introduction.

14 T. H. Fleisch and G. J. Mains, *J. Chem. Phys.*, **76**, 780 (1982).

15 W. E. Swartz, Jr., and D. M. Hercules, *Anal. Chem.*, **43**, 1774 (1971).

16 G. M. Varga, Jr., E. Papaconstantinou, and M. T. Pope, *Inorg. Chem.*, **9**, 662 (1970).

17 J. M. Fruchart, G. Herve, J. P. Launay, and R. Massart, *J. Inorg. Nucl. Chem.*, **38**, 1827 (1976).

18 L. P. Kazansky, I. V. Potapova, and V. I. Spitsyn, *Proc. Int. Conf. Chem. Uses Molybdenum, 3th*, **1979**, 67.

19 A. Aoshima and T. Yamaguchi, *Nippon Kagaku Kaishi*, **1986**, 641 and 1161.

Chapter 5

Kinetics of Oxygen-Transfer Reactions of the α-Dodecamolybdophosphate Anion Salt and of the A-Type Molybdenum-Trisubstituted Dodecatungstophosphate Anion Salt with Triphenylphosphine in Non-Aqueous Solution

5.1 Introduction

Oxygen-transfer reactions of oxomolybdenum complexes have been well-established with regard to the mechanisms and kinetics as model systems for molybdoenzymes [1, 2]. In these systems it was demonstrated that substrates abstract the terminal oxygen atom of an Mo=O bond in the dioxomolybdenum complexes, whereas the bridging oxygen atom of an Mo–O–Mo bond in the μ-oxo dinuclear complex is unreactive. In contrast to these findings, the oxygen-transfer reactions of α-$[PMo_{12}O_{40}]^{3-}$ and of A-β-$[PMo_3W_9O_{40}]^{3-}$ anion salts with PPh_3 revealed that PPh_3 did not abstract the terminal oxygen atom, but, rather, the bridging one in the Mo–O–Mo bond, according to the reactions (Eqs. 4–1 and 4–3), as described in chapter 4. In this chapter, kinetic studies of these oxygen-transfer reactions were discussed.

5.2 Experimental

Materials. Preparations of α-$(NBu^n_4)_3[PMo_{12}O_{40}]$ and α-$(NBu^n_4)_3[PW_{12}O_{40}]$ were described in chapter 4. Preparation of A-β-$(NBu^n_4)_3[PMo_3W_9O_{40}]$ was described in chapter 1. Acetonitrile was distilled from calcium hydride and deoxygenated by bubbling nitrogen before use.

Reactions and Kinetics. The reactions of α-$(NBu^n_4)_3[PMo_{12}O_{40}]$ and of A-β-$(NBu^n_4)_3[PMo_3W_9O_{40}]$ with PPh_3 were carried out in acetonitrile at different temperatures using a thermostated bath under a nitrogen atmosphere. The progress of the reactions was followed by the amount of $OPPh_3$ formed in the solutions, which was determined based on the intensity of the FT-IR bands of $OPPh_3$, as described in chapter 4.

Electrochemical Measurements. The cyclic voltammetry and controlled-potential electrolysis of α-$(NBu^n_4)_3[PMo_{12}O_{40}]$, A-β-$(NBu^n_4)_3[PMo_3W_9O_{40}]$, and α-$(NBu^n_4)_3[PW_{12}O_{40}]$, ($1.0 \times 10^{-3}$ mol dm^{-3}) in acetonitrile were conducted with a BAS CV-50W in the presence of $NBu^n_4ClO_4$ (1.0×10^{-1} mol dm^{-3}) as a supporting electrolyte, using a glassy carbon working electrode for cyclic voltammetry, a platinum working electrode for controlled-potential electrolysis, a platinum counter electrode, and a saturated calomel reference electrode.

5.3 Results and discussion

Reactions of α-$(NBu^n_4)_3[PMo_{12}O_{40}]$ and of A-β-$(NBu^n_4)_3[PMo_3W_9O_{40}]$ with PPh_3 in Acetonitrile. Oxygen-transfer reactions of dioxomolybdenum complexes ($Mo^{VI}O_2L_n$; L = S_2CNR_2, S_2PR_2, cysteinato, 8-quinolinolato, acetylacetonato, etc., n = 2; L = tetradentate S_4 or N_2S_2 donor ligand, n = 1) with PR_3 (R = aryl or alkyl) are known to produce monooxomolybdenum complexes ($Mo^{IV}OL_n$) at first, followed by dimerization of $Mo^{IV}OL_n$ with unreacted $Mo^{VI}O_2L_n$ to afford μ-oxo dinuclear complexes ($Mo^{V}_2O_3L_{2n}$), which complicates the kinetics of the reactions [1, 2]. However, under the conditions of the absence of a dinuclear $Mo^{V}_2O_3L_{2n}$ complex, the oxygen-transfer reaction of a dioxomolybdenum complex containing a bulky ligand [3, 4] or a Shiff base ligand [5] showed fairly simple kinetics of the reaction, being of first order in both the $Mo^{VI}O_2L_n$ complex and the substrate [2]. For the present study, although the one oxygen-deficient reduced species, α-$[PMo_{12}O_{39}]^{3-}$, formed by reaction (Eq. 4–1) could be further reduced by an excess of PPh_3, the secondary reduction was considerably slow compared with the primary one, as described in chapter 4. Furthermore, from reaction (Eq. 4–1) with equimolar amounts of α-$(NBu^n_4)_3[PMo_{12}O_{40}]$ and PPh_3, no other polyanion species different from α-$[PMo_{12}O_{39}]^{3-}$ were obtained, even under the refluxing conditions. Thus, the second-order rate law (Eq. 5–1) is applicable to the kinetics of reaction (Eq. 4–1); its integrated form is given in Eq. 5–2, where $[PMo_{12}]$ and $[PMo_{12}]_0$ are the concentration and the initial one of

α-$(NBu^n_4)_3[PMo_{12}O_{40}]$, respectively:

$$-d[PMo_{12}]/dt = k_2[PMo_{12}][PPh_3] \quad (5–1)$$

$$1/[PMo_{12}] = k_2t + 1/[PMo_{12}]_0 \quad (5–2)$$

Plots of $1/[PMo_{12}]$ vs. time for the reaction of α-$(NBu^n_4)_3[PMo_{12}O_{40}]$ (6.00×10^{-3} mol dm^{-3}) with an equimolar amount of PPh_3 at 23°C are shown in Fig. 5–1. A linear correlation between them is observed up to 65% completion of the reaction. From the slope of these plots the second-order rate constant k_2(23°C) was evaluated to be 6.53×10^{-4} (dm^3 mol^{-1} s^{-1}). Reactions of α-$(NBu^n_4)_3[PMo_{12}O_{40}]$ and PPh_3 in the molar ratio of 1:2, 1:3, and 1:0.5 were also carried out at 23°C. Based on the kinetic data treated in second-order forms, the resulting rate constants were calculated to be 6.50×10^{-4}–6.61×10^{-4} (dm^3 mol^{-1} s^{-1}). As shown in Fig. 5–1, linear relationships between $1/[PMo_{12}]$ and reaction time are also observed for the reactions of α-$(NBu^n_4)_3[PMo_{12}O_{40}]$ (7.85×10^{-3} mol dm^{-3}) with an equimolar amount of PPh_3 at 40, 60, and 82°C.

The kinetic data for reaction (Eq. 4–3) were also treated in second-order forms. Linear correlations between $1/[PMo_3W_9]$ ($[PMo_3W_9]$ is the concen-

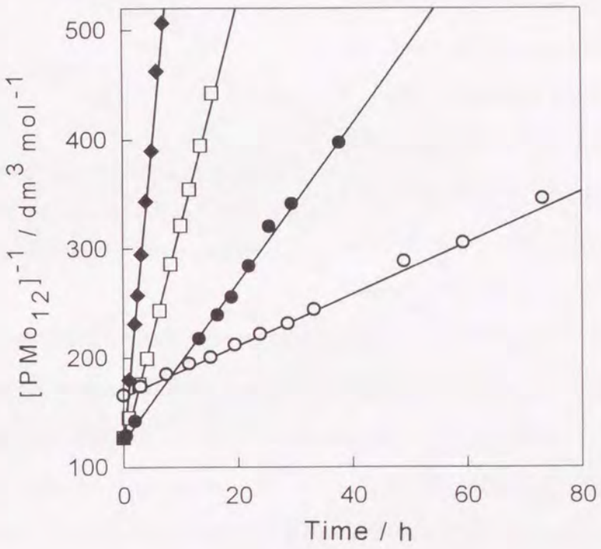

Figure 5–1. Plots of $1/[PMo_{12}]$ vs. time for the reaction of α-$(NBu^n_4)_3[PMo_{12}O_{40}]$ with an equimolar amount of PPh_3 in acetonitrile at 23 (○), 40 (●), 60 (□), and 82°C (◆).

tration of A-β-$(NBu^n_4)_3[PMo_3W_9O_{40}]$) and the reaction time are observed for the reactions of A-β-$(NBu^n_4)_3[PMo_3W_9O_{40}]$ (5.30×10^{-3} mol dm^{-3}) with an equimolar amount of PPh_3 at various temperatures, as shown in Fig. 5–2.

The rate constants determined from the slopes of these plots for reactions (Eqs. 4–1 and 4–3) are summarized in Table 5–1. Figure 5–3 shows Eyring plots for the rate constants of both reactions obtained at various temperatures. The activation parameters were calculated using the Eyring equation: $\Delta H^{\ddagger}$ = 43.6 and 43.4 (kJ mol^{-1}) and $\Delta S^{\ddagger} = -158$ and -181 (J K^{-1} mol^{-1}) for reactions (Eqs. 4–1 and 4–3), respectively (Table 5–1). These values in each parameter are almost identical for both reactions. Negative activation entropies indicate an associative mechanism for these reactions.

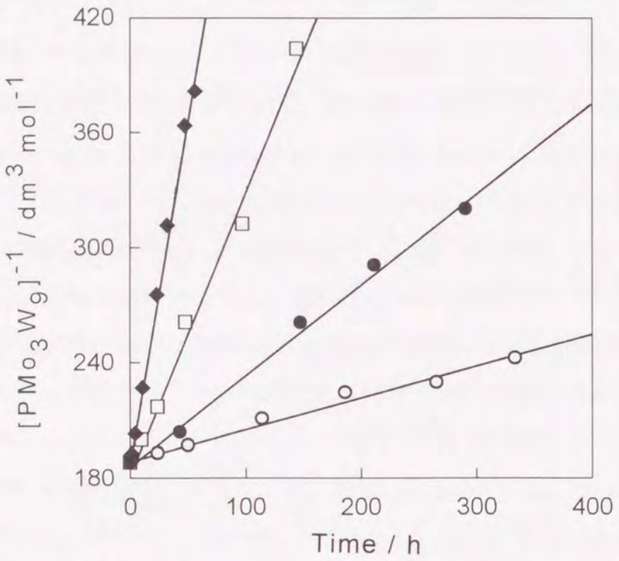

Figure 5–2. Plots of $1/[PMo_3W_9]$ vs. time for the reaction of A-β-$(NBu^n_4)_3[PMo_3W_9O_{40}]$ with an equimolar amount of PPh_3 in acetonitrile at 23 (○), 40 (●), 60 (□), and 82°C (◆).

Reduction Mechanisms of α-$(NBu^n_4)_3[PMo_{12}O_{40}]$ and A-β-$(NBu^n_4)_3[PMo_3W_9O_{40}]$. The redox behavior and oxidizing power of heteropoly compounds can be evaluated in connection with their redox potentials [5–9]. Cyclic voltammograms of α-$(NBu^n_4)_3[PMo_{12}O_{40}]$ and A-β-$(NBu^n_4)_3[PMo_3W_9O_{40}]$ measured in acetonitrile are illustrated in Fig. 5–4. The first and second highest reversible couples observed for both heteropolyanion salts correspond to each one-electron reduction-oxidation

Table 5–1. Kinetic and Activation Parameters[a] for the Oxygen-Transfer Reactions of Heteropolyanion Salts with PPh_3

Salt	10^4k_2 / dm^3 mol^{-1} s^{-1}				$\Delta H^{\ddagger}$ / kJ mol^{-1}	$\Delta S^{\ddagger}$ / J K^{-1} mol^{-1}
	23°C	40°C	60°C	82°C		
α-$(NBu^n_4)_3[PMo_{12}O_{40}]$	6.53 (±0.05)	20.3 (±0.3)	56.1 (±0.7)	151 (±2)	43.6 (±2.7)	−158 (±8)
A-β-$(NBu^n_4)_3[PMo_3W_9O_{40}]$	0.458 (±0.005)	1.31 (±0.08)	4.06 (±0.23)	10.0 (±0.2)	43.4 (±3.0)	−181 (±9)

a) Errors estimated at the 95% confidence level in parentheses.

transfer between Mo(VI) and Mo(V). The one-electron transfer for each couple was confirmed by controlled-potential electrolysis, which was consistent with the results of the Keggin-type polyanion in an aprotic solvent [10]. The voltammetric data are summarized in Table 5–2. The half-wave potentials ($E_{1/2}$) of A-β-$(NBu^n_4)_3$-$[PMo_3W_9O_{40}]$ are observed to be higher than the corresponding potentials of α-$(NBu^n_4)_3[PMo_{12}O_{40}]$. The positive shifts of the

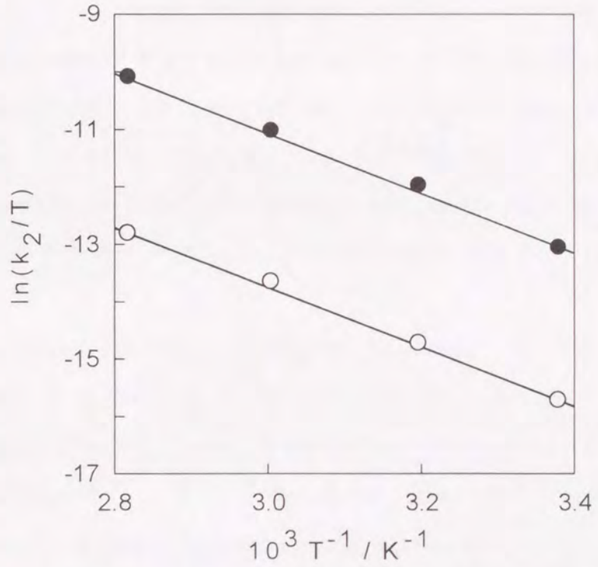

Figure 5–3. Eyring plots of the rate constants for the reductions of α-$(NBu^n_4)_3[PMo_{12}O_{40}]$ (●) and of A-β-$(NBu^n_4)_3[PMo_3W_9O_{40}]$ (○) with PPh_3.

Mo(VI)/Mo(V) redox potentials of mixed molybdotungstophosphate anions, compared with those of the molybdophosphate anion, were also observed [6, 8, 9, 11]. In addition, the reduction of a β-isomer polyanion is known to occur at a higher potential than the corresponding α-isomer polyanion [12]. On the other hand, the W(VI)/W(V) redox couples

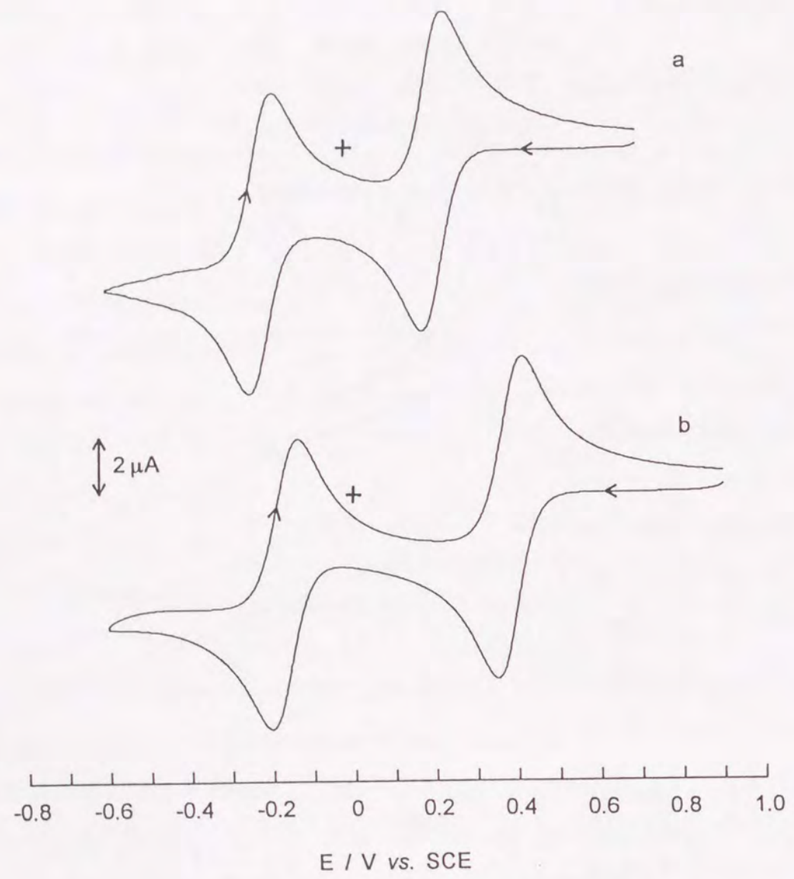

Figure 5–4. Cyclic voltammograms of α-$(NBu^n_4)_3[PMo_{12}O_{40}]$ (a) and A-β-$(NBu^n_4)_3[PMo_3W_9O_{40}]$ (b) (1.0×10^{-3} mol dm^{-3}) in acetonitrile containing $NBu^n_4ClO_4$ (1.0×10^{-1} mol dm^{-3}): scan rate, 10 mV s^{-1}; initial potential, +0.700 (a) and +0.900 V vs. SCE (b); initial scan direction cathodic.

Table 5–2. Voltammetric Data for Heteropolyanion Salts[a)]

Salt	$E_{1/2}$[b)]/V	ΔE[c)]/mV	i_{pc}/i_{pa}[d)]
α-$(NBu^n_4)_3[PMo_{12}O_{40}]$	+0.204	61	1.04
	−0.218	60	0.94
A-β-$(NBu^n_4)_3[PMo_3W_9O_{40}]$	+0.374	60	1.01
	−0.175	63	0.99

a) In acetonitrile containing $NBu^n_4ClO_4$ (1.0×10^{-1} mol dm^{-3}), scan rate 10 mV s^{-1}.
b) Half wave potential (V vs. SCE) for the Mo(VI)/Mo(V) redox couple.
c) Separation of cathodic and anodic peaks.
d) Ratio of cathodic and anodic peak currents.

of α-$(NBu^n_4)_3[PW_{12}O_{40}]$ were observed at lower potential regions ($E_{1/2}$ = −0.224 and −0.745 V vs. SCE) in acetonitrile. Accordingly, the reduction of the W(VI) atoms in A-β-$(NBu^n_4)_3[PMo_3W_9O_{40}]$ would occur at lower potentials than that of Mo(VI) atoms. Such an electrochemical redox behavior is consistent with the findings that α-$(NBu^n_4)_3[PW_{12}O_{40}]$ was not reduced by PPh_3 and that the reduction of A-β-$(NBu^n_4)_3[PMo_3W_9O_{40}]$ with PPh_3 did not occur on W atoms, but, rather, on Mo atoms; the bridging oxygen atoms in the W–O–W and Mo–O–W bonds were not transferred to PPh_3, as described in chapter 4.

Although the electrochemical reduction of the Mo(VI) atom in A-β-$(NBu^n_4)_3[PMo_3W_9O_{40}]$ occurs at a higher potential compared with that in α-$(NBu^n_4)_3[PMo_{12}O_{40}]$, the k_2 value of reaction (Eq. 4–3) is smaller than that of reaction (Eq. 4–1) at the same temperature by more than one order of magnitude (Table 5–1). These findings indicate that the difference in the rates of the present reactions can be ascribed to the number of active sites for the oxygen-transfer reaction of these two heteropolyanion salts, rather than the reduction potentials of the Mo(VI) atoms of these salts.

The reduction of A-β-$(NBu^n_4)_3[PMo_3W_9O_{40}]$ with PPh_3 does not occur on W(VI) atoms, but on Mo(VI) atoms, accompanied by the elimination of one of the O_{bc} atoms in the

Mo(VI)–O–Mo(VI) bonds, as described in chapter 4. There are only three O_{bc} atoms in Mo–O–Mo bonds of A-β-$(NBu^n_4)_3[PMo_3W_9O_{40}]$, whereas twelve O_{bc} and twelve O_{be} atoms exist in those of α-$(NBu^n_4)_3[PMo_{12}O_{40}]$. The activation enthalpies and entropies are, however, almost identical in each parameter for reactions (Eqs. 4–1 and 4–3) (Table 5–1). These results suggest that the transition state for the oxygen-transfer reaction via the Mo–O–Mo site of A-β-$(NBu^n_4)_3[PMo_3W_9O_{40}]$ (Eq. 4–3) is the same as that of α-$(NBu^n_4)_3[PMo_{12}O_{40}]$ (Eq. 4–1).

5.4 Conclusion

The kinetics of the oxygen-transfer reactions of α-$(NBu^n_4)_3[PMo_{12}O_{40}]$ and of A-β-$(NBu^n_4)_3[PMo_3W_9O_{40}]$ with PPh_3 revealed that each reaction was first order in both the heteropolyanion salt and PPh_3. The second-order rate constant of the latter reaction was smaller than that of the former one by more than one order of magnitude. This difference was ascribed to the number of active sites for the oxygen-transfer reaction of these two heteropolyanion salts, rather than the reduction potentials of the Mo(VI) atoms of them. The activation parameters were, however, almost identical for both reactions, which suggested that the transition state for the oxygen-transfer reaction via the Mo–O–Mo site of A-β-$(NBu^n_4)_3[PMo_3W_9O_{40}]$ was the same as that of α-$(NBu^n_4)_3[PMo_{12}O_{40}]$.

5.5 References

1 R. Barral, C. Bocard, I. Sérée de Roch, and L. Sajus, *Tetrahedron Lett.*, **1972**, 1963.

2 R. H. Holm, *Chem. Rev.*, **87**, 1401 (1987) and the references cited therein.

3 I. W. Boyd and J. T. Spence, *Inorg. Chem.*, **21**, 1602 (1982).

4 B. E. Schultz, S. F. Gheller, M. C. Muetterties, M. J. Scott, and R. H. Holm, *J. Am. Chem. Soc.*, **115**, 2714 (1993); B. E. Schultz and R. H. Holm, *Inorg. Chem.*, **32**, 4244 (1993) and the references cited therein.

5 J. Topich and J. T. Lyon, III, *Inorg. Chim. Acta*, **80**, L41 (1983); J. Topich and J. T. Lyon, III, *Polyhedron*, **3**, 61 (1984); J. Topich and J. T. Lyon, III, *Inorg. Chem.*, **23**, 3202 (1984).

6 M. Misono, *Proc. Int. Conf. Chem. Uses Molybdenum, 4th*, **1982**, 289, and references therein.

7 K. Katamura, T. Nakamura, K. Sakata, M. Misono, and Y. Yoneda, *Chem. Lett.*, **1981**, 89; M. Misono, T. Komaya, H. Sekiguchi, and Y. Yoneda, *Chem. Lett.*, **1982**, 53; N. Mizuno, K. Katamura, Y. Yoneda, and M. Misono, *J. Catal.*, **83**, 384 (1983).

8 M. Otake and T. Onoda, *Shokubai*, **18**, 169 (1976) and the references cited therein.

9 E. G. Zhizhina, L. I. Kuznetsova, R. I. Maksimovskaya, S. N. Pavlova, and K. I. Matveev, *J. Mol. Catal.*, **38**, 345 (1986).

10 R. A. Prados, P. T. Meiklejohn, and M. T. Pope, *J. Am. Chem. Soc.*, **96**, 1261 (1974).

11 J. P. Ciabrini, R. Contant, and J. M. Fruchart, *Polyhedron*, **2**, 1229 (1983).

12 M. T. Pope, "Heteropoly and Isopoly Oxometalates," Springer-Verlag, Berlin (1983), p. 73.

Chapter 6

Summary

This thesis dealt with the syntheses, structural characterization, and redox properties of the A-type metal-trisubstituted dodecatungstophosphate anion salts. The results obtained through this work are summarized as follows.

In chapter 1, α- or β-isomers of the A-type vanadium-, niobium-, and molybdenum-trisubstituted dodecatungstophosphate anion salts, A-$[PM_3W_9O_{40}]^{n-}$ (M = V and Nb, n = 6; M = Mo, n = 3), were prepared as single species by using A-$Na_9[PW_9O_{34}]$ as a precursor. Each of the isomers was successfully obtained under the different conditions of reactions of the same precursor, which suggested that the precursor, A-$Na_9[PW_9O_{34}]$, was a β-isomer. The behavior of protonation of the $[PM_3W_9O_{40}]^{6-}$ (M= V and Nb) anions was clarified by their NMR spectra.

In chapter 2, the structures of the metal(V, Nb, and Mo)-trisubstituted dodecatungstophosphate anion salts were clarified by single-crystal X-ray analyses as A-type metal-trisubstituted, geometrical β-isomers of the Keggin type, A-β-$Cs_{5.4}H_{0.6}[PV_3W_9O_{40}]$, A-β-$Cs_6[PNb_3W_9O_{40}]$, and A-β-$(NMe_4)_3[PMo_3W_9O_{40}]$, in which three substituted metals formed the corner-shared M_3O_{13} unit of the A-type through the three corner-sharing oxygen atoms. The structural characteristics of these polyanions were reflected in the differences between the ion radii of the substituted metals. In the crystal structure of A-β-$Cs_{5.4}H_{0.6}[PV_3W_9O_{40}]$, one cesium atom was disordered with a proton, which afforded structural information concerning protonation to the oxygen atom of the $[PV_3W_9O_{40}]^{6-}$ anion.

In chapter 3, A-β-$(NBu^n_4)_4H_2[PV_3W_9O_{40}]$ was found to be isomerized to A-α-$(NBu^n_4)_4H_2[PV_3W_9O_{40}]$ both in the solid state and in solution under mild conditions. The isomerization process was directly followed by FT-IR and ^{31}P NMR spectroscopies, which afforded its kinetics as a first-order reaction in the β-isomer. In contrast, the other β-isomers of A-type metal-trisubstituted dodecatungstophosphate anion salts, A-β-$[PM_3W_9O_{40}]^{n-}$ (M = V and Nb, n = 6; M = Mo, n = 3), containing one proton or less in their cation parts did not isomerize under the same conditions. It was suggested that the β-to-α isomerization was promoted by protonation to the bridging oxygen atom in the W–O–W bond of the polyanion.

In chapter 4, reductions of α-$(NBu^n_4)_3[PMo(VI)_{12}O_{40}]$ and of A-β-$(NBu^n_4)_3[PMo(VI)_3W_9O_{40}]$ with PPh_3 in acetonitrile were found to proceed homogeneously, accompanied by the transfer of the bridging oxygen atoms in the Mo(VI)–O–Mo(VI) bonds to PPh_3. The ^{31}P NMR and X-ray photoelectron spectra of the isolated reduced species revealed that they were single species of oxygen-deficient reduced forms of α-$(NBu^n_4)_3[PMo(VI)_{10}Mo(V)_2O_{39}]$, α-$(NBu^n_4)_3[PMo(VI)_8Mo(V)_4O_{38}]$, and A-β-$(NBu^n_4)_3[PMo(VI)Mo(V)_2W_9O_{39}]$. Among the bridging oxygen atoms in the Keggin-type polyanion, the corner-sharing one in the Mo–O–Mo bond was reactive for the oxygen-transfer reaction upon the reduction of the polyanion.

In chapter 5, the kinetics of the above-mentioned oxygen-transfer reactions revealed that each reaction was first order in both the heteropolyanion salt and PPh_3. The second-order rate constant of the reaction of A-β-$(NBu^n_4)_3[PMo_3W_9O_{40}]$ was smaller than that of α-$(NBu^n_4)_3[PMo_{12}O_{40}]$ by more than one order of magnitude. This difference was ascribed to the number of active sites for the oxygen-transfer reaction of these two heteropolyanion salts, rather than the reduction potentials of the Mo(VI) atoms of them. The activation parameters were, however, almost identical for both the reactions, which suggested that the transition state for the oxygen-transfer reaction via the Mo–O–Mo site of A-β-$(NBu^n_4)_3[PMo_3W_9O_{40}]$ was the same as that of α-$(NBu^n_4)_3[PMo_{12}O_{40}]$.

Acknowledgement

The author would like to express his gratitude to Professor Gen-etsu Matsubayashi, Osaka University, for his continuous guidance, valuable suggestions, and hearty encouragement throughout this work.

The author also wishes to express his appreciation to Professor Gin-ya Adachi and Professor Hideo Kurosawa, Osaka University, for their thoughtful direction and helpful suggestions.

The author is deeply grateful to Dr. Hatsue Tamura, Osaka University, for her invaluable discussions and help in X-ray analyses.

The author desires to express his sincere thanks to Professor Toshihiro Yamase, Tokyo Institute of Technology, and Professor Kenji Nomiya, Kanagawa University, for their fruitful suggestions and discussions.

The author would like to acknowledge Dr. Yoshio Tominaga, Director of Osaka Municipal Technical Research Institute, and Dr. Hidehiko Enomoto, Manager of Inorganic Chemistry Department of Osaka Municipal Technical Research Institute, for their encouragement and giving me the opportunity to conduct the present research.

Grateful acknowledgements are given to Dr. Masanari Takahashi, Inorganic Chemistry Department of Osaka Municipal Technical Research Institute, for his help and useful discussions and all other members of Osaka Municipal Technical Research Institute for their friendship and cooperation.

The author is so much obliged to Mr. Hideaki Okumura, Mr. Hisanori Kobayashi, Mr. Seigo Noguchi, Mr. Masafumi Ueshima, Mr. Hiroki Matsunaka, Mr. Tsuyoshi Nakajima, Mr. Kotaro Nishimura, Mr. Masaaki Iino, Mr. Tsutomu Abe, Mr. Seiya Murao, Mr. Keiji Koyama, and Mr. Masanori Nakatani, graduates of Osaka Institute of Technology, for giving me their helpful assistance.

Finally, the author is particularly grateful to the late Professor Emeritus Toshio Tanaka, Osaka University, for his worthwhile advice and hearty suggestions at the beginning of this work.